INVESTIGATION OF APPLICABLE SEISMIC RESPONSE MODIFICATION FACTOR FOR THREE-HINGE GLULAM TUDOR ARCHES USING FEMA P-695

Jonathan Robert Eberle

Thesis submitted to the faculty of the Virginia Polytechnic Institute and State University in partial fulfillment of the requirements for the degree of

Master of Science

In

Civil Engineering

Finley A. Charney, Chair

Matthew R. Eatherton, Member

Daniel P. Hindman, Member

May 8, 2013

Blacksburg, VA

Keywords: Three Hinge Glulam Tudor Arch, Dynamic Analysis, P-695, Seismic Response Modification Factor

INVESTIGATION OF APPLICABLE SEISMIC RESPONSE MODIFICATION FACTOR FOR THREE-HINGE GLULAM TUDOR ARCHES USING FEMA P-695

Jonathan Robert Eberle

ABSTRACT

The objective of this research project involves determining a seismic response modification factor for three-hinge glulam Tudor arches. In an attempt to meet this objective, the methods and procedures outlined in FEMA technical document P-695 were implemented on the provided arch designs. Computational models were created using finite elements within OpenSees to accurately depict the behavior of the arch. Incremental dynamic analyses were conducted on each of the provided designs and collapse margin ratios were determined allowing performance groups to be evaluated for each of seven design R-values within two gravity load cases. With the performance groups evaluated, it was determined that only groups within the low gravity load level designs were successfully able to pass, none of the groups designed for high gravity loads passed the evaluations. Within P-695, all performance groups associated with a given design R-value must pass the evaluations for that R-value to be deemed acceptable for use in designs. Because of the implications of this requirement, a seismic response modification factor could not be determined for this type of structural system within the scope of this project.

Acknowledgements

I would like to thank Dr. Finley A. Charney for serving as my academic and research project advisor. His help as a professor, advisor, and mentor throughout my education at Virginia Tech have proved invaluable. I would like to thank Dr. Matthew R. Eatherton for serving as a member of my committee and providing suggestions and guidance relating to my research project. The suggestions provided from his expertise in earthquake engineering were vital to the project. I would also like to thank Dr. Daniel P. Hindman for serving as committee member for my thesis project. His expertise in timber engineering and valuable suggestions and guidance throughout my research project were greatly appreciated.

I would like to thank the American Wood Council (AWC) and the National Association of Home Builders (NAHB) for sponsoring this research project. In particular, I would like to thank Phil Line, Brad Douglas, and Vladimir Kochkin for their assistance in providing information and suggestions throughout the research project.

Completion of this project would not have been possible without the computational tools provided by previous graduate from Virginia Tech, Amber Verma and doctoral student at Virginia Tech, Andy Hardyniac. The GUI that was created and modified with extensive help from Amber Verma made the creation of computational models possible in a timely manner, while the toolkit created by Andy Hardnyiac and modified with his assistance made it possible to conduct the thousands of dynamic analyses required for this project in a timely and organized manner.

I would also like to thank my friends and family for their support and encouragement throughout my graduate education and research project, especially my loving parents John and Christa Eberle and wonderful girlfriend Erin Singleton. Without their continued support, completion of my thesis and graduate education would not have been possible.

Table of Contents

List of Figures

List of Tables

Chapter 1 : Introduction

1.1 Problem Statement

Glued laminated lumber (glulam) has been utilized within the building industry for several decades, and continues to gain popularity with today's demands for larger spans within structures and reduced cost. North America, in addition to many other regions around the world, has abundant supplies of softwood trees, which provide a cost-efficient material for use within structures. One of the disadvantages of these softwood trees is that to accelerate the production of a forest, trees are harvested when they are still smaller than dimensions would require for many large span applications within structures. The benefit of glulam is that smaller dimension lumber (typically 2x material) can be glued together to create an overall member dimension great enough to span large areas and create irregular geometries. One common use of glulam is that of arches. The large open spaces created by glulam arches allow for multiple uses while the prefabrication of arch members speeds erection time. For these reasons, popularity and demand for three-hinge glulam Tudor arches continues (Linville, 2007). The ability to efficiently design arches for seismic loadings then becomes necessary to allow for the market share to expand to regions where seismic demands may control designs.

For structural systems that are pre-approved by ASCE 7-10 (ASCE, 2010) and included in Table 12.2-1, the seismic response modification factor, R, is provided. These R-values theoretically represent the ratio of elastic system response to the inelastic system response and are used to account for four factors. These factors include system ductility, system overstrength, damping within the structure (values are based upon an assumed value of 5% of critical damping), and experience relating to the behavior of the given systems during previous earthquakes. The structural system evaluated within this project of three-hinge glulam Tudor arches, however, are not included within ASEC 7-10 Table 12.2-1. This is because sufficient experience is not present in that there is not sufficient data showing how these systems respond during an earthquake. Because an R-value is not provided for the arch systems, it is necessary to determine an appropriate R-value for these systems which can be used to design the arches for lateral loads resulting from an earthquake.

To allow the systems not addressed within ASCE 7-10 to be designed for seismic loads using the Equivalent Lateral Force (ELF) method, methodology has been developed to aid in the determination of a design R-value. The procedure for determining an acceptable R-value is outlined within FEMA's (Federal Emergency Management Agency's) technical document P-695 (FEMA, 2009b). Determining an R-value for a structural system involves first designing each structure of interest using a range of assumed R-values. For this project, designs were provided within a white paper to be published by the American Wood Council (AWC) along with the National Association of Home Builders (NAHB) for R-values of 1.5, 2, 2.5, 3, 4, 5, and a minimum design was provided which had no R-value associated with it. This was due to the fact that the systems were not designed for seismic loads, but rather all members and connections were simply designed for gravity loads. All of the designs were then arranged into performance groups based upon several factors. Once the models were created and grouped, analyses were conducted to determine a CMR (Collapse Margin Ratio) and subsequently determine if a given

performance group is capable of resisting the forces induced by ground motions with an acceptable probability of collapse.

1.2 Objectives

The objective of this research was to determine an appropriate seismic response modification factor, R, for structural seismic force resisting systems consisting of three-hinge glulam Tudor arches. To fulfill this objective, several smaller objectives had to be met including:

- Determine an acceptable method of modeling the glulam elements within a Tudor arch
- Determine an acceptable method of computationally modeling the connections at the base and crown including any non-linear behavior deemed applicable within the scope of this project
- Computationally determine the CMR's (Collapse Margin Ratio) of the arches through use of non-linear incremental dynamic analyses
- Evaluate the arch performance groups to determine which pass in an attempt to determine an acceptable R-value

1.3 Significance

Three-hinge glulam Tudor arches currently have no associated R-value to allow for the seismic design to be completed using the methods outlined in ASCE 7-10. A white paper to be published by the AWC and NAHB outlines the steps necessary to design and detail these arches for seismic loads and is currently under development and a design R-value is needed to allow the arches to be designed without the use of complex and time consuming non-linear dynamic analyses.

Chapter 2 : Literature Review

2.1 Introduction

The use of FEMA P-695 to determine a seismic response modification factor, *R*, involves running several sets of non-linear dynamic analyses. The need to accurately model the behavior of the timber material within the arch, as well as the connections, requires the understanding of glulam material and timber connections. Within this chapter a review of literature pertinent to the arch designs, modeling, and analysis of glulam arches is included.

2.2 Glulam Bending Behavior

Glued laminated timber (glulam) is a composite material made by gluing laminations together as shown in Figure 2.1. The benefit of using glulam over typical dimension lumber is threefold. The first benefit is that more readily available sizes of dimension lumber (2x material) can be laminated together to make larger sections which can span farther than solid timber is capable of. These cross sections can also be manufactured to be much larger than a single timber cut from a log. The second benefit of glulam is that the individual pieces of dimension lumber comprising a glulam beam do not need to be as long as the total span that is being created. As shown in the figure below, shorter pieces of dimension lumber can be spliced together within the laminations as long as the splices are staggered. The final benefit of glulam is that a higher grade of lumber can be used in the outside laminations where the stresses are the largest and weaker, more cost efficient grades of lumber can be used for the inner laminations where the required strength is less.

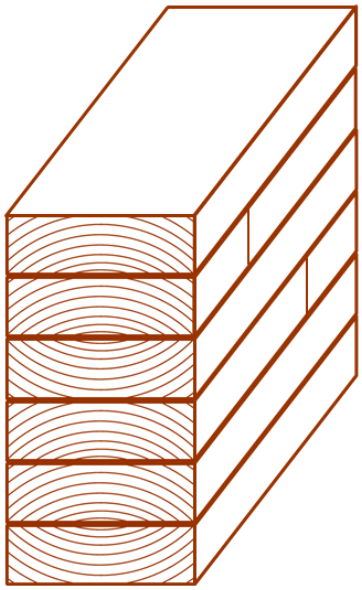

Figure 2.1: Glued laminated timber (glulam)

Considering that glulam is almost completely comprised of timber (excluding the glue), it is important to first understand the behavior of wood as a material. Although the laminating process used to create glulam could be expected to produce slightly different material response, the fundamental behavior of

glulam can be related directly back to the behavior of wood as a material. For the purposes of this study it was necessary to determine the response of wood subjected to bending.

Studies conducted at the College of Engineering and Technology at Northern Arizona University showed, among other things, the response of ponderosa pine subjected to bending (Larson et al., 2004). Within these tests, tapered ponderosa pine logs were subjected to a single point load at mid-span and were tested to failure. The resulting load vs. deflection plot from one of these tests is shown in Figure 2.2.

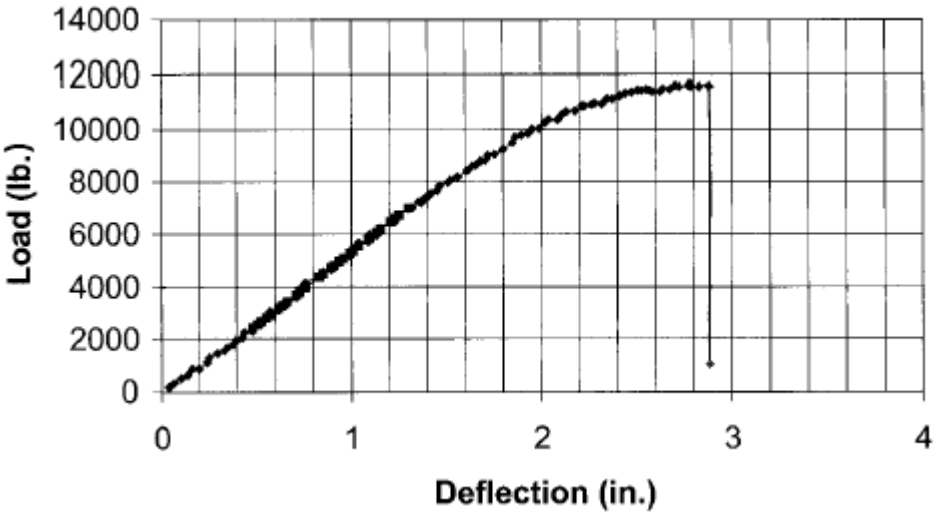

Figure 2.2: Load deflection plot for tapered ponderosa pine logs tested in bending (Larson et al., 2004)

As this figure shows, the logs responded with very linear behavior through the majority of loading and showed very limited amounts of non-linearity before failure. These results support the ability to model timber as a linear elastic material. This was expected as timber structures typically depend on the connections to provide ductility within a structural system. To ensure that the composite material glulam would perform with similar results, further investigation was done. Studies conducted for the Forest Products Lab (FPL) investigating the strengths of reinforced yellow-poplar glulam beams (Hernandez et al., 1997) provided some insight to the response of glulam beams. This study was intended to investigate the strength of glulam beams reinforced with glass fiber reinforced plastic (GFRP) on the tension and compression faces. Although the results from the composite beam tests are not of particular interest, issues during production of the beams caused one beam to have no GFRP attached and therefore was used as a control. The beams were loaded with a two point loading to produce a constant moment between the loading points and the load deflection data from the unreinforced beam is provided in Figure 2.3.

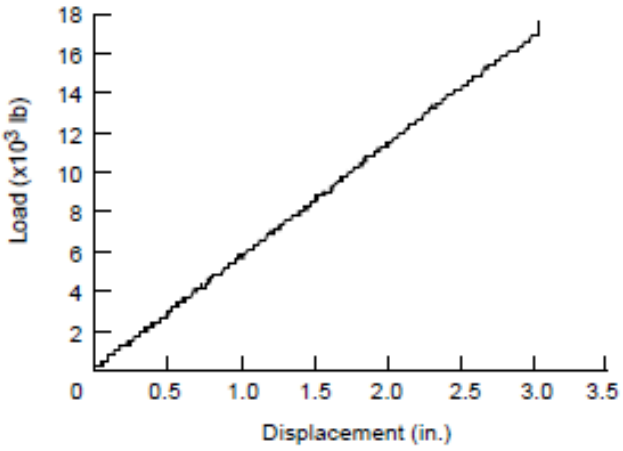

Figure 2.3: Load vs. deflection response for the unreinforced glulam beam (Hernandez et al., 1997)

As the results from this test show, the glulam beam without GFRP laminations performs linear right until the point of failure (where the plot ends) with no non-linear behavior, similar to the tapered ponderosa pines tested at Northern Arizona University. It is also important to note that the failure mechanism observed for this beam involved a rupture of one of the tension lamination finger joints. This failure mechanism could explain the highly linear behavior up to failure observed within the glulam beam.

Further support of the linear response of timber subjected to bending was found in a study investigating the bending response of water soaked glulam beams (Wolfe and Moody, 1978). Within these tests, dry glulam beams were tested along with the saturated beams for comparison purposes. The average load deflection curves from this study are presented in Figure 2.4.

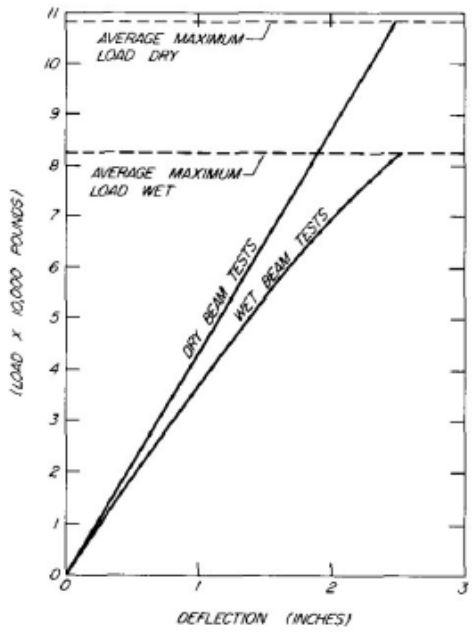

Figure 2.4: Load deflection plot for the studies conducted on dry and wet Douglas-fir glulam beams (Wolfe and Moody, 1978)

As seen in Figure2.4, it was found in this study that the wet glulam beams had a very limited amount of non-linear behavior, while for the dry beams, "The dry beam curves were nearly linear (elastic) all the way to failure" (Wolfe and Moody, 1978). The results of these studies provide sufficient evidence that glulam beams behave linearly until the failure point when subjected to bending and, therefore, modeling of the glulam within our models can be done with a linear elastic material.

2.3 Glulam Failure Limit

For the purposes of this project, the "nominal capacity" of the glulam material or of a connection will refer to the LRFD capacity of the given material or connection with a resistance factor, ϕ, equal to 1.0. The NDS (National Design Specification for Wood Construction) (AFPA, 2005) provides stress limits for several types of glulam. The reference values represent the allowable stress capacity of glulam, however, when conducting a P-695 analysis the expected strength is to be used when defining a NSC (Non Simulated Collapse) limit. It is well known that wood can achieve strengths in excess of its allowable capacity when subjected to non-static loads. One such study supporting this phenomenon was conducted on round timber piles (Wilkinson, 1968). Within this test it was found that the failure strengths of small samples subjected to impact loading were 1.86 to 3.24 times the load determined from statically loaded specimens. This study shows that the strength of wood is increased when loaded dynamically. However, these results are not directly related to the failure limits which are imposed on the glulam subjected to bending from dynamic earthquake accelerations. A more relevant study conducted by the Forest Products Lab (FPL) on the design of glulam utility structures (Hernandez et al., 1995) provides testing to support an increase from the allowable strength of glulam subjected to static loading to the expected strength of glulam subjected to short term loading, similar to that which would be observed during an earthquake. Within the tests conducted, it was determined that the ratio between the modulus of rupture (MOR) and allowable design stress is equal to 2.95 for glulam beams. This increase of strength can be used to determine the increase in bending stress which would be expected within the glulam arches when subjected to dynamic earthquake loading. The increase factor allows the nominal stress (LRFD bending stress limit with ϕ = 1.0 in accordance with NDS) to be increased by a factor of 1.15 to determine the expected stress which will be used as an NSC limit imposed upon bending stresses within the arch members.

2.4 Connection Capacities

The capacity of connections used as NSC limits within the structural models also needed to be determined for each of the connection types. The design capacity of each connection was provided within the white paper; however those values represented the nominal capacities of the connections. These values need to be increased from the nominal values to the expected values similar to the increase previously discussed on bending stresses.

2.4.1 Arch Base Connection Capacity

The shear capacity of the base connection is dependent upon the direction of loading. This is due to the geometry of the connection which creates two different failure mechanisms for the loading cases. The geometry of a typical base connection is shown in Figure 2.5.

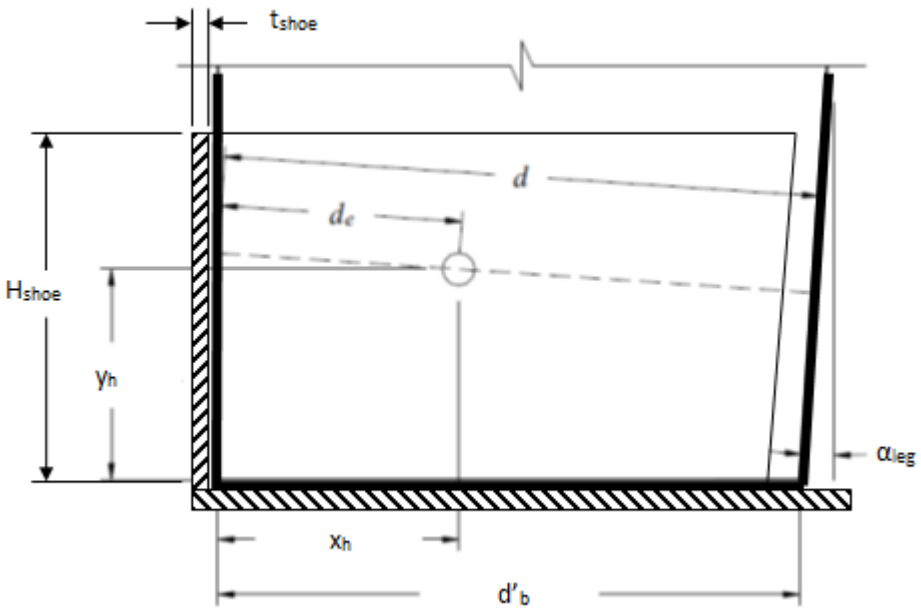

Figure 2.5: Geometry of typical shoe connection including dimensions (AWC, 2013)

When the load is applied toward the outside of the shoe (left in the above figure), such as the thrust resulting from gravity loading, the capacity of the connection is limited to the shear capacity of the timber. This is because the shoe thickness has been designed such that it is sufficient to resist any forces resulting from the arch without yielding, therefore causing wood shear failure at the base (AWC, 2013). The expected strength for this failure mode was taken as the LRFD capacity of the timber in shear with $\phi = 1.0$. It was determined that this failure mode would likely not control for any cases (which was later validated) so use of relevant test data to determine an increase in expected strength would not be useful for purposes of this project.

When the base connection is loaded toward the inside of the arch, which occurs during seismic ground motion accelerations, failure is resisted by the bolted connection. To determine the expected capacity of the bolted connection, a FPL report testing the capacity of bolted timber connections with steel side plates was referenced (Wilkinson, 1992). Within these tests, connection geometries involving both parallel to grain and perpendicular to grain loading were studied. For the purposes of this project, all of the loadings resulting from shear at the base connection involve loading the glulam member perpendicular to grain. The tests (Wilkinson, 1992) involving geometries similar to those seen in the arch base connections were found to have an ultimate capacity equal to three times the nominal design capacity ($\phi = 1.0$) determined in accordance with NDS. This was for connections failing due to Mode III_s as seen in Figure 2.6. The results for this type of failure were used in determining the increase in nominal strength because the design of the arch base connection for inward loading requires that the failure be controlled by Mode III_s (AWC, 2013). From these test results, it was determined that an increase factor of 3.0 was deemed applicable to convert the nominal connection capacities to the expected connection capacities to be used as a NSC limit.

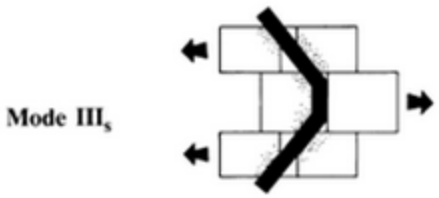

Figure 2.6: Failure mode III$_s$ as defined within the NDS for Wood Construction

2.4.2 Arch Peak Connection Capacity

The capacity of the peak connection to resist shear induced by lateral loads is controlled by the capacity of the shear plate connectors within the peak connection. A typical peak connection showing the shear plate location dimensions is shown in Figure 2.7. All designs utilized 4 inch diameter shear plates.

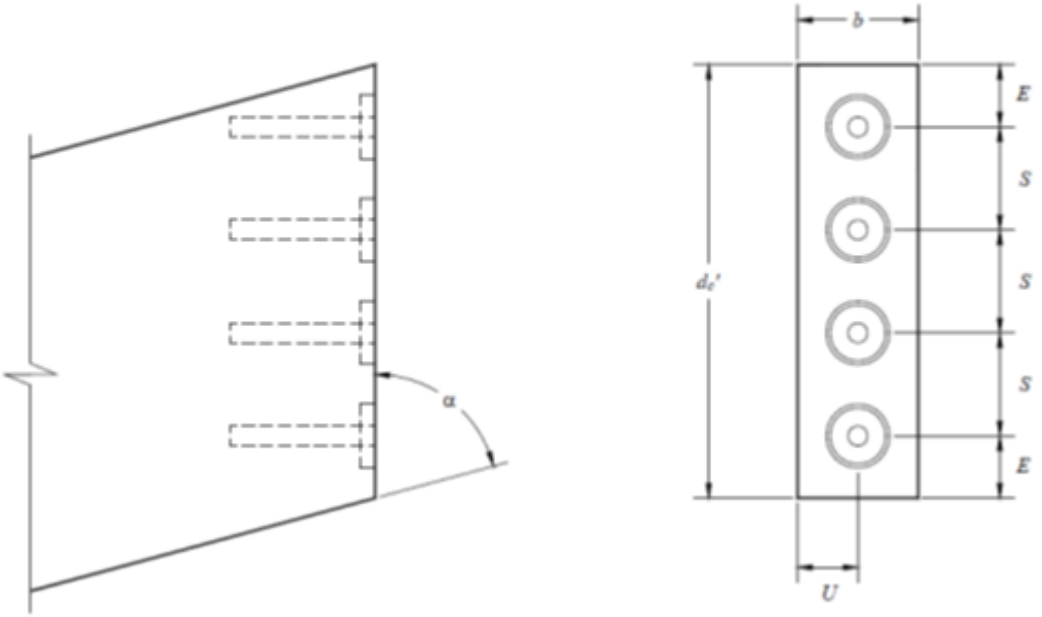

Figure 2.7: Summary of peak connection dimensions for typical shear plate connection (AWC, 2013)

To determine how the NDS nominal strength of the shear plate connectors (ϕ = 1.0) compared to the expected strength, a report on the behavior of shear plate connectors in sloped end grain (Longworth, 1967) was referenced. Within this report (Longworth, 1967), evidence was provided showing that the ultimate shear capacity of the shear plate connectors used in end grain was equal to 1.5 times the nominal strength determined in accordance with the NDS provisions. This increase in capacity above the values determined from the NDS are assumed to be the result of conservatism within the adjustment factors used to determine the capacity of shear plates at an angle to grain within the NDS. This increase factor is applicable to the shear plate connector capacities used within the arch designs and therefore the expected strength of the shear connections was determined as 1.5 times the nominal LRFD capacity with ϕ = 1.0 to provide the necessary NSC limits.

2.5 Damping in Timber Structures

Damping is an essential factor in the response of a structure to dynamic loadings. Whether the loads consist of seismic, wind, or cyclic loading applied from a mechanical unit within a structure, damping plays a large role in preventing failure and helping to meet serviceability limit states. A structure with a damping ratio equal to zero (although practically not feasible) could be set into a resonant like behavior, up until damage occurred and induced damping, by the smallest of dynamic loads and collapse under a slight breeze or a very low magnitude and distant earthquake. Although added dampers such as viscous fluid or friction dampers are used frequently in high seismic areas, structures without any added damping will always exhibit some amount of inherent damping. A damping ratio of 5% critical is commonly used when conducting dynamic analyses on conventional building systems such as steel moment frames. Although this value may be representative of steel moment frames for example, it does not necessarily well represent the damping ratio of all structural systems and takes no consideration for factors such as secondary framing, connections, etc. While trying to establish an appropriate damping ratio for the structural system consisting of three-hinge glulam Tudor arches, a significant issue arose. There is no material available defining the damping ratio of such a system, and the information on damping in any type of wood structure or timber itself seems to be in its infancy. For purposes of the project, it was determined that 2.5% critical damping would be a conservative estimate for damping within the structure. This literature review works to determine if a higher damping ratio could be applicable and works in parallel to determine the effects of varied damping ratio on the Collapse Margin Ratio (CMR) for the given 56 arch designs provided within this project.

Damping within timber structural systems is related to two components: the damping associated with the timber material itself and the damping associated with the connections between elements within the structural system (Yeh et al., 1971). The damping of timber as a material is generally thought to be negligible. This assumption is supported by a results presented by an article in the Journal of Sound and Vibration (Yeh et al., 1971). Within this study, the damping ratio of timber specimens was determined and the moisture content of each specimen was recorded. The results from this study are summarized in Figure 2.8..

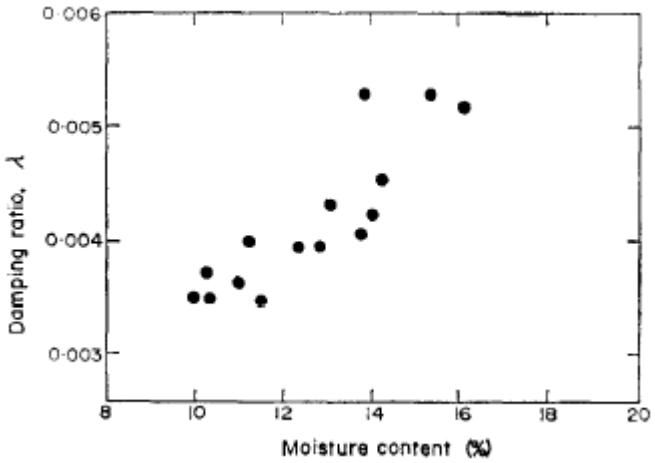

Figure 2.8: Results from damping tests showing damping ratio as a function of moisture content (Yeh et al., 1971)

As the results from this study show, the damping ratio of timber increases as the moisture content increases. The overall magnitude of the damping ratio is determined to vary between values of approximately 0.0035 and 0.0055. These results would support an assumed damping ratio of timber as a material equal to 0.5%.

This paper also presents results from a study where the damping ratio of T-beams was evaluated. Within this study, the beams consisted of a 2x4 which was attached to plywood by means of gluing and nailing at various spacing's (Yeh et al., 1971). Figure 2.9 shows the results of the test and provides damping ratio at a function of amplitude of vibration.

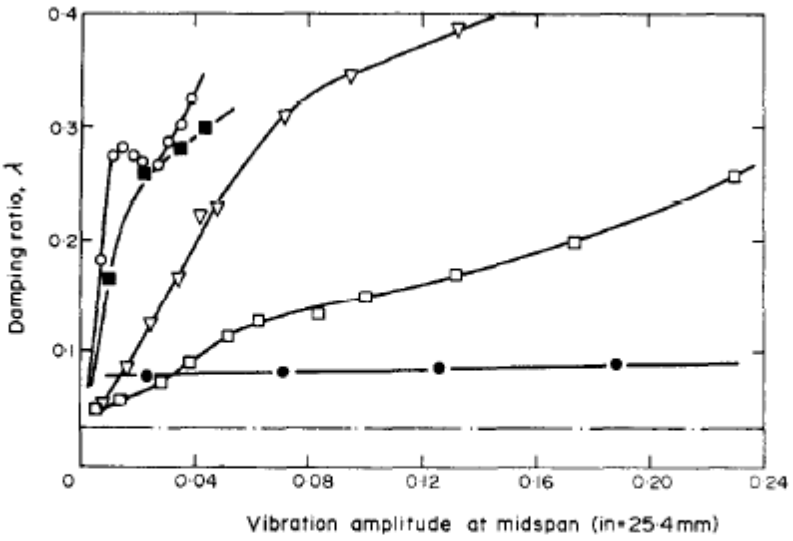

Figure 6. Comparison of damping in beams [T-beams, nailed and glued; solid, 2 in × 4 in (5·08 cm × 10·16 cm)]. 140·84 in (3·577 m) beams: o——o, $C = 72$ in; ■——■, $C = 36$ in. ▽——▽, $C = 18$ in; □——□, $C = 8$ in. Nailed T-beam, ●——●, glued (3M adhesive, $\frac{3}{32}$ in) T-beam: —·—, 2 in × 4 in.

Figure 2.9: Damping ratio as a function of vibration amplitude for wood T-beams with varied connection methods (Yeh et al., 1971)

As these results show, the T-beams which are only nailed or only glued have damping ratios that are effectively independent of amplitude. However the cases where both glue and nails are used provides a varied damping ratio for the range of deflection amplitudes studied; specifically, the larger the nail spacing, the higher the damping ratio and the greater the increase of damping as a function of deflection amplitude. The beam which is only glued exhibits approximately 3-4% damping and the beam which is only nailed exhibits approximately 8% damping. The cases where both gluing and nailing are used have damping ratios varying from 5% to 40% depending on the nail spacing and deflection amplitude. These results show promise that the damping within the timber arches is certainly greater than the 0.5% damping present in timber alone but also that the damping ratio could be well in excess of the assumed 2.5% value used in analyses. Particularly, the connections between the arches and the timber decking fastened with nails could be similar to the nailed only results in that both are using small dowel type connections. Additionally, wood structural panels are commonly placed over the timber decking and nailed to the decking to act as a structural diaphragm.

In an effort to determine the damping of the arch system itself, the availability of research relating to free vibration or dynamic testing of timber arches was investigated. Although not the exact structural system used for the purposes of the project, a report was found outlining studies conducted on a glulam frame. Within this report, pseudo-dynamic (cyclic) testing was done on a Tudor arch with a design as shown in Figure 2.10 (Isoda, 2000).

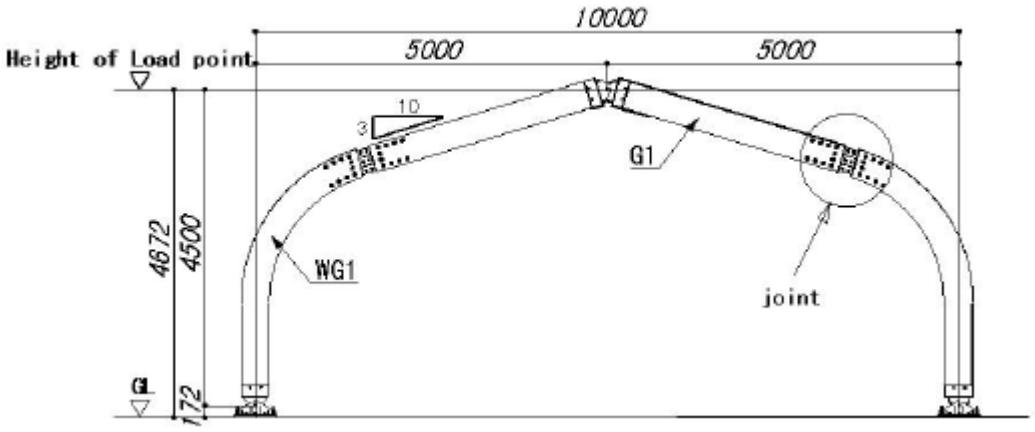

Figure 2.10: Glulam Tudor arch used within cyclic testing in Japan (Isoda, 2000)

Although the overall shape of the arch used in this study is similar to the arches within the scope of this project, the connections within this arch are significantly different. These arches have “true” steel pin connections at the base and peak which could provide some amount of damping; however the joint in the arm is likely to provide a large amount of damping through friction between the steel and timber. For this test, the damping ratio was determined as a function of the displacement amplitude as seen in Figure 2.11 (Isoda, 2000).

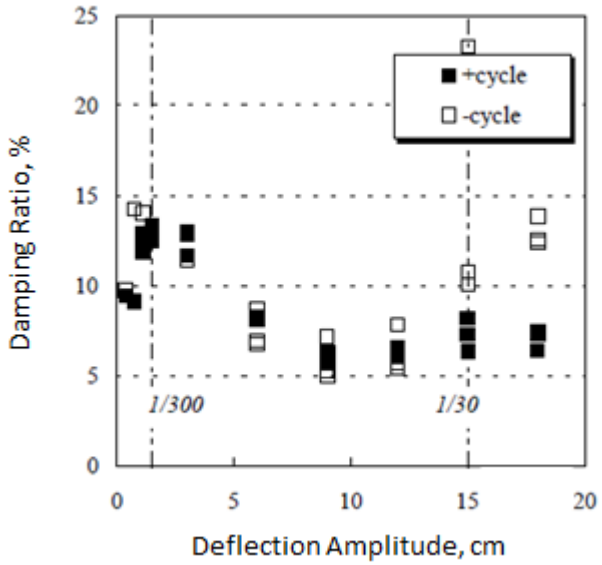

Figure 2.11: Damping results from arch test as a function of displacement amplitude (Isoda, 2000)

As this figure shows, the damping ratio of the given arch varies from 5% to near 15 % depending on the displacement amplitude. Although the connections within this system may vary and provide more damping than the systems being studied within this project, this test included only the arch within testing without any attachments. The connections between the arch and decking and wall will provide additional damping as discussed from the previous study. The results of this study conclude that a constant value 6% damping be used for the system studied (Isoda, 2000). This further supports the idea that a damping ratio greater than the 2.5% of critical used could be applicable.

The final research project referenced for the purposes of this literature review relates to the damping of two single story wood frame structures. Within this project, the damping ratio was determined based upon multiple different earthquakes (Sutoyo and Hall, 2006). Although this structural system is drastically different than the arches within this project, the fundamentals can be related back to the systems of interest for this project. As previously discussed, the damping within timber structures comes mainly from the connections between structural elements. The building investigated within this study involves conventional frame construction where shear walls would be designed to resist the lateral loads. In contrast, the arch is designed to resist the lateral loads for the structural system of this project. The slight similarity between the two systems is that both have some form of sheathing and/ or decking attached to the main structural elements and the connections between those sheathings and the elements are capable of dissipating energy and therefore provide damping to the system. The damping ratios determined for these structures varied depending on the ground motion but the range of values was found to be between 8.9% and 17.2% (Sutoyo and Hall, 2006). Again, although these damping ratios would be expected to be higher than the damping ratios of the arches being analyzed within the context of this project, this provides further evidence that the connections used in timber construction are capable of providing significant amounts of damping.

In conclusion, the damping ratio used for dynamic analyses for this project equal to 2.5% is likely a conservative value based upon the findings of related studies. However, proving that a much higher damping ratio is reasonable for these structures would be difficult without some experimental results relating to an arch similar to those provided for analysis.

2.6 Summary

Based on the review of pertinent literature, several important modeling and evaluation assumptions were determined. It was determined that glulam responds linearly to the point of failure and therefore modeling of the glulam as linear elastic is appropriate. It was also determined that the glulam bending stress limit used as a NSC limit could be increased by a factor of 1.15 times the nominal bending stress capacity determined in accordance with the NDS. The NSC limits for the inward base shear and peak connection shear were determined to be 3 times the nominal value for the base connection and 1.5 times the nominal value for the shear plate capacities for the shear within the peak. It was also determined that a conservative damping ratio for use in dynamic analyses is 2.5% of critical.

Chapter 3 : Arch Designs and Analysis Methodology

3.1 Design Methodology

Designs were provided within the AWC white paper for 56 arches. These designs were conducted and detailed using the methods outlined in *Special Requirements for Seismic Design of Structural Glued Laminated Timber (Glulam) Arch Members and Their Connections in Three-hinge Arch Systems (2009 NEHRP Provisions, Part III Resource Paper).* The AWC white paper also references ASCE 7-10 and the 2012 National Design Specification (NDS) for Wood Construction (AWC, 2013).

The provided designs represent several variations of four typical archetypes as seen in Figure 3.1. The ID numbers, ranging from one to four, define the exterior dimensions of the arches which range in span from 40 ft to 165 ft and range in height from 40 ft to 65 ft.

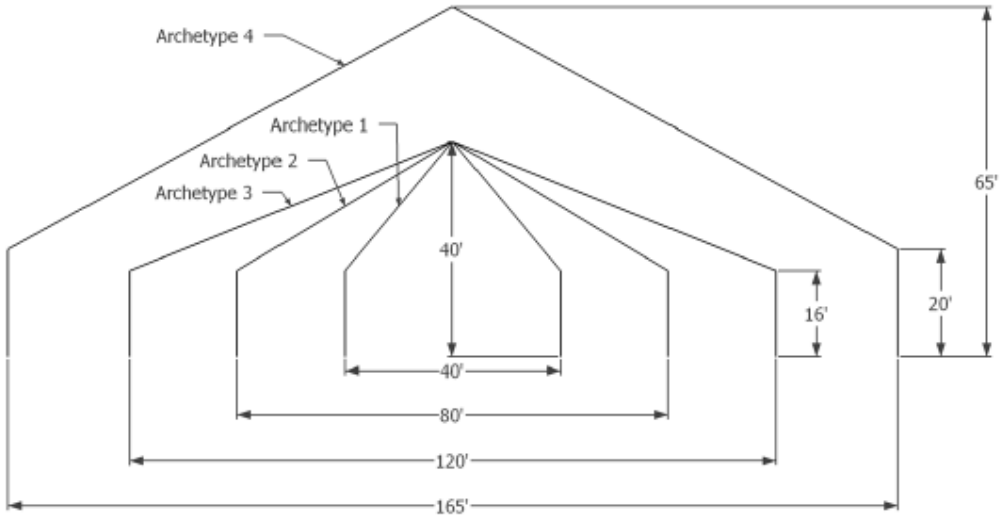

Figure 3.1: Exterior arch dimensions and arch ID numbering convention

Ground motion intensities of Seismic Design Category (SDC) D_{max} were used to determine the seismic demands for the given arches (AWC, 2013). Given SDC D_{max}, Tables 5-1A and 5-1B within FEMA P-695 provide that $S_{DS} = 1.0$ g and $S_{D1} = 0.6$ g. The fundamental period of each of the given arches was determined using Equation 12.8-7 from ASCE 7-10 (ASCE, 2010).

$$T_a = C_t h_n^x \quad (1)$$

where for wood structures with S_{D1} = 0.6 g:

C_t = 0.02

x = 0.75

C_u = 1.4 = coefficient for upper limit on calculated period

h_n = structural height (ft) defined in Section 11.2 as the distance from the base to the average height of the roof for structures with pitched or sloped roofs (ASCE, 2010)

So for the arch designs provided, h_n is equal to:

$$h_n = \frac{H_c + H_w}{2} \quad (2)$$

where:

H_c = height of the structure (ft) measured from the base to outside of crown

H_w = height of wall (ft) measured from base to outside of haunch

The fundamental periods for the provided arch designs ($C_u T_a$) were calculated as the product of the coefficient for upper limit on calculated period, C_u, and the approximate fundamental period, T_a, (ASCE, 2010) for use in the P-695 procedure and are summarized for each archetype in Table 3.1. Note that because the approximate method outlined in ASCE 7-10 is dependent only upon the height of the structure for these arches, the fundamental period for arch ID's 1, 2, and 3 are all the same.

Table 3.1: Summary of wall height, peak height, and fundamental period of vibration for each arch ID

Arch ID	Wall Height [ft]	Peak Height [ft]	$C_u T_a$ [sec]
1L	16	40	0.34
2L	16	40	0.34
3L	16	40	0.34
4L	20	65	0.47
1H	16	40	0.34
2H	16	40	0.34
3H	16	40	0.34
4H	20	65	0.47

The span between arches within a system is equal to 12 ft for all archetypes. This spacing was representative of the typical span which lumber decking could be used to support the roofing (AWC, 2013).

The design loads used to size members (excluding seismic loads) were also provided within the white paper and are summarized in Table 3.2. For purposes of the seismic design, wind and snow loads were neglected.

Table 3.2: Summary of loads used in determination of member and connection demands (AWC, 2013)

Load Type	**Load**	**Description**
Dead Load, Roof	Light: 15 psf Heavy: 30 psf	Light: Lumber decking, panel overlay, roof membrane, and light weight roof covering. Heavy: Same as light except with heavy roof covering such as clay tile.
Dead Load, Wall	Light: 11 psf Heavy: 50 psf	Light: Wood frame wall with interior gypsum board, exterior wood sheathing, cavity insulation and light siding such as vinyl. Heavy: Wood frame wall with heavy veneer.
Roof Live Load	20 psf	Minimum value of roof live load per ASCE 7-10. Balanced and unbalanced roof live load is considered.
Wind Load, Roof	8 psf	Minimum value of roof wind load per ASCE 7-10. Applied to windward side of vertical projection of roof surface.
Wind Load, Wall	16 psf	Minimum value of wall wind load per ASCE 7-10. Applied to windward side of vertical projection of wall surface.
Minimum Integrity	-	Anchorage of structural walls per ASCE 7-10 Section 1.4.5. A horizontal force perpendicular to the plane of the wall equal to 0.2 times the weight of the wall tributary to the connection, but not less than 5 psf.

Designs were provided for two load cases: light and heavy. The light gravity load designs consist of an assumed heavy wall dead load of 50 psf from the previous table in addition to a light roof dead load of 30 psf as defined previously. The heavy gravity load case includes the same heavy wall loads from the light case, but the roof dead loads are increased to a heavy roof load of 30 psf as previously defined (AWC, 2013). This division of designs into heavy and light load cases separates the 4 arch ID's into the eight archetype ID's: 1L, 2L, 3L, 4L, 1H, 2H, 3H, and 4H. Within each of these eight archetype ID's, designs are provided for a range of seismic response modification (*R*) factors including 1.5, 2, 2.5, 3, 4, 5, and a "minimum design" which is sized for minimum loads excluding seismic. Together, these seven designs for each of the eight archetype ID's provide the 56 designs discussed in the subsequent sections.

In addition to designing the arches to resist the applied loads, there were also several other limits applied to the arch designs including deflection limits and arch dimension limits as summarized in Table 3.3 (AWC, 2013).

Table 3.3: Deflection and dimension limits imposed on arch designs (AWC, 2013)

Limit Type	Description
1. Roof live load deflection limits	a. $L_L/180$ for the arm b. $H_w/120$ for lateral deflection at the haunch
2. Arch dimension limits	a. Leg taper angles of 5° or less and arm taper angles of 3° or less b. Tangent point depths limited to a maximum of six times the width c. Tangent point depths in arm and leg portion (i.e. above and below the haunch) are approximately equal d. Depth at the ends, such as the peak and base, are limited to no less than 1.5 times the width

Deflection limits provided are vertical deflections at the peak for deflection limit (a.) and lateral deflections at the haunch for deflection limit (b.), both of which are compared to the deflections resulting from roof live loads. The arch dimension limits are mainly imposed for aesthetic and manufacturing purposes. Additionally, the limit imposed on tangent point depth is applied for stability in accordance with the NDS Section 5.3 (AWC, 2013).

3.1.1 Arch Member Designs

The arch member dimensions were sized for each of the 56 provided designs with the necessary dimensions summarized in Figure 3.2.

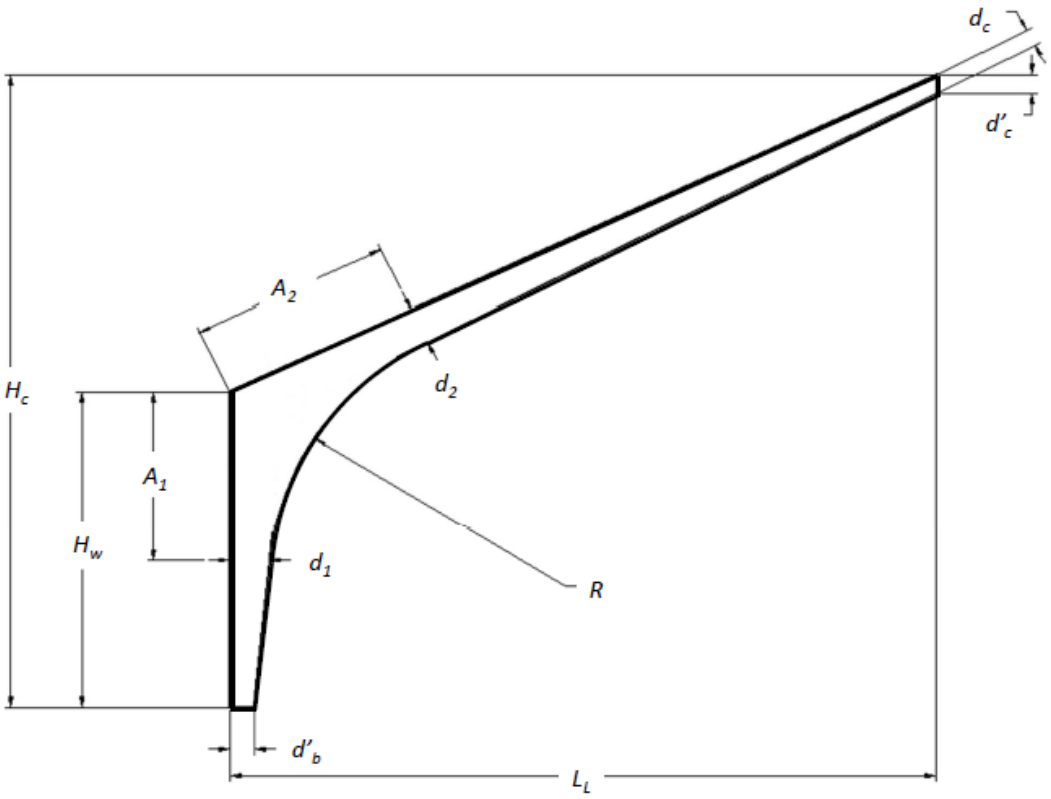

Figure 3.2: Summary of necessary arch dimensions (AWC, 2013)

where:

b = width of arch

d'_c = depth of vertical section at crown

d_c = depth of section at crown measured perpendicular to laminations

d'_b = depth of section at base measured perpendicular to wall

A_1 = vertical distance from haunch to lower tangent

A_2 = distance from haunch to upper tangent measured along roof

d_1 = depth of lower tangent point measured perpendicular to wall

d_2 = depth of upper tangent point measured perpendicular to roof

H_c = height of roof at crown

H_w = height of wall

L_L = span of arch segment

R = radius of curved face of arch segment

It is important to note that, for ease of shipping, some manufacturers provide splices within the arm section of the arch that is the section that extends from the haunch to the peak. Although a splice may be present within the arm, it was suggested that the entire half-span of the arch be modeled as continuous, assuming that the splice would be capable of transferring applied forces across the connection adequately. Another note on arch construction is that some manufacturers form the arch as one whole member and "overbuild" the outside of the haunch section, which would be trimmed to form the straight sections after the adhesive has set. Other manufacturers may, however, form the arch member such that the section depth between the arm and leg tangent points is equal to the greater of the depths at those two points. Following the setting of the adhesive, a "cap" would then be attached to the outside of the haunch to provide the geometry shown above. It was also suggested that this "cap" be assumed integral with the arch member and therefore the material was modeled continuously throughout this region. The necessary dimensions are provided in Tables 3.4 and 3.5 for each of the 56 arch designs. Note that the designs shown in red italic have the same member dimensions as the design with the next lower R-value. This occurs when the design of the arch is controlled by minimum loads applied to the structure rather than the seismic lateral loads. In this case, the arch designs are not dependent on the design R-value so several of the design R-values can have the same arch dimensions. For the larger arches, the large spans cause the gravity loads to drive the sizing requirements for the arch members rather than seismic loads.

Table 3.4: Arch dimensions for low gravity load level designs (AWC, 2013)

Arch ID	R	b [in]	d'_b [in]	d_c [in]	d'_c [in]	d_1 [in]	d_2 [in]	A_1 [in]	A_2 [in]	R [in]
1L	1.5	5.125	24	23.71	37	35.82	35.22	63.73	68.48	180
	2	5.125	18	16.66	26	29.19	29.53	60.2	67.55	180
	2.5	5.125	14	16.66	26	27.29	25.34	62.34	64.48	180
	3	5.125	12	12.81	20	23.59	23.12	59.22	65.45	180
	4	5.125	10	8.33	13	19.32	19.23	60.06	64.88	180
	5	5.125	9.5	8.01	12.5	16.36	16.58	61.3	66.08	180
	Min.	5.125	8	7.68	12	11.33	11.34	64.61	67	180
2L	1.5	6.75	23	16.3	19	33.47	33.07	76.85	81.55	120
	2	6.75	20	14.15	16.5	28.15	27.68	76.31	79.5	120
	2.5	6.75	18	12.87	15	25.26	25.15	75.07	78.74	120
	3	6.75	17	11.37	13.25	23.78	24.22	73.91	78.54	120
	4	*6.75*	*17*	*11.37*	*13.25*	*23.78*	*24.22*	*73.91*	*78.54*	*120*
	5	*6.75*	*17*	*11.37*	*13.25*	*23.78*	*24.22*	*73.91*	*78.54*	*120*
	Min.	*6.75*	*17*	*11.37*	*13.25*	*23.78*	*24.22*	*73.91*	*78.54*	*120*
3L	1.5	8.75	28	18.57	20	33.7	33.83	96.74	101.24	120
	2	*8.75*	*28*	*18.57*	*20*	*33.7*	*33.83*	*96.74*	*101.24*	*120*
	2.5	*8.75*	*28*	*18.57*	*20*	*33.7*	*33.83*	*96.74*	*101.24*	*120*
	3	*8.75*	*28*	*18.57*	*20*	*33.7*	*33.83*	*96.74*	*101.24*	*120*
	4	*8.75*	*28*	*18.57*	*20*	*33.7*	*33.83*	*96.74*	*101.24*	*120*
	5	*8.75*	*28*	*18.57*	*20*	*33.7*	*33.83*	*96.74*	*101.24*	*120*
	Min.	*8.75*	*28*	*18.57*	*20*	*33.7*	*33.83*	*96.74*	*101.24*	*120*
4L	1.5	8.75	39	19.73	23	51.03	52.5	85.69	94.08	120
	2	*8.75*	*39*	*19.73*	*23*	*51.03*	*52.5*	*85.69*	*94.08*	*120*
	2.5	*8.75*	*39*	*19.73*	*23*	*51.03*	*52.5*	*85.69*	*94.08*	*120*
	3	*8.75*	*39*	*19.73*	*23*	*51.03*	*52.5*	*85.69*	*94.08*	*120*
	4	*8.75*	*39*	*19.73*	*23*	*51.03*	*52.5*	*85.69*	*94.08*	*120*
	5	*8.75*	*39*	*19.73*	*23*	*51.03*	*52.5*	*85.69*	*94.08*	*120*
	Min.	*8.75*	*39*	*19.73*	*23*	*51.03*	*52.5*	*85.69*	*94.08*	*120*

Note: Red italic values denote a design with dimensions equal to the design with the next lower R-value.

Table 3.5: Arch dimensions for high gravity load level designs (AWC, 2013)

Arch ID	R	b [in]	d'_b [in]	d_c [in]	d'_c [in]	d_1 [in]	d_2 [in]	A_1 [in]	A_2 [in]	R [in]
1H	1.5	6.75	27	26.91	42	38.82	38.12	64.93	69.41	180
	2	6.75	21	20.5	32	30.79	30.94	62.77	69.28	180
	2.5	6.75	17	16.65	26	26.69	26.26	62.86	67.29	180
	3	5.125	19	17.94	28	27.87	28.03	62.86	68.68	180
	4	5.125	16	15.37	24	23.4	23.67	62.92	68.82	180
	5	5.125	14	14.09	22	21.17	21.21	62.98	68.13	180
	Min.	5.125	10	10.24	16	13.85	13.53	65.6	67.39	180
2H	1.5	6.75	32	21.46	25	42.41	41.62	82.1	85.13	120
	2	6.75	28	18.88	22	37.52	37.46	79.33	83.87	120
	2.5	6.75	25	17.16	20	34.28	33.95	78.27	82.18	120
	3	6.75	23	16.3	19	32.7	31.1	78.94	80.09	120
	4	6.75	21	16.3	19	28.85	29.41	76.89	80.29	120
	5	*6.75*	*21*	*16.3*	*19*	*28.85*	*29.41*	*76.89*	*80.29*	*120*
	Min.	*6.75*	*21*	*16.3*	*19*	*28.85*	*29.41*	*76.89*	*80.29*	*120*
3H	1.5	8.75	35	25.08	27	43.48	43	100.6	106.34	120
	2	8.75	34	25.08	27	41.19	41.26	99.8	105.89	120
	2.5	*8.75*	*34*	*25.08*	*27*	*41.19*	*41.26*	*99.8*	*105.89*	*120*
	3	*8.75*	*34*	*25.08*	*27*	*41.19*	*41.26*	*99.8*	*105.89*	*120*
	4	*8.75*	*34*	*25.08*	*27*	*41.19*	*41.26*	*99.8*	*105.89*	*120*
	5	*8.75*	*34*	*25.08*	*27*	*41.19*	*41.26*	*99.8*	*105.89*	*120*
	Min.	*8.75*	*34*	*25.08*	*27*	*41.19*	*41.26*	*99.8*	*105.89*	*120*
4H	1.5	10.75	42	20.59	24	55.15	55.22	88.85	94.37	120
	2	10.75	38	20.59	24	51.93	51.35	87.43	92.19	120
	2.5	*10.75*	*38*	*20.59*	*24*	*51.93*	*51.35*	*87.43*	*92.19*	*120*
	3	*10.75*	*38*	*20.59*	*24*	*51.93*	*51.35*	*87.43*	*92.19*	*120*
	4	*10.75*	*38*	*20.59*	*24*	*51.93*	*51.35*	*87.43*	*92.19*	*120*
	5	*10.75*	*38*	*20.59*	*24*	*51.93*	*51.35*	*87.43*	*92.19*	*120*
	Min.	*10.75*	*38*	*20.59*	*24*	*51.93*	*51.35*	*87.43*	*92.19*	*120*

Note: Red italic values denote a design with dimensions equal to the design with the next lower R-value.

As these tables show, a conscience effort was made to attempt to keep the depth of the arch designs the same for each arch ID within the light and heavy gravity load designs. The radius around the inside of the arch haunch was also kept the same for each arch ID with only radiuses of 120 in. and 180 in. used. These values are the same for all design R-values because this radius was designed with a large amount of conservatism during the design process. This was to ensure that failure would not occur due to radial tension stresses within the haunch, but rather failure would be driven to one of the other modes discussed within this report.

3.1.2 Arch Connection Designs

Also provided within the white paper were the designed connection capacities. At the base connection, capacity values were provided for the strength of the connection when subjected to inward or outward shear. The steel arch shoe was designed such that applied outward shear would not cause any yielding or other failure of the shoe back, but rather failure would result from the glulam member shear at the base. Design to resist shear induced toward the inside of the arch is resisted by the bolted connection within the shoe. This connection is forced through design to experience significant yielding of the bolt prior to shear failure of the glulam or failure of the shoe material (AWC, 2013). Figure 2.5 provides the relevant dimensions of the base connections.

The capacities of the base connections are summarized within the following tables for both low gravity and high gravity designs. The dimensions of the base connection are also summarized for each arch design. Again, values in red italic represent designs which are the same, with respect to both dimensions and capacities, as the design for the next higher R-value.

Table 3.6: Shoe connection dimensions and capacities for low gravity load designs (AWC, 2013)

									Inward loading		Outward loading
		Bolt Diameter	No. of bolts	Bolt Spacing	x_h	y_h	H_{shoe}	t_{shoe}	Connector Strength (ϕ = 1.0)	Notch Shear Strength (ϕ = 1.0)	Shear Strength (ϕ = 1.0)
Arch ID	R	[in]		[in]	[in]	[in]	[in]	[in]	[lbs]	[lbs]	[lbs]
1L	1.5	0.813	2	3.25	18.25	6.5	9	0.625	13825	18906	46100
	2	0.625	2	2.5	14.25	6.5	9	0.625	11699	15758	34840
	2.5	1	1	-	10.5	6.5	9	0.625	7657	10242	27333
	3	0.688	1	-	8.75	6.5	9	0.625	6317	8639	22641
	4	0.625	1	-	7.75	6.5	9	0.625	5850	7986	19589
	5	0.625	1	-	7.5	6.5	9	0.625	5850	8140	18444
	Min.	0.625	1	-	3.75	6.5	9	0.625	5850	1478	15280
2L	1.5	1.25	1	-	15	6.5	9	0.625	11205	15024	58246
	2	0.688	1	-	11.75	6.5	9	0.625	6954	9592	50417
	2.5	0.625	1	-	10.25	6.5	9	0.625	5850	7851	45383
	3	0.625	1	-	10	6.5	9	0.625	5850	8152	42916
	4	*0.625*	*1*	*-*	*10*	*6.5*	*9*	*0.625*	*5850*	*8152*	*42916*
	5	*0.625*	*1*	*-*	*10*	*6.5*	*9*	*0.625*	*5850*	*8152*	*42916*
	Min.	0.625	1	-	5.5	6.5	9	0.625	5850	1356	42916
3L	1.5	0.625	1	-	12.75	6.5	9	1.125	5850	8220	90809
	2	*0.625*	*1*	*-*	*12.75*	*6.5*	*9*	*1.125*	*5850*	*8220*	*90809*
	2.5	*0.625*	*1*	*-*	*12.75*	*6.5*	*9*	*1.125*	*5850*	*8220*	*90809*
	3	*0.625*	*1*	*-*	*12.75*	*6.5*	*9*	*1.125*	*5850*	*8220*	*90809*
	4	*0.625*	*1*	*-*	*12.75*	*6.5*	*9*	*1.125*	*5850*	*8220*	*90809*
	5	*0.625*	*1*	*-*	*12.75*	*6.5*	*9*	*1.125*	*5850*	*8220*	*90809*
	Min.	0.625	1	-	7	6.5	9	1.125	5850	1360	90809
4L	1.5	1.25	1	-	21.25	6.5	9	1.125	14525	19642	126770
	2	0.625	1	-	15.75	6.5	9	1.125	5850	7998	126770
	2.5	*0.625*	*1*	*-*	*15.75*	*6.5*	*9*	*1.125*	*5850*	*7998*	*126770*
	3	*0.625*	*1*	*-*	*15.75*	*6.5*	*9*	*1.125*	*5850*	*7998*	*126770*
	4	*0.625*	*1*	*-*	*15.75*	*6.5*	*9*	*1.125*	*5850*	*7998*	*126770*
	5	*0.625*	*1*	*-*	*15.75*	*6.5*	*9*	*1.125*	*5850*	*7998*	*126770*
	Min.	0.625	1	-	9.25	6.5	9	1.125	5850	1620	126770

Note: Red italic values denote a design with dimensions equal to the design with the next lower R-value.

Table 3.7: Shoe connection dimensions and capacities for high gravity load level (AWC, 2013)

									Inward loading		Outward loading
		Bolt Diameter	No. of bolts	Bolt Spacing	x_h	y_h	H_{shoe}	t_{shoe}	Connector Strength (ϕ = 1.0)	Notch Shear Strength (ϕ = 1.0)	Shear Strength (ϕ = 1.0)
Arch ID	R	[in]		[in]	[in]	[in]	[in]	[in]	[lbs]	[lbs]	[lbs]
1H	1.5	0.813	2	3.25	21.75	6.5	9	0.625	17713	33474	68133
	2	0.688	2	2.75	17	6.5	9	0.625	13909	26839	52331
	2.5	0.625	2	2.5	14	6.5	9	0.625	11699	22213	43112
	3	1	1	-	14.25	6.5	9	0.625	7657	14332	36456
	4	0.625	1	-	11.75	6.5	9	0.625	5850	11318	30687
	5	0.625	1	-	10.75	6.5	9	0.625	5850	11278	26893
	Min.	0.625	1	-	4.25	6.5	9	0.625	5850	1385	19042
2H	1.5	1.25	1	-	20.75	6.5	9	0.625	11205	20825	80492
	2	0.688	1	-	16.25	6.5	9	0.625	6954	13016	70528
	2.5	0.625	1	-	14.25	6.5	9	0.625	5850	10985	63005
	3	0.625	1	-	13.5	6.5	9	0.625	5850	11033	57924
	4	0.625	1	-	12.75	6.5	9	0.625	5850	11128	52918
	5	*0.625*	*1*	*-*	*12.75*	*6.5*	*9*	*0.625*	*5850*	*11128*	*52918*
	Min.	0.625	1	-	6.25	6.5	9	0.625	5850	1311	52918
3H	1.5	0.625	1	-	16.25	6.5	9	1.125	5850	10871	113954
	2	0.625	1	-	16	6.5	9	1.125	5850	11013	110490
	2.5	*0.625*	*1*	*-*	*16*	*6.5*	*9*	*1.125*	*5850*	*11013*	*110490*
	3	*0.625*	*1*	*-*	*16*	*6.5*	*9*	*1.125*	*5850*	*11013*	*110490*
	4	*0.625*	*1*	*-*	*16*	*6.5*	*9*	*1.125*	*5850*	*11013*	*110490*
	5	*0.625*	*1*	*-*	*16*	*6.5*	*9*	*1.125*	*5850*	*11013*	*110490*
	Min.	0.625	1	-	8	6.5	9	1.125	5850	1377	110490
4H	1.5	1.25	1	-	24	6.5	9	1.125	16097	30038	167556
	2	0.625	1	-	16	6.5	9	1.125	5850	10842	151810
	2.5	*0.625*	*1*	*-*	*16*	*6.5*	*9*	*1.125*	*5850*	*10842*	*151810*
	3	*0.625*	*1*	*-*	*16*	*6.5*	*9*	*1.125*	*5850*	*10842*	*151810*
	4	*0.625*	*1*	*-*	*16*	*6.5*	*9*	*1.125*	*5850*	*10842*	*151810*
	5	*0.625*	*1*	*-*	*16*	*6.5*	*9*	*1.125*	*5850*	*10842*	*151810*
	Min.	0.625	1	-	8.5	6.5	9	1.125	5850	1626	151810

Note: Red italic values denote a design with dimensions equal to the design with the next lower R-value.

The other connection present within the arch is located at the peak. This connection is comprised of shear plate connectors which act to carry shear induced due to lateral loads across the peak. Shear plate connectors have been used for decades as a way of transferring shear forces which are larger than a

typical bolted connection is capable of resisting. Figure 3.3 shows 4 inch shear plates which are made of cast iron.

Figure 3.3: 4 inch shear plate connectors used in arch peak connections (Portland Bolt & Manufacturing Company, 2012b)

Shear plates are used in timber construction by cutting grooves into the timber members using a "dapping tool". This tool cuts the necessary profile into the members which allows the shear plate to be recessed into the member with the flat face of the shear plate being flush with the connection plane. Figure 3.4 shows the profile cut into the member by the dapping tool (left) and the dapping tool above the member with the shear plate placed into the grooves made by the tool (right).

Figure 3.4: Grooves created by the dapping tool to accept the shear plate (left) and dapping tool above the shear plate which has been placed into the grooves cut by the tool (Portland Bolt & Manufacturing Company, 2012a)

Once the grooves have been cut into the members on each side of the connection, the shear plates can be placed into the grooves and the connection can be made. Because the geometry of such a connection creates two flat surfaces for connecting, some sort of a dowel connector is necessary to transfer the shear forces across the connection. This can be done with one of two connectors, the first being bolts which can be seen in the Figure 3.5 which shows a cut away of an assembled connection utilizing a bolted shear plate connection.

Figure 3.5: Cut away of an assembled bolted shear plate connection placed in member side grain (Portland Bolt & Manufacturing Company, 2012)

The benefit of using bolts as the dowel connector is that in addition to providing a path for shear to be transferred between structural elements, the bolt also prevents the connected members from pulling apart in a direction perpendicular to the shear plane. The other connector which can be used to transfer shear forces across the shear plane is a steel dowel. Steel dowels provide the same shear capacity as the bolts but with the downside that they are unable to prevent the connection from separating. Although dowels present this issue, they are typically what are used within the connection at the peaks of the arches being analyzed. This is because the angles associated with the peak connections are connecting the arch elements near perpendicular to grain and therefore bolts would have to be very long to extend out of the arch member on either side. To avoid this issue, dowels are commonly used which can be located on the inside of the member and do not have to protrude through the elements. This can be seen in Figure 2.7 which shows a typical peak connection utilizing shear plate connectors and dowels.

To prevent the connection from separating perpendicular to the shear plane when dowels are used, steel plates are commonly used. Within this connection, steel plates which are 0.25” thick are placed on both sides of the arch and bolted to prevent this connection from separating. The detail of this connection can be seen in Figure 3.6.

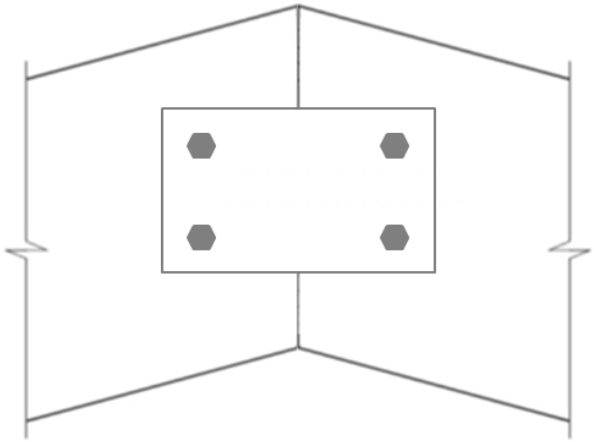

Figure 3.6: Detail of steel plates which prevent the connection from separating

Tables 3.8 and 3.9 below show a summary of the connection dimensions and LRFD capacities of the connections including applicable resistance factors. Within these tables, the values in red italic denote that the design is the same as the design with the next highest design R-value.

Table 3.8: Peak shear connection capacity summary for light gravity load level (AWC, 2013)

Arch ID	R	Angle of Load to Grain	Edge Distance	Overstrength Load Combinations			Basic Load Combinations			Notch Shear Strength at Peak, lb
				n	Spacing	Design Strength, lb	*n*	Spacing	Design Strength, lb	
		[Degrees]	[in.]		[in.]	[ϕ=0.65]		[in.]	[ϕ=0.65]	[ϕ=1.0]
1L	1.5	37.3	5.25	4	8.83	22060	2	26.5	11844	32901
	2	37.3	5.25	3	7.75	17230	2	15.5	11844	20186
	2.5	37.7	5.25	2	15.5	11770	2	15.5	11770	20186
	3	37.7	4.75	2	10.5	11770	2	10.5	11770	14708
	4	37.7	3.75	2	5.5	7470	2	5.5	7470	9435
	5	38.2	3.5	2	5.5	7430	2	5.5	7430	9525
	Min.	31.1	3.5	2	5	6060	2	5	6060	8948
2L	1.5	56.9	4.25	2	10.5	9530	2	10.5	9530	26287
	2	57.3	4.25	2	8	9490	2	8	9490	21284
	2.5	57.5	3.5	2	8	8630	2	8	8630	21843
	3	57.5	3.5	2	6.25	8560	2	6.25	8560	18305
	4	*57.5*	*3.5*	*2*	*6.25*	*8560*	*2*	*6.25*	*8560*	*18305*
	5	*57.5*	*3.5*	*2*	*6.25*	*8560*	*2*	*6.25*	*8560*	*18305*
	Min.	*57.5*	*3.5*	*2*	*6.25*	*8560*	*2*	*6.25*	*8560*	*18305*
3L	1.5	66.9	4	3	6	11260	3	6	11260	41436
	2	*66.9*	*4*	*3*	*6*	*11260*	*3*	*6*	*11260*	*41436*
	2.5	*66.9*	*4*	*3*	*6*	*11260*	*3*	*6*	*11260*	*41436*
	3	*66.9*	*4*	*3*	*6*	*11260*	*3*	*6*	*11260*	*41436*
	4	*66.9*	*4*	*3*	*6*	*11260*	*3*	*6*	*11260*	*41436*
	5	*66.9*	*4*	*3*	*6*	*11260*	*3*	*6*	*11260*	*41436*
	Min.	*66.9*	*4*	*3*	*6*	*11260*	*3*	*6*	*11260*	*41436*
4L	1.5	57.1	4.25	3	7.25	13870	3	7.25	13870	44593
	2	*57.1*	*4.25*	*3*	*7.25*	*13870*	*3*	*7.25*	*13870*	*44593*
	2.5	*57.1*	*4.25*	*3*	*7.25*	*13870*	*3*	*7.25*	*13870*	*44593*
	3	*57.1*	*4.25*	*3*	*7.25*	*13870*	*3*	*7.25*	*13870*	*44593*
	4	*57.1*	*4.25*	*3*	*7.25*	*13870*	*3*	*7.25*	*13870*	*44593*
	5	*57.1*	*4.25*	*3*	*7.25*	*13870*	*3*	*7.25*	*13870*	*44593*
	Min.	*57.1*	*4.25*	*3*	*7.25*	*13870*	*3*	*7.25*	*13870*	*44593*

Note: Red italic values denote a design with dimensions equal to the design with the next lower R-value.

Table 3.9: Peak shear connection capacity summary for heavy gravity load level (AWC, 2013)

Arch ID	R	Angle of Load to Grain	Edge Dist.	Overstrength Load Combinations			Basic Load Combinations			Notch Shear Strength at Peak, lb
				n	Spacing	Design Strength, lb	*n*	Spacing	Design Strength, lb	
		[Degrees]	[in.]		[in.]	[ϕ=0.65]		[in.]	[ϕ=0.65]	[ϕ=1.0]
1H	1.5	37.3	3.75	6	6.875	28510	3	17.2	15484	57026
	2	37.3	4.75	4	7.5	22700	2	22.5	11993	37571
	2.5	37.7	5	3	8	18030	2	16	12325	27466
	3	37.7	5	3	9	17050	2	18	11753	23164
	4	37.7	5	2	14	11680	2	14	11680	18571
	5	38.2	5	2	12	11650	2	12	11650	16308
	Min	31.1	3.5	2	9	10141	2	9	10141	13525
2H	1.5	56.9	4.25	3	8.25	13860	2	16.5	9240	38523
	2	57.3	4.25	3	6.75	13840	2	13.5	9230	32374
	2.5	57.5	3.5	3	6.5	12550	2	13	8370	32105
	3	57	3.25	3	6.25	12100	2	12.5	8070	31362
	4	57.5	3.5	3	6.25	12060	2	12.5	8040	31362
	5	*57.5*	*3.5*	*3*	*6.25*	*12060*	*2*	*12.5*	*8040*	*31362*
	Min	*57.5*	*3.5*	*3*	*6.25*	*12060*	*2*	*12.5*	*8040*	*31362*
3H	1.5	66.9	4	4	6.5	15720	4	6.5	15720	63551
	2	*66.9*	*4*	*4*	*6.5*	*15720*	*4*	*6.5*	*15720*	*63551*
	2.5	*66.9*	*4*	*4*	*6.5*	*15720*	*4*	*6.5*	*15720*	*63551*
	3	*66.9*	*4*	*4*	*6.5*	*15720*	*4*	*6.5*	*15720*	*63551*
	4	*66.9*	*4*	*4*	*6.5*	*15720*	*4*	*6.5*	*15720*	*63551*
	5	*66.9*	*4*	*4*	*6.5*	*15720*	*4*	*6.5*	*15720*	*63551*
	Min	*66.9*	*4*	*4*	*6.5*	*15720*	*4*	*6.5*	*15720*	*63551*
4H	1.5	57.1	4.25	3 × 2	7.75	27350	2 × 2	15.5	18230	58050
	2	57.1	4.25	3 × 2	7.75	27290	2 × 2	15.5	18190	58050
	2.5	*57.1*	*4.25*	*3 × 2*	*7.75*	*27290*	*2 × 2*	*15.5*	*18190*	*58050*
	3	*57.1*	*4.25*	*3 × 2*	*7.75*	*27290*	*2 × 2*	*15.5*	*18190*	*58050*
	4	*57.1*	*4.25*	*3 × 2*	*7.75*	*27290*	*2 × 2*	*15.5*	*18190*	*58050*
	5	*57.1*	*4.25*	*3 × 2*	*7.75*	*27290*	*2 × 2*	*15.5*	*18190*	*58050*
	Min	*57.1*	*4.25*	*3 × 2*	*7.75*	*27290*	*2 × 2*	*15.5*	*18190*	*58050*

Note: Red italic values denote a design with dimensions equal to the design with the next lower R-value.

3.2 FEMA Technical Document P-695

Technical document P-695 titled *Quantification of Building Seismic Performance Factors* was published by the Federal Emergency Management Agency (FEMA) in June of 2009. This document uses the research completed for the Applied Technology Council's (ATC) project ATC-63 along with other

nonlinear response and collapse simulation research, and other applicable seismic evaluations to present a methodology which allows building system performance and response parameters to be determined for use in seismic design. The main factor of interest which P-695 provides methodology for determining is the seismic response modification coefficient, also known as an R-factor or R-value. Although ASCE 7-10 provides R-values for 83 different systems within Table 12.2-1 (ASCE, 2010), there are numerous remaining structural systems in use today which require seismic designs. To allow for a simplified method for calculating the seismic design, it is advantageous to determine an R-value for a system which is not currently included within ASCE 7-10 Table 12.2-1. By using the methodology outlined in P-695, an R-value can be determined for a given structural system.

The methodology outlined in P-695 is consistent with NEHRP Recommended Provisions and ASCE 7-10 provisions in that it addresses the primary "life safety" performance objective for the given structure. To address the life safety performance objective, this methodology works to provide protection of the structural system from collapse. By limiting the probability of collapse to an acceptable value, it is assumed that fatal injuries and death will in turn be limited. The methodology assesses only structural components included within the lateral force resisting system and therefore does not address the non-structural components nor does it address the gravity system. When determining the probability of collapse for a given structure, the methodology does so in reference to the Maximum Considered Earthquake (MCE) ground motion intensity level (FEMA, 2009b).

The general process for determining an R-value for a new structural system is outlined in Figure 3.7. These steps are described in detail throughout the methodology of P-695.

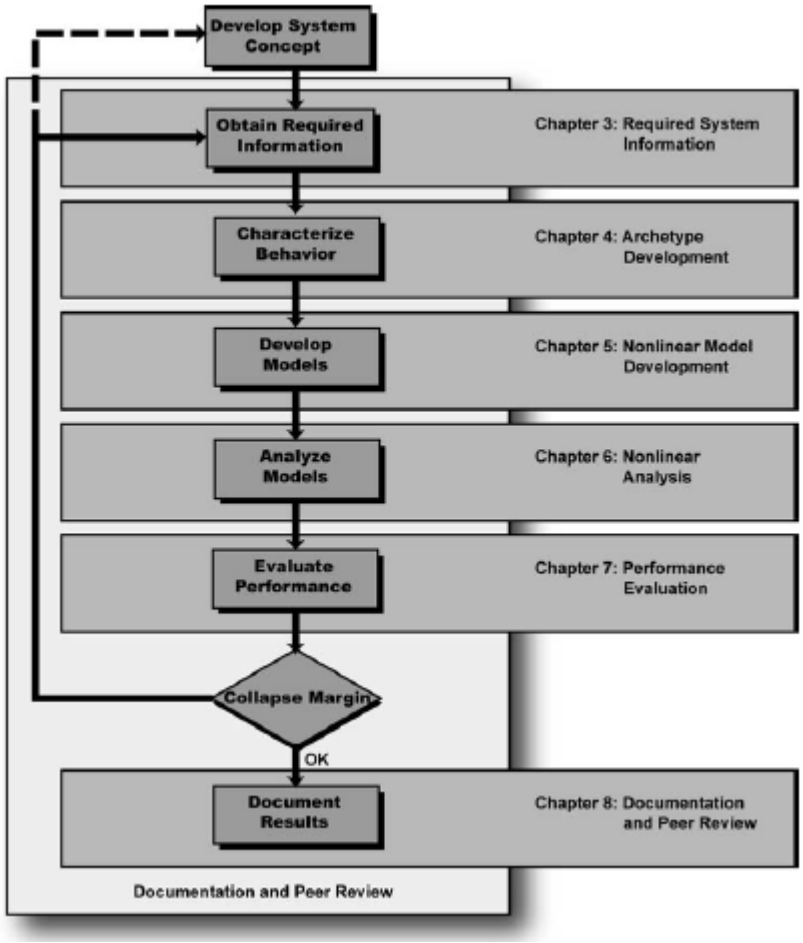

Figure 3.7: Flow chart defining the general steps required for a P-695 analysis (FEMA, 2009b)

The first step within the process of developing a system concept has already been completed for this project as three-hinge glulam Tudor arches have been used as structures for several decades. As previously discussed, the reason for evaluating this set of structures which have previously established concepts is to determine an R-value for SDC D_{max}, as one has not previously been assigned for this SDC. A white paper within FEMA P-750 includes R-values for SDC A, B, and C (FEMA, 2009a).

The next step involves obtaining required information about the structural system of interest. This general structure information includes a comprehensive description of the purposed system, a complete set of design requirements and specifications, and test data and other supporting evidence (FEMA, 2009b). For the purposes of this project, much of this information was provided within the previously discussed AWC white paper.

The third step within the process involves characterizing the behavior of the system. In particular, this part of the process involves the development of archetypes within the structural system (FEMA, 2009b). As previously discussed, the archetypes were defined for four exterior arch dimensions associated with arch ID's 1-4 and further separated into heavy and light gravity load cases. This provides the eight index archetypes which are to be used within this P-695 evaluation. The last part of this step involves defining the performance groups to be evaluated later. The performance groups are generally divided according

to the index archetypes, and then further divided into high or low gravity load level, then if applicable these can be further divided based upon seismic design category and period domain. The main rule to consider when creating these archetypes is that each should contain a minimum of three index models (FEMA, 2009b).

After the behavior has been characterized, the models can next be developed. This involves designing models for a range of assumed design R-values for each index archetype. These designs were created and outlined within the AWC white paper as previously discussed. Using the designs, computational models must then be created which accurately model the behavior of the designed structural system.

Once the computational models have been created, the models must be analyzed. The first step in analyzing the models is to apply the gravity loads. The methodology within P-695 defines the gravity load to be applied to the structure in Equation 6-1 (FEMA, 2009b) as:

$$1.05D + 0.25L \tag{3}$$

where:

D = nominal dead load of the structure plus the superimposed dead load

L = nominal live load

Once the gravity loads have been applied to the structure, static pushover or nonlinear dynamic analyses can then be conducted. The ground motions used for dynamic analyses are defined within the P-695 with 2 sets to choose from. These sets include the near field set which includes 28 component pairs (56 records) which were taken from recording sites stations no more than 10 kilometers from the earthquake epicenter, and the far field set which includes 22 component pairs (44 records) which were taken from recording stations at least 10 kilometers from the earthquake epicenter (FEMA, 2009b). The far field set is applicable to this project and was used for all dynamic analyses. The ground motion records are scaled to the MCE level shaking based upon P-695 requirements. This scaling involves two components, the first of which is the anchoring scale factor which is the same for each ground motion within a set. The anchoring scale factor ensures that the median spectral acceleration of the record set matches the spectral acceleration at the fundamental period of the index archetype (FEMA 2009). The second factor applied is the normalization scaling factor which varied for each component pair. This factor is intended to remove variability between records due to several site, event, and distance differences without eliminating record-to-record variability (FEMA 2009).

The first sets of analyses to be conducted in a P-695 evaluation are nonlinear static pushover analyses. These analyses provide a pushover curve of roof displacement vs. base shear and allow two important factors to be determined. These values include the static overstrength of the system and the period-based ductility. These values are necessary when determining the record-to-record uncertainty and spectral shape factor as discussed later.

Once the static pushover analyses have been conducted, the nonlinear response history analyses can be conducted. To perform the nonlinear dynamic analyses, the previously defined dead loads are applied to the structure and then the scaled ground motions are used to conduct dynamic analyses. These analyses

are done at a range of scale factors applied to the factored ground motions to create what is known as an Incremental Dynamic Analysis (IDA). By conducting the IDA, a Collapse Margin Ratio (CMR) can then be determined.

When evaluating the safety associated with a given structure, this methodology defines a value known as the CMR. This value is defined as the ratio of the median 5% damped spectral acceleration of the collapse level ground motions to the 5% damped spectral acceleration of the MCE ground motions at the fundamental period of the seismic-force resisting system as shown below (FEMA 2009).

$$CMR = \frac{\hat{S}_{CT}}{S_{MT}} \tag{4}$$

For practical applications, determining the CMR involves scaling all ground motions to the MCE level and then incrementing the scale factor applied to the scaled ground motions. As the scale factor is increased, failure will be observed within the structural model for some of the ground motions. The first scale factor at which 50% of the ground motions within the set cause collapse is taken as the CMR. When conducting analyses on structural models with large amounts of non-linearity, several sets of incremental dynamic analyses will have to be conducted to obtain a precise CMR.

The final major step within the process involves evaluating the performance groups. Once the CMR values have been determined for each index model, the Adjusted Collapse Margin Ratio (ACMR) can next be determined. This is done by multiplying the CMR by a Spectral Shape Factor (SSF) as given in Equation 7-1 of P-695 (FEMA, 2009b):

$$ACMR_i = SSF_i \times CMR_i \tag{5}$$

Within this equation, the subscript i simply denotes that the ACMR will be evaluated for each index model. The spectral shape factor is determined from Table 7-1a or 7-1b of P-695 and is a function of both the fundamental period of the structure as well as the period-based ductility, which is determined from the nonlinear pushover analyses.

Once the ACMR values have been determined, it is necessary to determine what values of ACMR are acceptable. To determine this, all of the sources of uncertainty within the P-695 evaluation need to be determined. The sources of uncertainty include record-to-record uncertainty, design requirements uncertainty, test data uncertainty, and modeling uncertainty. The record-to-record uncertainty results from the wide range of variability of response of the index models to the various ground motion records within the given set. The record to record uncertainty is a function of the period based ductility and is given by P-695 Equation 7-2 (FEMA, 2009b):

$$\beta_{RTR} = 0.1 + 0.1\mu_T \leq 0.40 \tag{6}$$

The design requirement uncertainty, β_{DR}, is related to robustness of the design requirements used for the structural system and also relates to how well the requirements prevent unanticipated failures. The test data uncertainty, β_{TD}, relates to the certainty of the test data used within the structural model as well as the applicability of the test data to the structural system of interest. The modeling uncertainty, β_{MDL}, is related to the certainty that the model is capable of capturing the true behavior of the structural

system of interest as well as the ability of the model to capture failure modes within the lateral force resisting system (FEMA 2009).

The total system uncertainty is determined as the square root of the sum of the squares of the individual uncertainty components as given by P-695 Equation 7-5 (FEMA, 2009b):

$$\beta_{TOT} = \sqrt{\beta_{RTR}^2 + \beta_{DR}^2 + \beta_{TD}^2 + \beta_{MDL}^2} \quad (7)$$

The total system uncertainty calculated is then to be rounded to the nearest 0.025. Given the range of possible individual uncertainties, the total uncertainty can vary from 0.275 to 0.950. The rounded total system uncertainty value is then used within P-695 Table 7-3 to determine the acceptable AMCR values for a given collapse probability. Of particular interest in determining an R-value are the 10% and 20% probabilities of collapse as these are used to determine if a given performance group passes or not. For a given performance group to pass, each individual ACMR value within the performance group must be greater than or equal to the $ACMR_{20\%}$ and the average of the ACMR values within the performance group must be greater than or equal to the $ACMR_{10\%}$. If both of these criteria are met, the performance group passes, if either or both of these are not met, the performance group fails. The performance group with the highest R-value which passes defines the design R-value for the structural system of interest (FEMA, 2009b).

Once a design R-value is determined for the system, the final steps of the P-695 evaluation are to document the process and results, and have a peer review conducted. A peer review is required to ensure that the methods, modeling, uncertainty values, etc. are determined acceptable to an independent panel of professionals.

Chapter 4 : Methods and Modeling

4.1 Structural Modeling

The design of the arches within the general size constraints of the Tudor arches provides glulam members with irregular geometry and section properties which vary nonlinearly along the length of the members as depicted in Figure 3.2. Due to this irregular geometry, it was determined at an early point within the project that beam column elements would not be able to adequately model the behavior of the structure, nor would they allow stresses within the arch to be determined accurately. For these reasons, it was decided that finite elements would need to be implemented.

Having determined that finite elements would be required to accurately model the arches, there were two structural analysis programs readily available to the research group which were considered for use including SAP2000 (SAP2000, 2009) and OpenSees (OpenSees, 2000). Both programs were used for preliminary analyses but OpenSees was ultimately chosen to conduct all of the dynamic analyses required by P-695 because of the available toolkit (P695, 2012) created during previous research at Virginia Tech. The tookit is a MATLAB (MATLAB, 2011) Graphical User Interface (GUI) which automates and greatly accelerates the process outlined in P-695 for conducting analyses and evaluating performance groups. Within both programs, planar "membrane" elements were utilized for the arch members because the arches are assumed to be fully braced out of plane by the timber decking and wall framing which connects the arches to one another (AWC, 2013).

The large number of models required for the P-695 analyses coupled with the fact that each model would involve hundreds if not thousands of nodes and elements contributed to the necessity for a program to help create the computational models. Through the use of a GUI, the calculation of nodal coordinates and element connectivity was generalized given the arch dimensions summarized in the above figure. This GUI was created within MATLAB and can be seen in Figure 4.1.

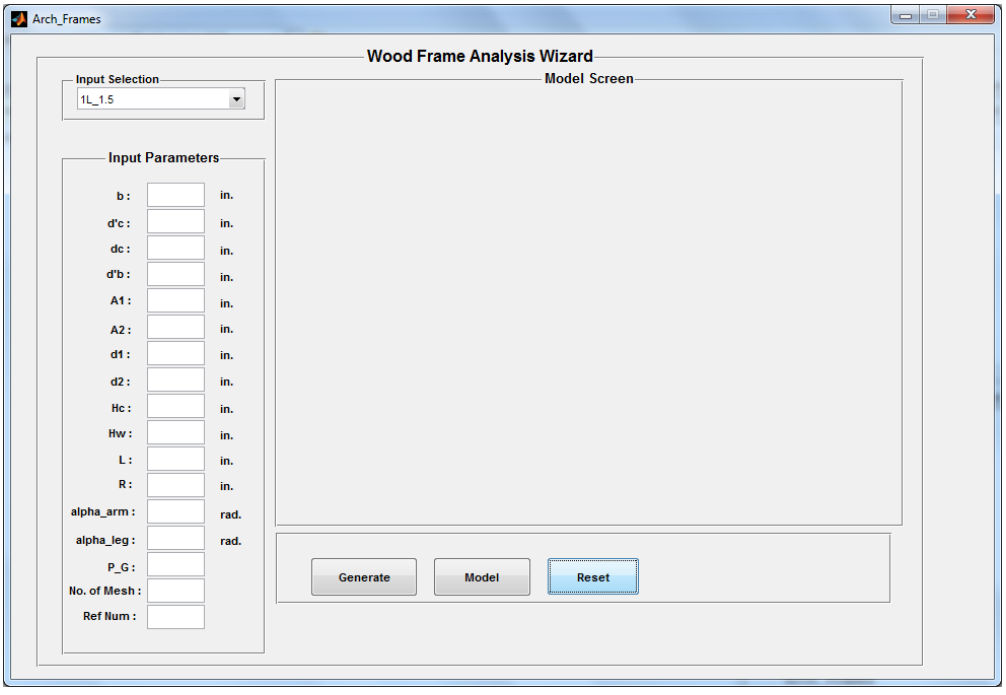

Figure 4.1: GUI created within MATLAB to aid creation of OpenSees Models

The GUI allows for the user to select one of the 56 given arches from the drop down menu on the upper left section of the GUI, which automatically inputs the arch dimensions into the input parameter fields. Alternatively, the dimensions of another arch design could be manually input into the parameter fields to create a model for an arch outside the scope of this project. A user guide for the GUI is provided in Appendix A for user reference.

The GUI works to first run a routine that determines the nodal coordinates, masses, gravity loads, and element connectivity for the given arch inputs. The nodal coordinates within the arch are created such that there are 4 elements across the depth of the member (the GUI defaults to 4 elements when the drop down list is used but other even values can be used) and the length of the elements are created in an effort to limit the aspect ratio of the finite elements to a maximum of 1.5:1. Once the nodal coordinates have been determined, the masses and loads associated with the nodes are next calculated.

The gravity loads applied to the arch include the "factored" dead load of the arch members themselves as well as the superimposed dead loads associated with the roof loads as required per P-695 Equation 6-1 (FEMA, 2009b). The forces associated with the wall loads of 50 psf are not applied to the arch because these loads are carried to the foundation through the walls themselves as they are typically traditional stud frame walls. The roof loads associated with either the light or heavy gravity load cases of 15 psf or 30 psf, respectively, are affixed to the outside nodes of the arch along the arm. These loads are calculated using the assumed 12 ft spacing between arches and using tributary area between the nodes on the outside of the arm. The gravity loads associated with the arch members themselves are calculated by assuming a density of wood equal to 35 pcf comparable to southern pine G = 0.55, ρ = 34.3 pcf (Berman et al., 2010). This assumed density is then distributed to each node within the arch using tributary area principles along with the known thickness of the arch members. The area of each quadrilateral finite element is calculated and then the associated weight of that element is determined and distributed to each of the four nodes equally assuming the elements are approximately rectangular. All of these gravity dead loads have the load factor of 1.05 applied as required by P-695 Equation 6-1 (FEMA, 2009b). Live loads are also to be applied to the computational models with a load factor of 0.25 but the only live loads used for design of these arches are roof live loads. Because the probability that any roof live loads would be present at the time of a seismic event is relatively low, the roof live loads were neglected for the purposes of these evaluations. This assumption was validated by Charles Kircher, Project Technical Director for FEMA P-695 project.

The masses applied at the nodes of the arch include the masses associated with the arch members themselves and the masses associated with the gravity dead loads which are affixed to the arch. The masses associated with the arch members are determined by again assuming a unit weight of the arch material equal to 35 pcf which is equal to a mass density of 0.00783 kip*in/s^2 per cubic in., and distributing the mass associated with each finite element to the four nodes associated with that element. The masses associated with the roof dead loads are again calculated using the assumed arch spacing of 12 ft and then distributed to the nodes on the outside of the arch arm using tributary area. Although the forces associated with the wall dead loads were not included for the analyses because the forces are carried to the foundation through the wall, the walls are still affixed to the arch and will therefore move with the arch. Because stud frame walls will likely be used in construction, the walls will be connected to the arch at the outside of the haunch and to the ground at the base of the arch. To accurately model the resulting dynamic behavior, the masses associated with the top half of the wall are affixed to the outside of the haunch and the masses associated with the bottom half of the wall are not included as they would be attached to the ground and not act with the arch. The tributary wall masses applied to the arch haunch are only applied to the global x degree of freedom (acting in lateral motion) because the masses in the vertical direction are assumed to not be transferred to the arch. Even if the

vertical masses were included, the effects would be minimal as the arch haunch movement is dominated by lateral motion and the vertical motion is minimal. Once the nodal coordinates, masses, and forces are determined, the model is ready to be created.

The previously determined information is then used when the "Model" button is pressed to write a .tcl file that defines the computational model for the given arch. The file first dictates the number of dimensions of the model and the number of degrees of freedom of the model. For the planar quad elements being utilized within OpenSees, there are 2 dimensions of the model and 2 degrees of freedom. Next the file defines the geometry of the arch by defining the coordinates of each node. After the nodal coordinates have been defined, the masses associated with the global x and y degrees of freedom are defined for each node. Next the arch material is defined as an elastic material with a modulus of elasticity equal to 1,700 ksi (AWC, 2013). After the material has been defined, it can be used to create the quad elements that comprise the arch members. The quad elements are defined using a counter-clockwise definition around the associated nodes as required by OpenSees. Once the elements are defined, the gravity loads associated with each node are applied within the model. Following the application of gravity loads, the fixities and connectivity at the arch peak are defined for the model.

The GUI also works to write a text file, when the "Model" button is clicked, that defines the necessary recorders for the model. Within OpenSees, when an analysis is conducted, no information is output from the analysis; rather recorders have to be defined to extract the relevant information during the analysis. The text file created by the GUI defines the types of recorders required, the locations where the recorders should measure (i.e. node numbers where displacements should be checked, element numbers where forces should be checked, etc.), and the NSC limits associated with the recorded information. This file is then read by the P-695 toolkit to automatically recover the necessary information from the dynamic analyses.

The last thing which is done when the "Model" button is clicked is that the GUI plots the membrane elements (called quad elements within OpenSees) as seen in Figure 4.2 below which allows the user to visually ensure that no errors have occurred during the dimension input or creation of the model.

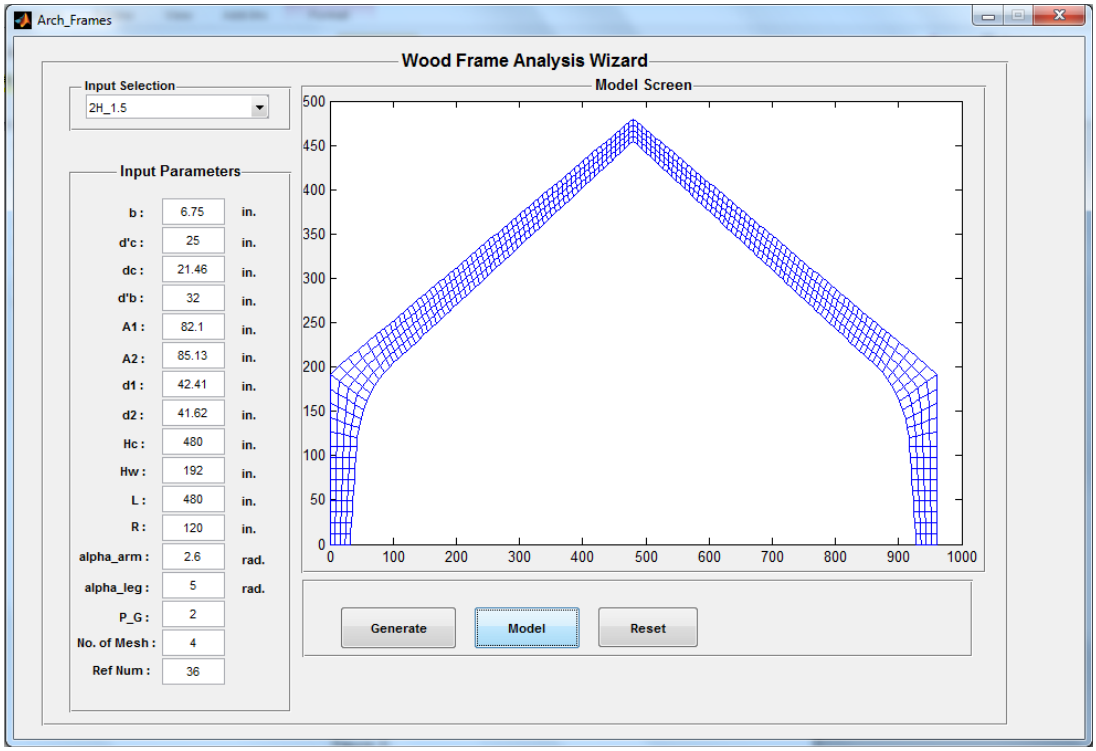

Figure 4.2: GUI showing model geometry after model has been created

4.1.1 OpenSees Modeling Validation

To ensure that the OpenSees models were providing reasonable results, several comparisons between OpenSees and SAP2000 were conducted. For these preliminary analyses, the base supports were modeled as pin supports and the connection at the crown was modeled as a hinge at the center of the interface. This method of modeling depicts the behavior of a true three-hinge arch.

The first check between the two programs was to compare the first four periods of vibration for the arch designs with a design R-value of 1.5. The observed first four mode shapes are shown in Figure 4.3 where the 1st and 4th modes are dominated by lateral acceleration and the 2nd and 3rd modes are dominated by vertical acceleration and are considered “breathing” modes. This was determined by visual observation in addition to a comparison of the relative modal participation factors (mass participating in the global X and Z directions) for each mode in the SAP output tables.

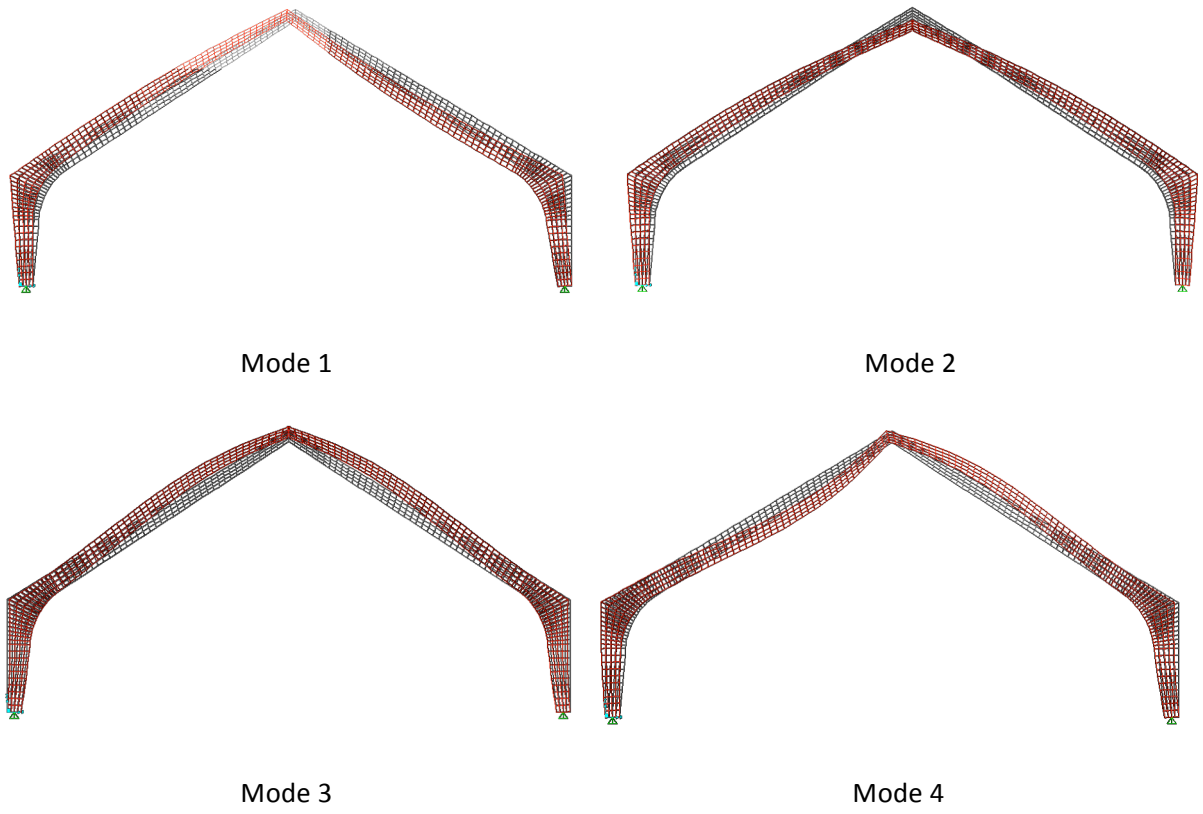

Figure 4.3: Mode shapes for arch ID 1L with an R-value of 1.5

Modal analyses conducted using SAP2000 provided the above figures and were done with Ritz Vectors implementing acceleration loads in the horizontal and vertical directions. Within OpenSees, the natural periods of vibration were determined by conducting eigenvalue analyses. The initial conditions used within the modal analyses for both programs were that of an unstressed state. After conducting eigenvalue analyses using both programs, the first four natural periods of vibration were calculated and are summarized in Table 4.1.

Table 4.1: Comparison of the first four natural periods of vibration (sec/cycle) determined using SAP2000 and OpenSees

	SAP2000				**OpenSees**				**Percent Difference**			
	Mode				**Mode**				**Mode**			
	1	**2**	**3**	**4**	**1**	**2**	**3**	**4**	**1**	**2**	**3**	**4**
1L	0.57	0.32	0.08	0.07	0.59	0.32	0.08	0.07	2.9%	2.1%	4.0%	3.3%
2L	0.87	0.49	0.21	0.17	0.87	0.49	0.21	0.17	-0.7%	-0.7%	-1.7%	-1.6%
3L	1.03	0.59	0.33	0.26	1.01	0.57	0.32	0.25	-2.1%	-2.0%	-2.4%	-2.4%
4L	1.27	0.79	0.40	0.31	1.29	0.81	0.41	0.32	2.2%	2.1%	1.6%	1.6%
1H	0.54	0.29	0.09	0.07	0.54	0.28	0.08	0.07	-1.6%	-1.8%	-4.4%	-4.4%
2H	0.75	0.41	0.19	0.15	0.74	0.41	0.19	0.15	-0.2%	-0.2%	-1.4%	-1.3%
3H	0.87	0.49	0.30	0.22	0.87	0.49	0.30	0.22	-0.7%	-0.5%	-1.1%	-1.0%
4H	1.33	0.83	0.43	0.32	1.40	0.87	0.44	0.34	5.2%	4.7%	4.5%	4.4%

As this table shows, the periods of vibration calculated using SAP2000 and OpenSees are very close (generally within 5%). The small amount of difference between the two programs is likely the result of different element formulations for the SAP2000 "membrane" element and the OpenSees "quad" element. Another small difference between the results could lie in the fact that the SAP models were not created using the GUI, but were rather created by manually inputting the outside nodes of the trapezoidal regions of the arch and automatically meshing the regions with SAP built in functions. This could have resulted in slightly varying element sizes.

The second comparison between SAP2000 and OpenSees related to the response of the models to lateral loads applied at the center of the peak connection. A lateral point load with magnitude equal to 1 kip was applied and the force effects being recorded for comparison to NSC limits were measured. In particular, the shear across the peak connection, shear at the base (left base only as they are equal for this case), and the stresses were determined within the element at the leg tangent point on the outside of the arch. The location where shear is measured is representative of a location where stresses are assumed to be critical which was later checked. However, for the purposes of this study only the magnitude of stresses was of interest not the location of maximum stress. The results from these analyses are summarized in Table 4.2. Again, the percent difference between SAP2000 and OpenSees are also provided for comparison.

Table 4.2: Deflection (in inches) resulting from point loads and comparison

Arch ID	R-value	Force Effect	SAP2000	OpenSees	% Difference
1H	2.5	Peak Shear (kips)	1.01	1.01	0.0%
		Base Shear (kips)	-0.50	-0.50	0.0%
		Bending Stress (ksi)	-0.07	-0.07	-6.4%
2H	1.5	Peak Shear (kips)	0.50	0.50	-0.1%
		Base Shear (kips)	-0.50	-0.50	0.0%
		Bending Stress (ksi)	-0.02	-0.02	-3.1%
3L	4	Peak Shear (kips)	0.33	0.33	0.0%
		Base Shear (kips)	-0.50	-0.50	0.0%
		Bending Stress (ksi)	-0.03	-0.03	0.4%
4L	Min	Peak Shear (kips)	0.40	0.40	0.0%
		Base Shear (kips)	-0.50	-0.50	0.0%
		Bending Stress (ksi)	-0.02	-0.02	-5.3%

As seen in Table 4.2, there is again a variation in results between the two programs however the variation is relatively small. In an effort to determine the cause of variation between SAP2000 and OpenSees analyses, a simple example consisting of a cantilevered column was analyzed using both programs as seen in Figure 4.4. The overall dimensions of the column are 12 inches wide and 48 inches tall.

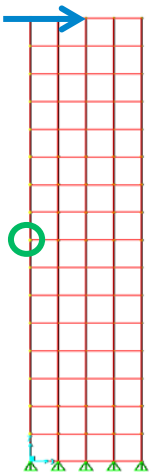

Figure 4.4: Simple example used to check results

This simple example was created in both SAP2000 and OpenSees and a lateral point load with a magnitude of 10 kips was applied at the center of the column top. With the load applied, deflections were measured at mid-height on the left side of the column (circled in green in above figure) and are summarized in Table 4.3.

Table 4.3: Deflection comparison for simple cantilever column example (inches) with varying mesh densities

Mesh Size	OpenSees		SAP		% Difference	
	X-Disp	Y-Disp	X-Disp	Y-Disp	X-Disp	Y-Disp
2 x 8	0.066	0.028	0.073	0.031	-10.8%	-11.6%
4 x 16	0.072	0.030	0.074	0.031	-2.8%	-3.0%
8 x 32	0.074	0.031	0.075	0.031	-0.7%	-0.8%
16 x 64	0.075	0.031	0.075	0.031	-0.2%	-0.1%

As these results show, the mesh density seems to have a significant impact on the results. This is assumed to be producing some of the difference between the two programs. The reason that the results vary by a much larger amount for coarser mesh densities is that SAP2000 uses incompatible modes to obtain results closer to the exact solution with a coarser mesh density. As the mesh density is refined, the results asymptotically approach the true value and the variation between the two programs diminishes. This shows that the mesh density might be causing some of the variation in results. In addition to the effects of mesh density, another thing that could be causing variation between the deflection results is the element formulation between the two programs.

To further investigate the effects of mesh density, the study on natural periods of vibration was expanded to include mesh densities that were doubled resulting in 8 elements across the depth of the arch for a few of the arches. The first four natural periods of vibration were again determined using both SAP and OpenSees and compared. The resulting natural periods are summarized in Table 4.4.

Table 4.4: Revised periods of vibration (cycles/second) with 8 elements across the depth of the arch

Archetype	SAP2000				OpenSees				Comparison			
	Mode				Mode				Mode			
	1	2	3	4	1	2	3	4	1	2	3	4
1L	0.60	0.33	0.09	0.08	0.60	0.33	0.09	0.08	-0.3%	-0.2%	1.2%	0.9%
2L	0.88	0.49	0.21	0.17	0.88	0.49	0.21	0.17	-0.6%	-0.6%	-0.1%	-0.1%
1H	0.55	0.29	0.09	0.07	0.55	0.29	0.09	0.07	-0.7%	-0.5%	0.8%	0.6%
2H	0.75	0.41	0.19	0.15	0.76	0.41	0.20	0.16	-1.4%	-1.3%	-0.7%	-0.8%

As seen in the table, the variations within the periods of vibration are generally reduced with the previous maximum of 4.4% difference reduced to a maximum of 1.4% difference. This further supports the idea that some of the discrepancy between the two programs is likely the result of the use of incompatible modes within SAP2000 which allow better results with a coarser mesh density of the models. OpenSees was investigated for the availability of incompatible modes however it was found to not available at this time.

To ensure that the density of the mesh used for analysis of 4 elements across the depth of the member was adequate, a small study was conducted. Within this study, arch ID 2L with a design R-value of 4 was selected for use to check the effects of mesh density. The number of elements across the depth of the arch member was varied with values of 2, 4, and 6. A lateral load equal to 1 kip was applied to the peak of the arch and three critical values were checked including the shear observed within the peak, the shear observed at the base, and the bending stresses observed at the leg tangent point on the outside of the arch. The resulting force effects from this study are summarized in Table 4.5.

Table 4.5: Mesh density check results

	# of Elements Across Section		
	2	4	6
Peak Shear (kips)	0.51	0.50	0.50
Base Shear (kips)	-0.50	-0.50	-0.50
Bending Stress (ksi)	0.069	0.081	0.084
Peak Shear Relative Error	-1.9%	-0.5%	0.0%
Base Shear Relative Error	0.0%	0.0%	0.0%
Bending Stress Relative Error	17.7%	2.9%	0.0%

From these results, it can be observed that with 6 elements across the depth of the arch member, the results are converging. By comparing the results from the models containing 2 and 4 elements across the depth, it can be observed that 2 elements provides a significant amount of error when observing the stresses, but 4 elements has very little error for any of the observed effects. The little amount of error (2.9%) is deemed acceptable within the context of this project especially when considering the impact of the number of elements on the run time for these analyses with 44 ground motions analyzed for each of the 56 models at each scale factor.

4.1.2 Effects of Rotational Connection Fixity

To better understand the effects of rotational fixity of the connections at the bases and crown, the periods of vibration for the 8 given arch ID's with an R-value of 1.5 were determined for every combination of fixed and pinned connections for the base and crown connections. The natural periods of vibration for the first mode of each of the arch ID's are given in Table 4.6 for the four resulting cases.

Table 4.6: Periods of vibration (seconds/cycle) with connection fixity varied for the first natural period

Arch ID	All Connections Pinned	Crown Connection Fixed, Base Connections Pinned	Base Connections Fixed, Crown Connection Pinned	All Connections Fixed
1L	0.59	0.59	0.36	0.36
2L	0.87	0.87	0.50	0.50
3L	1.01	1.01	0.55	0.55
4L	1.29	1.29	0.78	0.78
1H	0.53	0.53	0.34	0.34
2H	0.74	0.74	0.45	0.45
3H	0.87	0.87	0.53	0.53
4H	1.39	1.39	0.89	0.89

As seen, the periods of vibration are significantly reduced when the connections are all fixed as compared to all pinned. It can also be observed that the rotational fixity of the crown connection has a negligible effect on the first period of vibration. This can be seen in that the difference in natural period is not present for the cases when the base connection stiffness's are the same (ie. the first two columns and last two columns have almost exactly the same values).

The results from this study lead to the subsequent study to determine the effects of varied connection stiffness on the periods of vibration for the arches. For each of the given arches, curves were created by varying the connection stiffness's and determining the periods of vibration as seen in Figures 4.5 and 4.6. Note that all periods reported have been normalized by dividing by the period resulting when all connections are pinned. Figure 4.5 shows the effect on the first natural period of vibration resulting from varying the base rotational stiffness for arch ID 1L with a design R-value of 1.5. The fact that the curves representing fixed and pinned crown connections lie directly on top of each other again shows that the crown connection fixity has no effect on the first period of vibration.

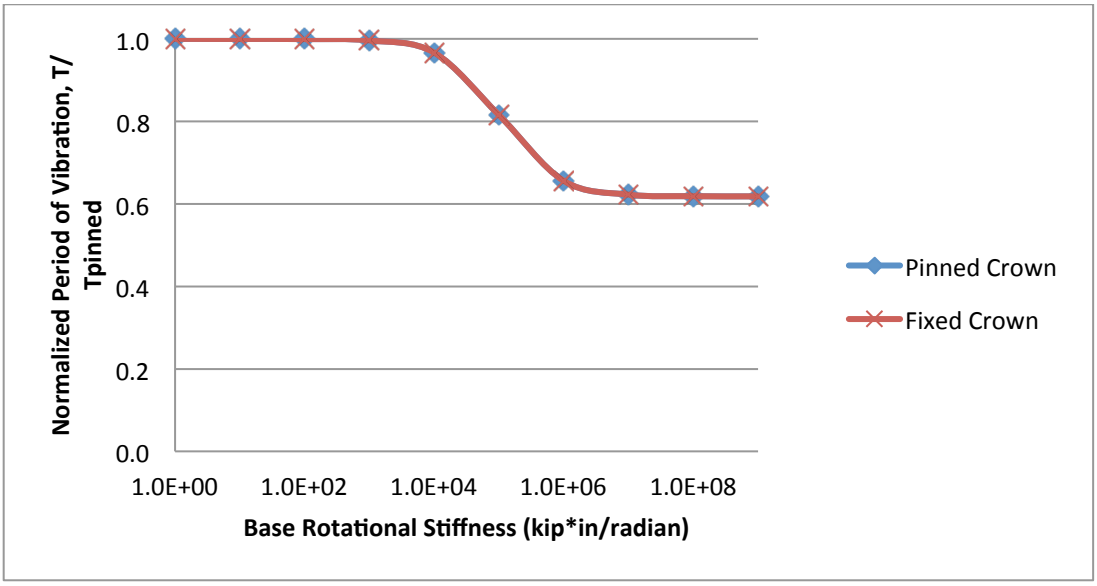

Figure 4.5: Effects of base connection rotational stiffness on the first natural period of vibration

Figure 4.6 shows results similar to the previous figure, but for all archetypes. As with arch ID 1L, the crown connection fixity has no effect on the first period of vibration and the curves lie directly on top of one another so only the case with the crown pinned is plotted.

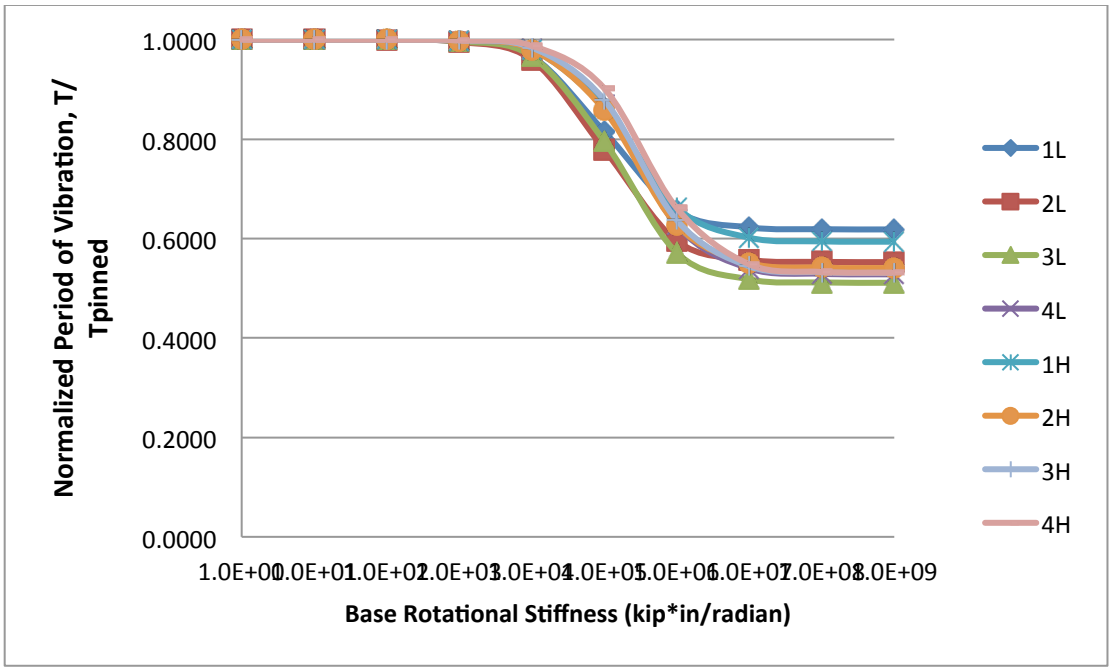

Figure 4.6: Effects of base connection rotational stiffness on the first natural period of vibration

It was assumed that the second and third modes would be impacted by the connection stiffness of the crown because their mode shapes included vertical displacements and would therefore cause rotation of the crown connection. To check this assumption, the second, third and fourth periods of vibration were determined for all archetypes. Mode 4 was expected to be similar to mode 1 in that the crown connection stiffness was expected to have little to no impact on the measured period. These

assumptions were checked by evaluating the results for arch ID 1L with R-value 1.5 which are given in Figures 4.7 through 4.9 for natural periods two through four.

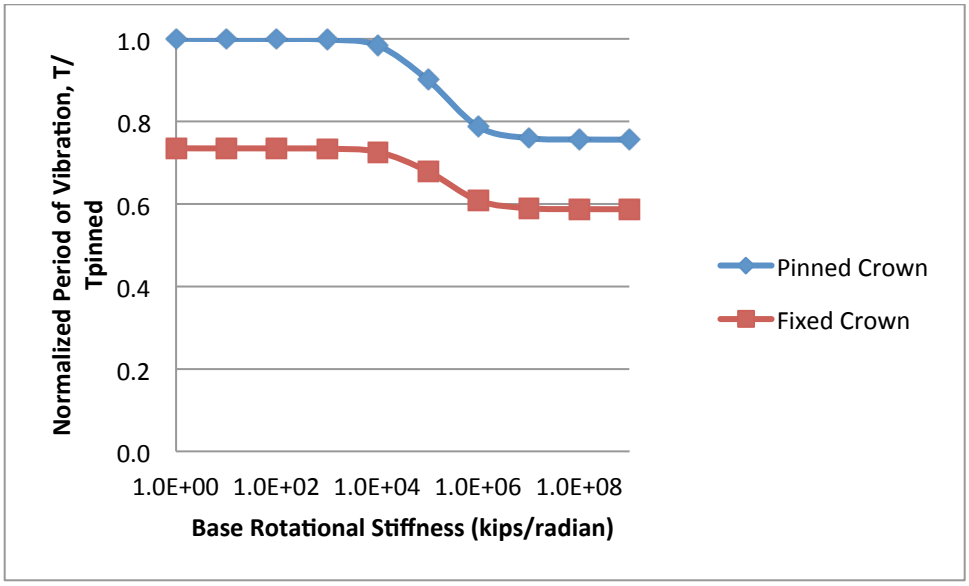

Figure 4.7: Effects of base connection rotational stiffness on the second natural period of vibration

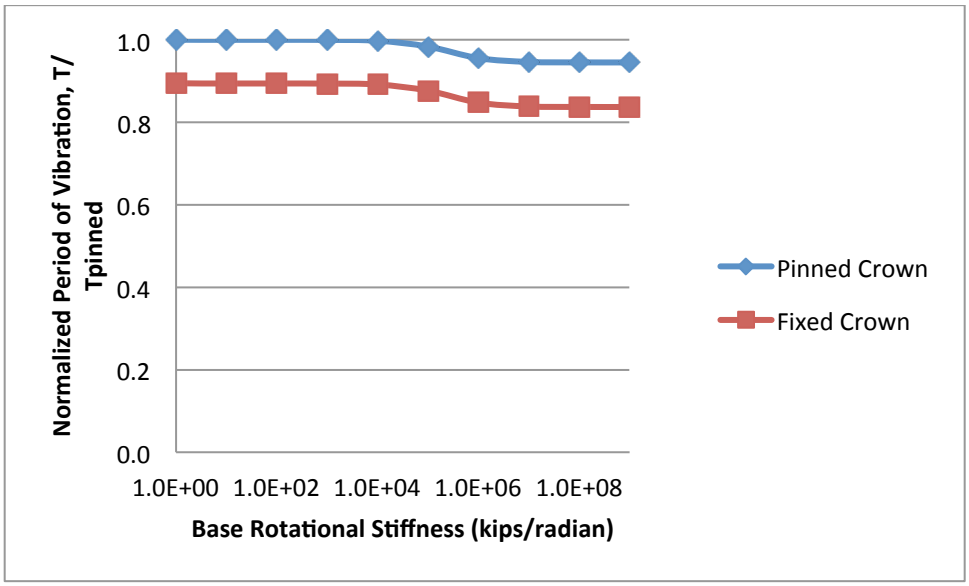

Figure 4.8: Effects of base connection rotational stiffness on the third natural period of vibration

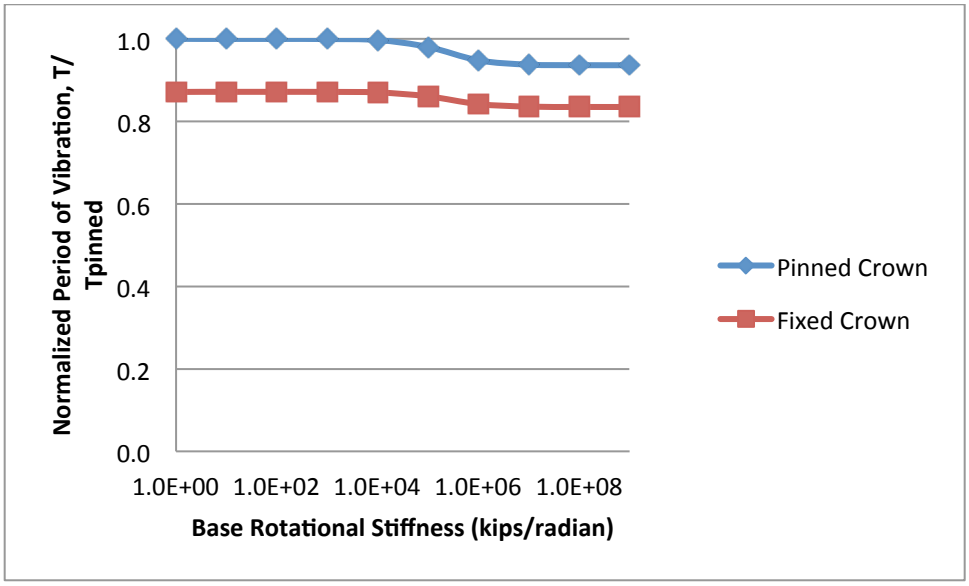

Figure 4.9: Effects of base connection rotational stiffness on the fourth natural period of vibration

The fact that the two curves relating to pinned and fixed crown connection are not lying on top of each other in the previous three figures shows that the crown connection stiffness does have an impact on the natural periods. This is present for natural periods two through four showing that within all of them, the connection stiffness is having an impact. The larger gap within the results of natural period two shows that the crown connection stiffness has a larger impact on the second mode. These results show that modeling of the stiffness within the crown connection could have an impact on the dynamic analyses.

Similar to the previous study conducted, the connection stiffness's for each of the arches were varied and the deflection at the crown was determined for two point loading cases. The first loading case included a lateral point load applied at the outside of one of the haunches, while the second case included a point load in the gravity direction applied at the crown. For these cases of lateral and gravity loading, the lateral and vertical deflections at the crown were measured, respectively. The measured deflections were normalized by dividing by the deflection observed when all connections are pinned. Figures 4.10 and 4.11 show the interaction of connection fixity and peak deflection for all 8 archetypes.

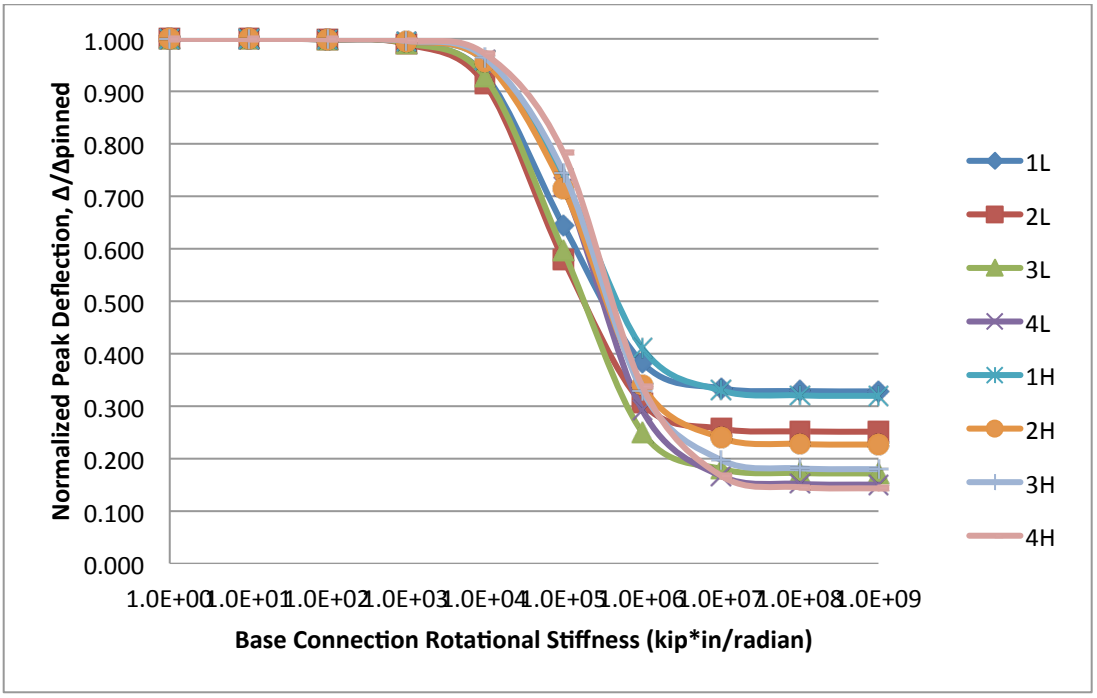

Figure 4.10: Effects of base connection rotational stiffness under lateral loading with crown pinned

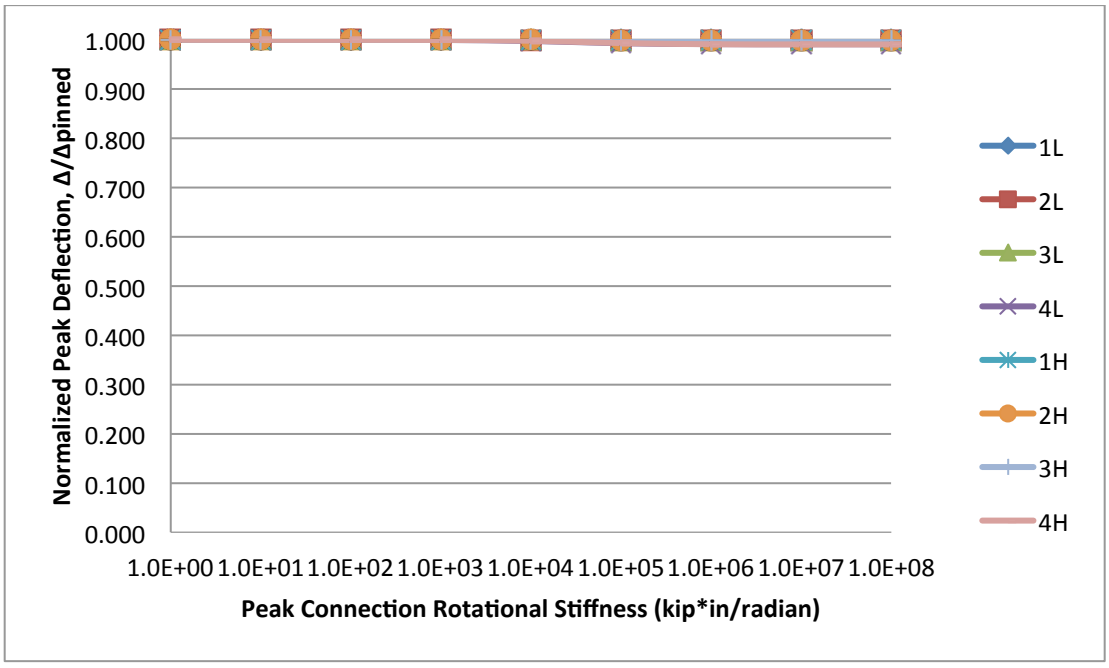

Figure 4.11: Effects of peak connection rotational stiffness under lateral loading with base pinned

Similar to the modal results for the first mode shape of the structure, these plots show that the crown connection stiffness does not have an impact on the lateral deflection of the arch as loaded for this study. This makes sense because the first mode shape is a lateral swaying motion similar to the lateral loading applied in this study. The results from the gravity loading studies conducted can similarly be compared to mode shapes 2 and 3 which are vertical modes. For this reason, it is expected that there will be an interaction between the vertical deflection and both the crown and base connection

stiffness's. This idea is investigated within Figures 4.12 and 4.13 by applying gravity loads at the peak and measuring the vertical deflection.

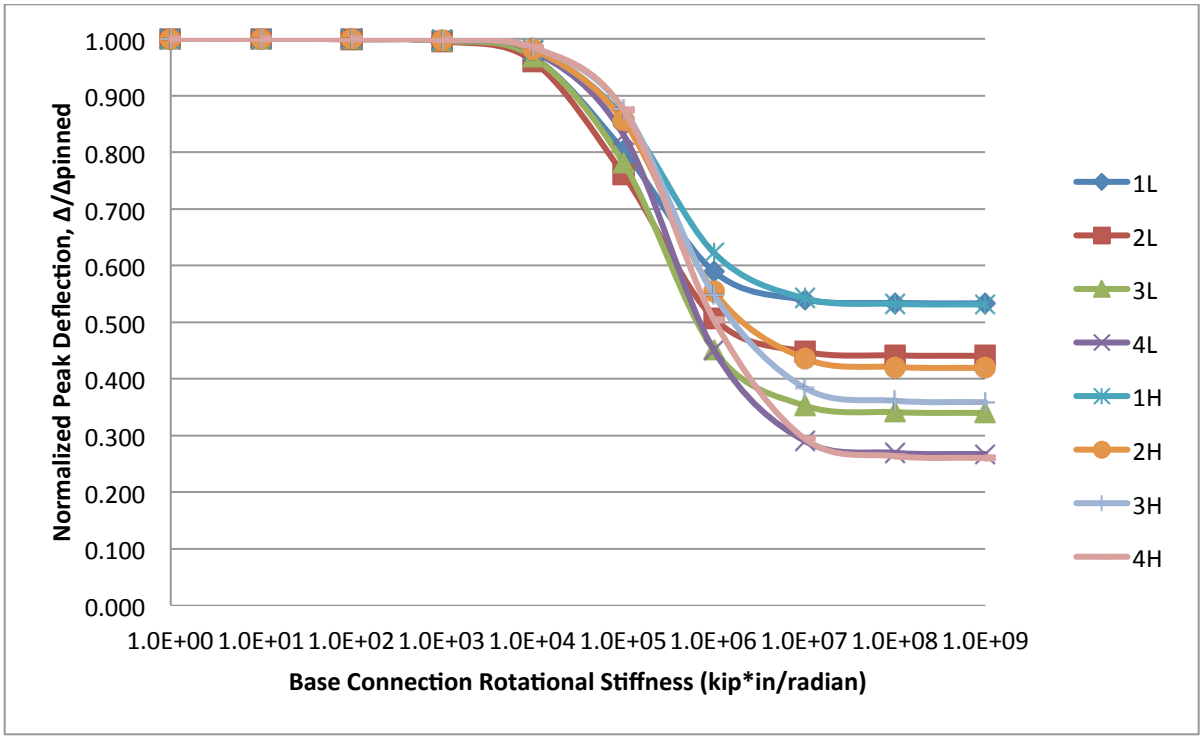

Figure 4.12: Effects of base connection rotational stiffness under gravity loading with crown pinned

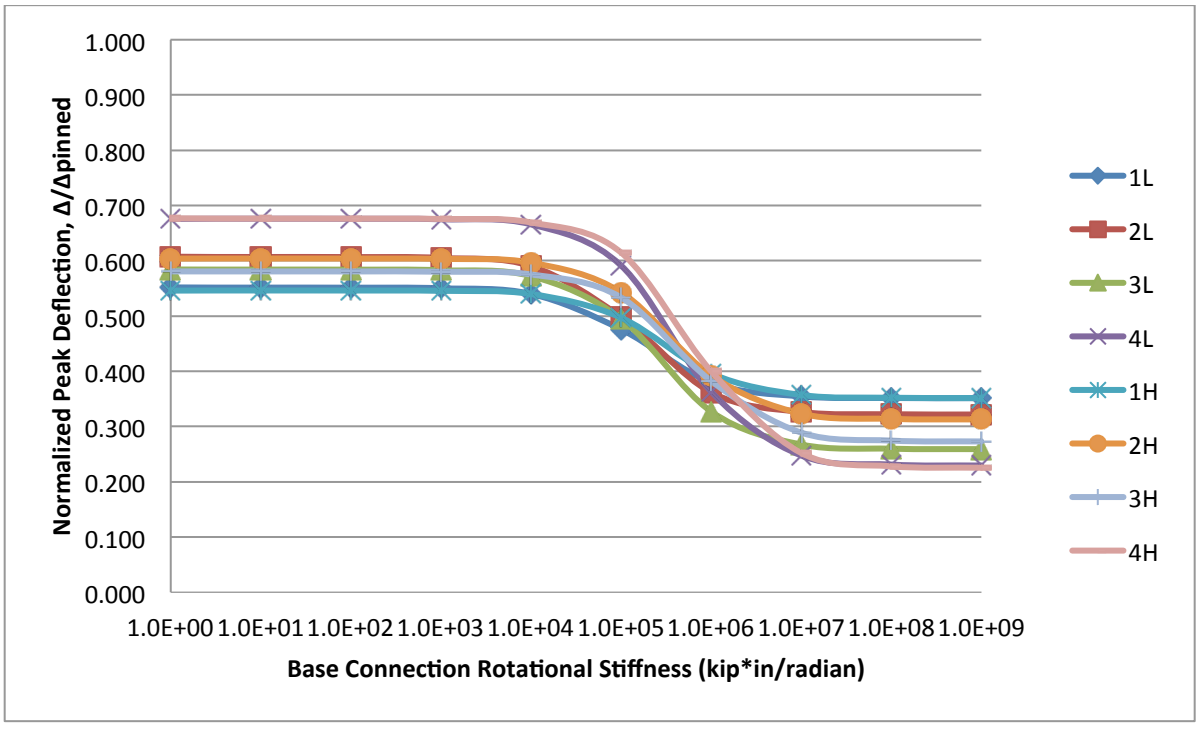

Figure 4.13: Effects of base connection rotational stiffness under gravity loading with crown fixed

As seen, these results represent the expected behavior that both the base and crown connection stiffness's have an impact on the vertical deflection. Similar to the modal analyses, the transition between pinned and fixed connections occurs between values of 1,000 and 10,000,000 kip*in/radian.

4.1.3 Determination of Shoe Connection Rotational Stiffness

According to the approximate load-deformation data provided in Table 5 of the AWC white paper, the rotational stiffness of the arch 2L shoe (with design R-value of 1.5) was determined to be 6.6 x 10^4 kip*in/radian for loading that compresses the arch into the toe of the shoe (AWC, 2013). This value is at the pinned end of the connection fixity as determined from previous studies. To check the provided stiffness, a more rigorous check involving a SAP2000 finite element model was completed. Figure 4.14 shows the solid model of the shoe created using SAP. The model included a detailed shoe as well as the full arch with a pinned crown connection. The full arch was included within the model to provide the appropriate thrust and compression within the arch base due to gravity loads. A lateral load was then applied following the gravity loads to allow the actual connection stiffness to be determined.

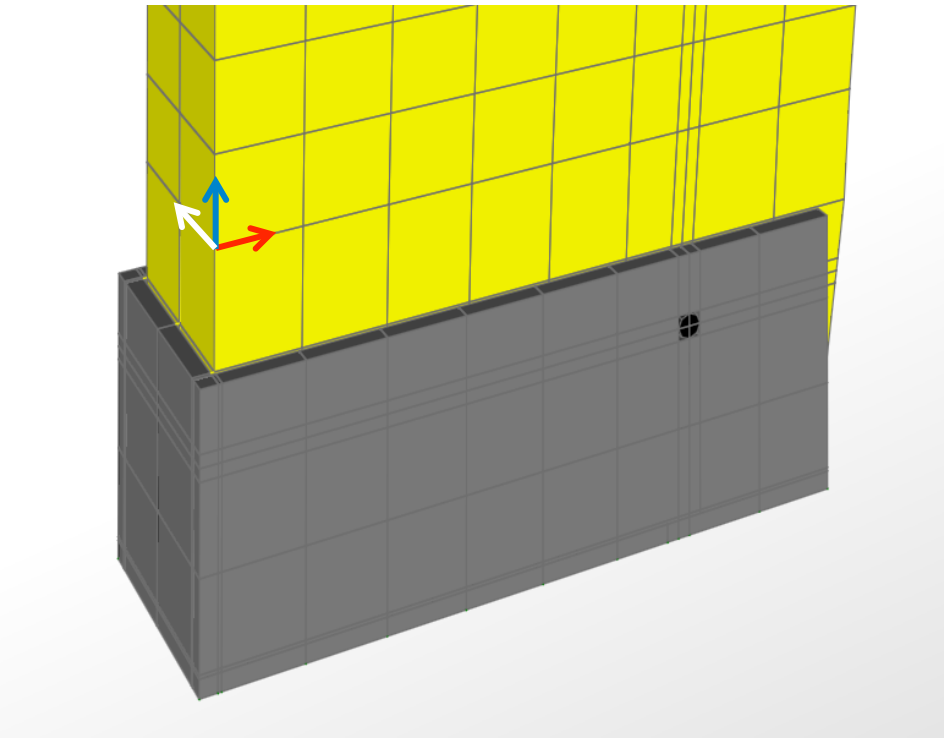

Figure 4.14: Finite element model of Arch ID 2L (R = 1.5) shoe created using SAP2000

Within the above figure, the red, white, and blue arrows represent the local 1, 2, and 3 axes, respectively. The modulus of elasticity in the longitudinal direction was provided as 1700 ksi (AWC, 2013). To determine the elastic modulus in the other 2 directions as well as the shear moduli in all three directions, ratios of the necessary factors to the longitudinal elastic modulus were found in the *Wood Handbook* (FPL, 2010). It was assumed that Douglas-Fir was the species used and that the tangential modulus would be used for both of the other axis because it is the lower of the tangential and radial values and is therefore conservative. The elastic and shear modulus values used within the model were determined to be:

E_1 = 85 ksi

E_2 = 85 ksi

E_3 = 1700 ksi

G_{12} = 11.9 ksi

G_{13} = 108.8 ksi

G_{23} = 108.8 ksi

With the modeling of the solid elements complete, links were used to connect the steel shoe to the timber arch. These links were defined to have a zero tensile strength and effectively infinite compression strength to model the interaction surface between the two materials. Two cases of loading were investigated involving loading that compresses the arch into the toe and loading that causes the arch to lift away from the toe. These two loading cases were then used to determine the rotational stiffness of the arch base for each of the rotational directions, with the assumption that they would vary significantly. The deflection within the shoe for each of these loadings can be seen below.

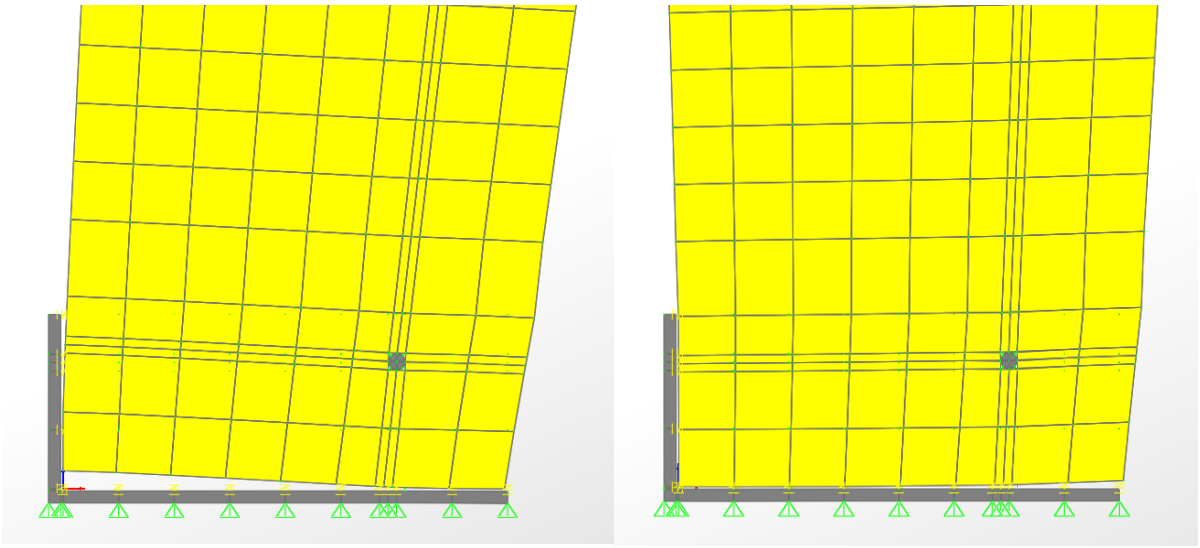

Figure 4.15: Deflection of the timber arch-shoe connection for loading toward the inside of the arch (image on left) and loading toward the outside of the arch (image on right)

To determine the rotational stiffness of the model, stresses were measured at two locations within the height of the arch and used to calculate the moment at those locations. These moments were then extrapolated linearly to determine the moment at the level of the bolt. The rotation within the model was calculated by measuring the displacement of each node at the horizontal plane of the bolt and calculating a corresponding rotation. These values were then averaged to determine the average rotation of the model. Using these values, the rotational stiffness's were determined to be 9 x 10^4 kip*in/radian and 6 x 10^5 kip*in/radian for the out of toe and into toe loading directions, respectively. These values lie within the transition range of connection stiffness as previously determined and are shown in Figure 4.16 as vertical blue lines. A vertical yellow line has also been included showing the rotational stiffness assumed within the timber arch report.

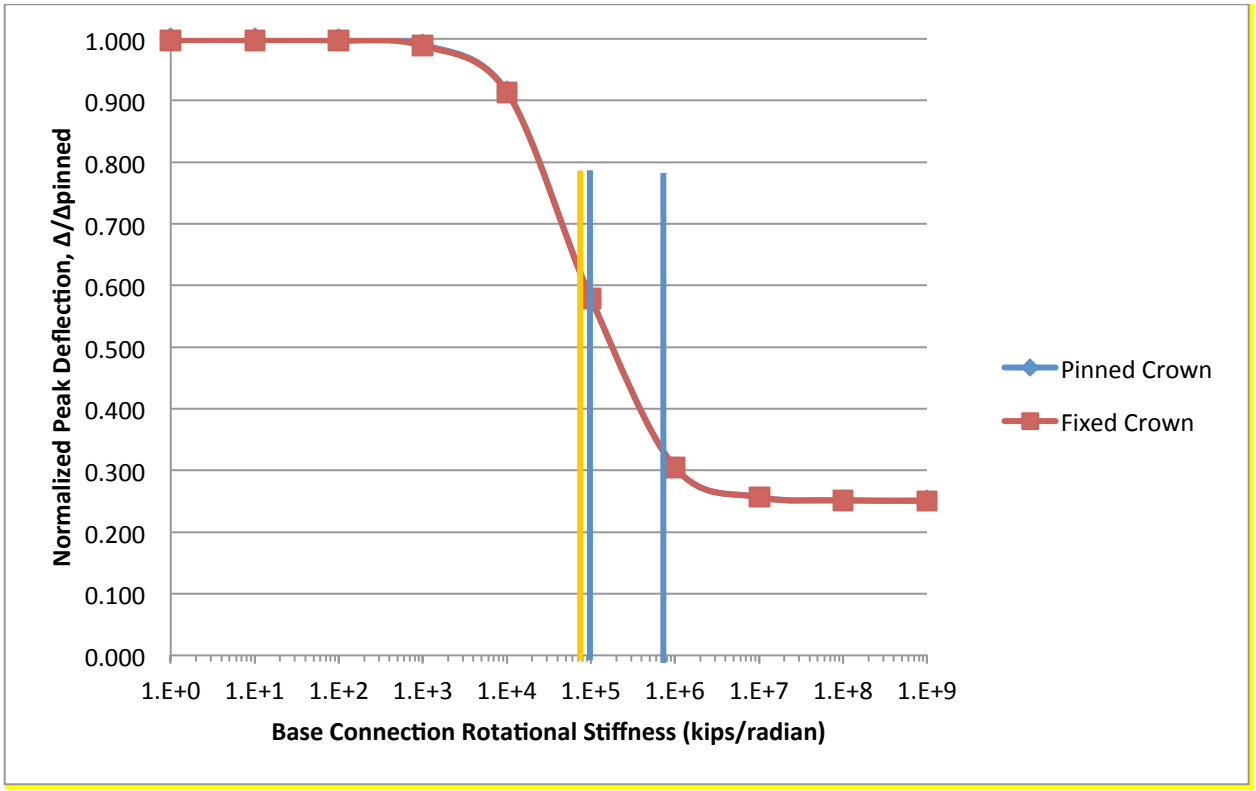

Figure 4.16: Plot showing the effects of base connection rotational stiffness resulting from lateral load

It is important to note that these values of rotational stiffness represent only the flexibility of the metal shoe and arch interaction, excluding any flexibility resulting from deformation of the shoe to concrete connection. Subsequently, the values provided would be assumed an upper bound of rotational stiffness. The significant amount of time required to create and analyze the full solid model was determined to be too great and therefore further models to evaluate the stiffness of the other arches would be beyond the scope of this project. Therefore, the project moved forward with all models having base connections modeled as pinned.

4.1.4 Non-Linear Base Connection Modeling

To determine what affect the non-linear behavior within the base connections has on the P-695 evaluations, the behavior of the bolted connections was implemented within a subset of the models. It is assumed that a large amount of non-linear behavior occurs when the base of the arch is pulled toward the inside of the arch and bearing/crushing of the timber material along with yielding of the bolt occurs. To model this behavior within the OpenSees models, a nonlinear truss element which has post yield strength was implemented at the arch bases. A small truss element was also input horizontally extending from the base connection toward the inside of the arch with a tension stiffness corresponding to the bearing of the arch against the shoe and zero compression strength where the nonlinear element will act. The properties of the nonlinear element are determined from the relationship given in the AWC white paper where the initial stiffness of the bolted connection is equal to (for the 3L arch including all design R-values):

$$k_i = 270{,}000(D)^{1.5} = 270{,}000(0.625)^{1.5} = 133{,}409\ lbf/in \quad (8)$$

The nominal yield capacity of the 0.625 in diameter bolt is defined as 10182 lbf (AWC, 2013). Using these two known values, the deformation at yield can be determined as:

$$\Delta_y = \frac{Nominal\ capacity}{k_i} = \frac{10{,}182\ lbf}{133{,}409\ lbf/in} = 0.0763\ in. \tag{9}$$

The maximum capacity of the connection is defined as 3 times the nominal capacity of the connection determined in accordance with the NDS assuming ϕ = 1.0. This gives an ultimate capacity of 30,546 lbf. To define the slope of the post yield response portion and to give the failure limit, the maximum deformation capacity of the bolted connection had to be determined. This value was calculated using the equations given in the white paper to give the NSC limit and determined to be (AWC, 2013):

$$\Delta_u = \frac{1.25(Wood\ bearing\ length)}{8.75} = \frac{1.25(8.75\ in.)}{8.75} = 1.25\ in. \leq 1.25\ in. \tag{10}$$

Next, the post yield stiffness needed to be determined, providing the nonlinear behavior of the connection. This was determined to be:

$$k_p = \frac{(P_u - P_y)}{(\Delta_u - \Delta_y)} = \frac{(30{,}546 lbf - 10{,}182\ lbf)}{(1.25\ in. - 0.0763\ in.)} = 17{,}350\ lbf/in \tag{11}$$

The stiffness of the connection when loaded in an outward direction also needed to be calculated. To find this, the modulus of elasticity needed to first be determined. The wood handbook published by the Forest Products Laboratory gives ratios of modulus of elasticity for the 3 principle axis of wood. The least value corresponding to the tangential direction was chosen in an effort to be conservative. The ratio between tangential and longitudinal modulus of elasticity is defined as 0.05 for douglas-fir, which is assumed to be acceptable softwood representative of the glulam (FPL, 2010). Multiplying the Longitudinal modulus of elasticity of 1,700 ksi by this ratio gives the tangential modulus as 85 ksi.

The general relationship used to relate the modulus of elasticity to an equivalent stiffness is:

$$\sigma = E\varepsilon \tag{12}$$

which can be expanded to:

$$\frac{P}{A} = E\frac{\Delta L}{L} \tag{13}$$

and rearranged to give us the desired stiffness:

$$k = \frac{P}{\Delta L} = \frac{AE}{L} \tag{14}$$

Having determined the modulus of elasticity, the only remaining unknowns are the area and length. Because the compression at the free surface on the inside of the arch is equal to zero, it was assumed that a linear stress distribution ranging from zero to the maximum value would provide an average on half of the stress value. To simplify the calculation of stiffness, the length under compression was set as half of the depth of the arch, which when a uniform stress distribution is assumed, is equal to the stiffness of the arch base where the stresses vary from zero to the maximum value. This gives L = 14 in for all arch ID 3L designs. The area under the given compression stress was calculated by multiplying the width of the arch by the depth of the shoe. For the arch 3L, this is equal to:

$$A = bH_{shoe} = 8.75in * 9in = 78.75in^2 \quad (15)$$

Knowing all of these values, the stiffness was determined to be:

$$k = \frac{P}{\Delta L} = \frac{AE}{L} = \frac{78.75in^2 * 85{,}000\ psi}{14\ in.} = 478.1\ kip/in \quad (16)$$

With all of the necessary values determined, the response of the arch shoe connection will be modeled as shown in Figure 4.17. The red line below the axis represents the NSC failure limit when the arch is loaded in an outward direction and the red and green lines above the axes represent the failure limits when the arch is loaded toward the inside.

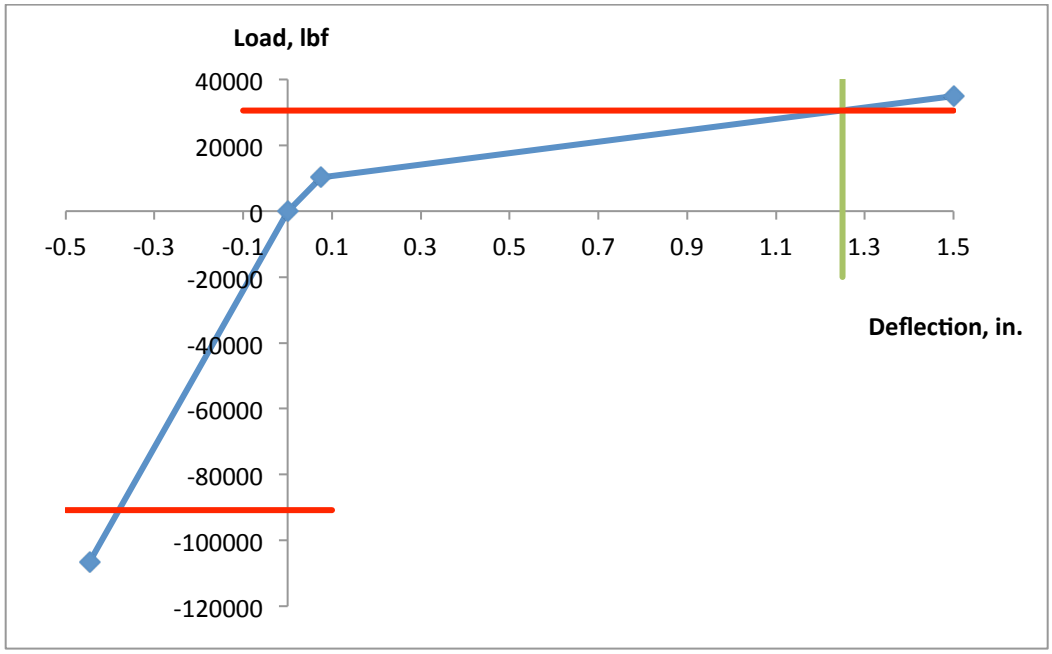

Figure 4.17: Load deformation response for bolted base connection of arch 3L

The cyclic response of the model when loaded toward the inside will look like Figure 4.18.

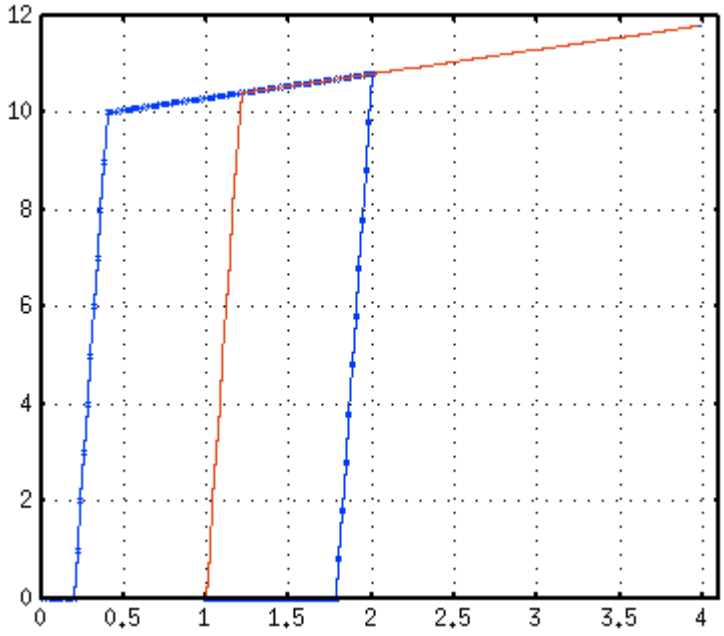

Figure 4.18: Expected cyclic response of bolted base connection caused by inward acting forces

4.1.5 Effects of Damping

To determine the effects of the damping ratio on the P-695 evaluation, analyses were conducted where the damping ratio was varied at values of 0.5%, 2.5%, 5%, and 10%. Analyses were run on all arches for both high and low gravity load levels. The resulting Collapse Margin Ratio's (CMR) (which are equal to the Adjusted Collapse Margin Ratio (ACMR)) were then averaged for the low and high gravity load cases and the results are summarized in Table 4.7.

Table 4.7: CMR results for varied damping ratio

Damping Ratio, ζ	CMR		Δ_{CMR} from ζ = 0.025	
	Gravity Load Level		Gravity Load Level	
	Low	High	Low	High
0.005	1.15	0.77	-24%	-21%
0.025	1.51	0.98	0%	0%
0.05	1.77	1.13	17%	15%
0.1	2.08	1.33	38%	36%

As these results show, increasing the damping ratio to 5% or 10% of critical would result in an increase of collapse margin ratio of around 15% and 35% on average. Therefore, if a higher damping ratio could be proven applicable, significant benefits could be obtained. Damping curves for a sample performance group are provided in Table 4.19. These results are representative of a low gravity load level and design R-value of 1.5.

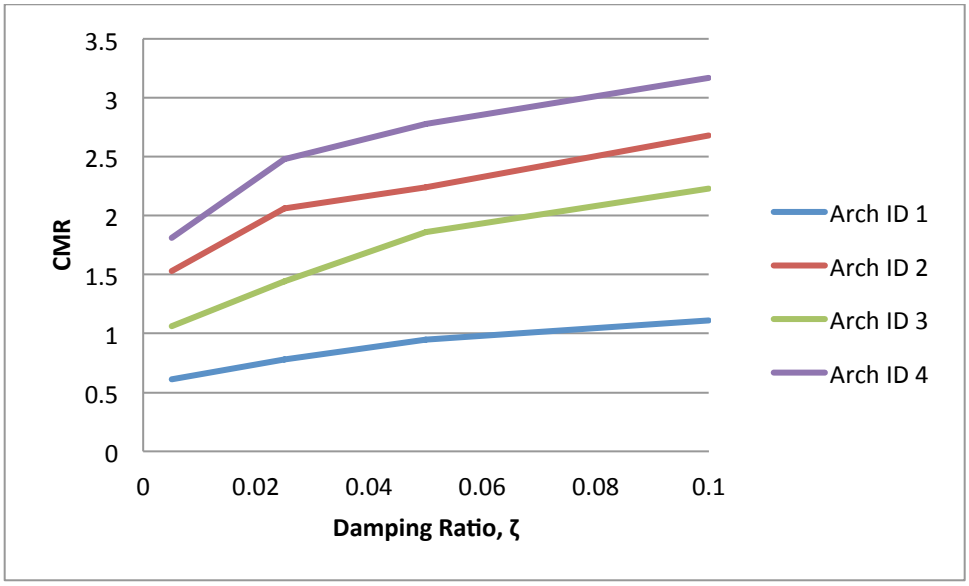

Figure 4.19: Plot of CMR vs. damping ratio for low gravity load level and design R-value = 1.5

Complete results from this study on damping ratio can be found in Appendix C.

4.2 P-Delta Effects

The impact of including P-delta effects were investigated in a limited capacity. To include P-delta effects, two leaner columns were included within the model, one on each side of the arch attached to the haunches. To determine if the inclusion of P-delta effects would significantly impact the results, the widest arch with the shorter height (arch 3) was chosen with a high gravity load level and the minimum design was analyzed. Within each of this model, half of the gravity load associated with the structure was attached to each leaner column and ground motion MUL009 was analyzed with a scale factor of 1.133 applied to the MCE level ground motion. This scale factor was greater than the CMR and therefore P-delta effects would be larger than those observed at the scale factor associated with the CMR. The haunch drift observed for this ground motion is plotted in Figure 4.20 for both models including and excluding the P-delta effects.

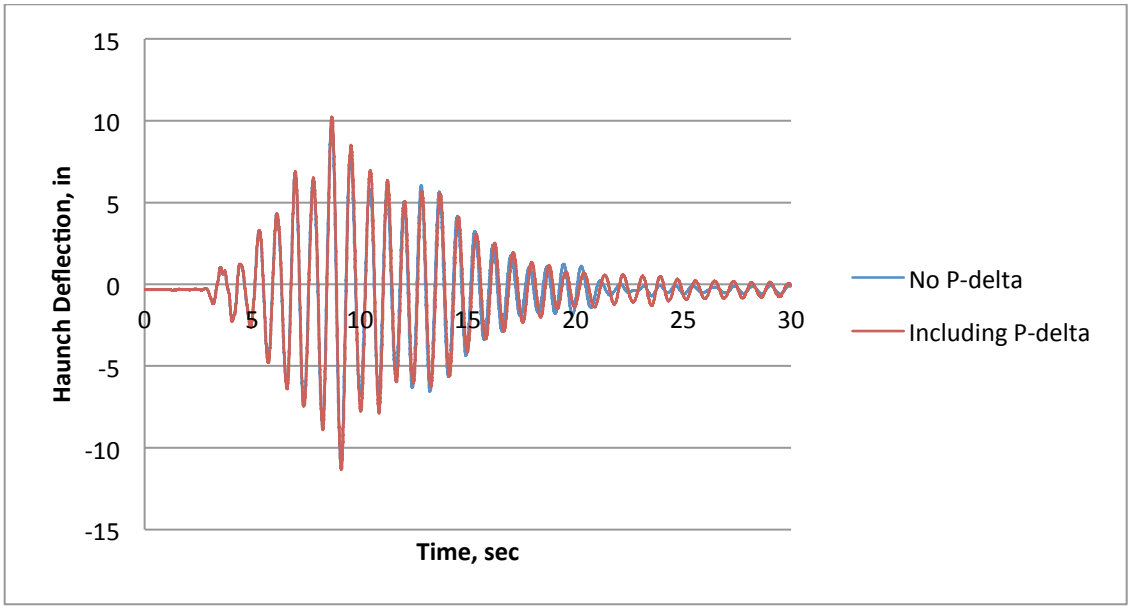

Figure 4.20: Haunch deflection response history for MUL009 ground motion with scale factor = 1.133

As this plot shows, the effects from including P-delta effects are minimal. The maximum haunch deflection is slightly increased. To ensure that the overall effects on the CMR values would not be significant, the controlling failure mode of base inward shear was checked to ensure there wasn't a significant change in base shear forces. To determine the base shear forces, the reaction at the base of the arch for the left side was added to the reaction of the left leaner column to provide the effective base shear reaction for the left side of the arch. When this was done for the previously mentioned ground motion, the differences in outward and inward base shear forces were compared for the left base of the arch and are presented in Table 4.8.

Table 4.8: Comparison of base shear reactions for ground motion MUL009

Left Base Shear Forces, kips				% Increase In Base Shear
No P-delta	Including P-delta			
Arch Reaction	Arch Reaction	Leaner Column Reaction	Total Reaction	
77.3	81.7	1.5	80.1	3.6%
-39.3	-40.1	-1.6	-38.7	-1.5%

As these results show, the effects from including P-delta effects within the models being analyzed are minimal. The difference in base shear between the case when P-delta effects were excluded and the case where they were included was -1.5 – 3.6%. This tells us that including the P-delta effects actually decreased the base shear forces slightly due to the limited impact on the response of the structure.

4.3 Performance Group Definition

Arch designs to be evaluated were divided first according to the gravity load applied to the structure, including both a low and high gravity load. The low gravity load scenario includes a light roof dead load of 15 psf which includes the self-weight of the arch throughout the arm as well as decking, panel

overlay, roof membrane, and light-weight roof covering. The high gravity load scenario includes a heavy roof dead load of 30 psf which includes the same dead loads as the light load case, but with a heavy roof covering. Both load scenarios also include a heavy wall dead load of 50 psf which contributes only to the masses attached to the arch because the walls are assumed to be self-supporting (AWC, 2013).

Once divided into heavy and light gravity load levels, the arch designs were further divided into their performance groups according to their design R-Values. The performance groups are summarized in Table 4.9.

Table 4.9: Summary of Performance Groups

Group No.	Performance Group Summary Grouping Criteria		Number of Archetypes
	Gravity Load Level	Design R-Value	
PG-1	Low	1.5	4
PG-2		2	4
PG-3		2.5	4
PG-4		3	4
PG-5		4	4
PG-6		5	4
PG-7		Min. Design	4
PG-8	High	1.5	4
PG-9		2	4
PG-10		2.5	4
PG-11		3	4
PG-12		4	4
PG-13		5	4
PG-14		Min. Design	4

All performance groups were designed for Seismic Design Category D_{max} (AWC, 2013). Table 6-1 in P-695 defines the variables S_{MS}, S_{M1}, and T_s as 1.5 g, 0.9 g, and 0.6 seconds, respectively (FEMA, 2009b). As previously discussed, the fundamental period of each arch was defined as $C_u T_a$ and was calculated using ASCE 7-10 Eq. 12.8-7 (ASCE, 2010):

$$T_a = C_t h_n^x \tag{17}$$

Where for wood structures with S_{D1} = 0.6 g:

C_t = 0.02

x = 0.75

C_u = 1.4

h_n = the distance from the base of the arch to the average height of the roof (28 ft and 42.5 ft for arches 1-3 and 4, respectively)

Using this equation, the fundamental periods were determined to be 0.34 seconds for arch ID's 1, 2, and 3 and 0.47 seconds for arch ID 4 as seen in Table 3.1.

The fundamental period of the arches is required to determine the anchoring scale factor. This anchoring scale factor is used in determining the total factor applied to each ground motion.

Because $T \leq T_s$ for all archetypes, S_{MT} is given by P-695 Eq. 6-2 as:

$$S_{MT} = S_{MS} = 1.50 \tag{18}$$

This also defines the period domain as short for all archetypes. The 4 archetypes for each performance group are defined by the index archetypes 1-4 with exterior dimensions summarized in Table 4.10.

Table 4.10: Summary of arch overall dimensions

Arch Index	Wall Height (ft)	Peak Height (ft)	Span (ft)	Aspect Ratio (Peak Height/Span)
1	16	40	40	1:1
2	16	40	80	1:2
3	16	40	120	1:3
4	20	65	165	1:2.3

4.4 P-695 Analyses

4.4.1 Performance Groups

Once the models have been created and arranged within their respective performance groups, the analyses required for P-695 can be conducted. The analyses necessary for the P-695 evaluations were all conducted using the P-695 toolkit created at Virginia Tech. This toolkit greatly accelerates and streamlines the P-695 process. The first step within the toolkit is to define the performance group by entering relevant information as seen in Figure 4.21.

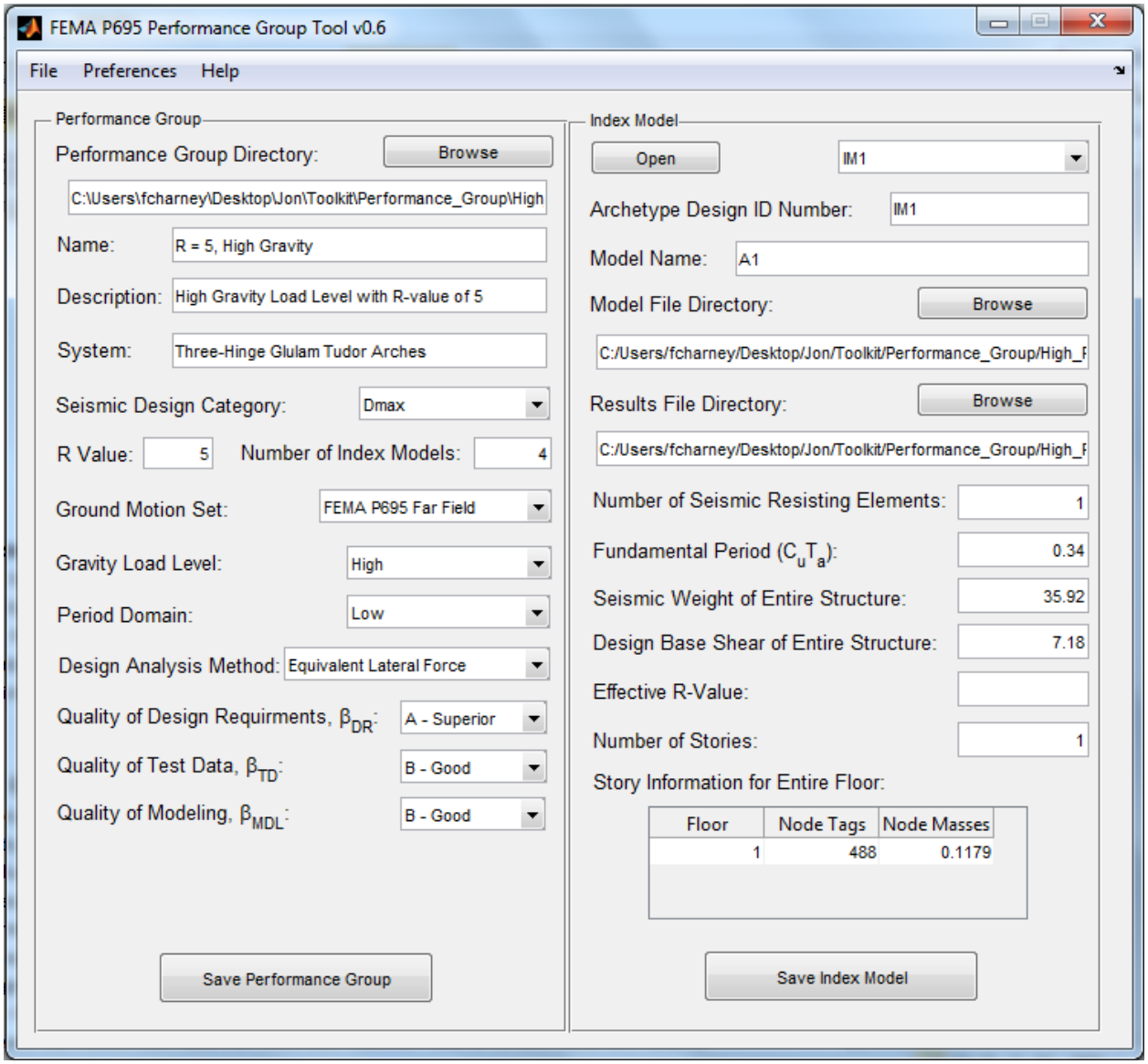

Figure 4.21: Performance group definition tool within P-695 toolkit

The seismic design category was defined as D_{max} within the AWC white paper and is input as the SDC for the toolkit (AWC, 2013). The design R-values range from 1.5 to the minimum design for the designs provided and there are four index models within each performance group evaluated which correspond to the four arch ID's. These structures are assumed to be more than 10 kilometers from the nearest fault so the Far-Field set containing 22 ground motion pairs was used for all evaluations. The gravity load level is defined as either high or low depending which scenario is being analyzed for the given performance group. To define the period domain, the transition period must be determined using P-695 Equation 5-1 (FEMA, 2009b):

$$T_S = \frac{S_{M1}}{S_{MS}} = \frac{0.9}{1.5} = 0.6\ sec \tag{19}$$

Because the transition period is larger than the fundamental periods for all archetypes, the period domain is defined as short for all performance groups. The design analysis method was defined as

Equivalent Lateral Force for all arch designs (AWC, 2013). The uncertainty values used will be discussed at a later point.

4.4.2 Pushover Analyses

Once the performance groups have been developed, analyses can then be conducted on the models within the performance groups. The first analyses to be conducted are static pushover analyses. Within the P-695 toolkit, the pushover tool is as seen in Figure 4.22.

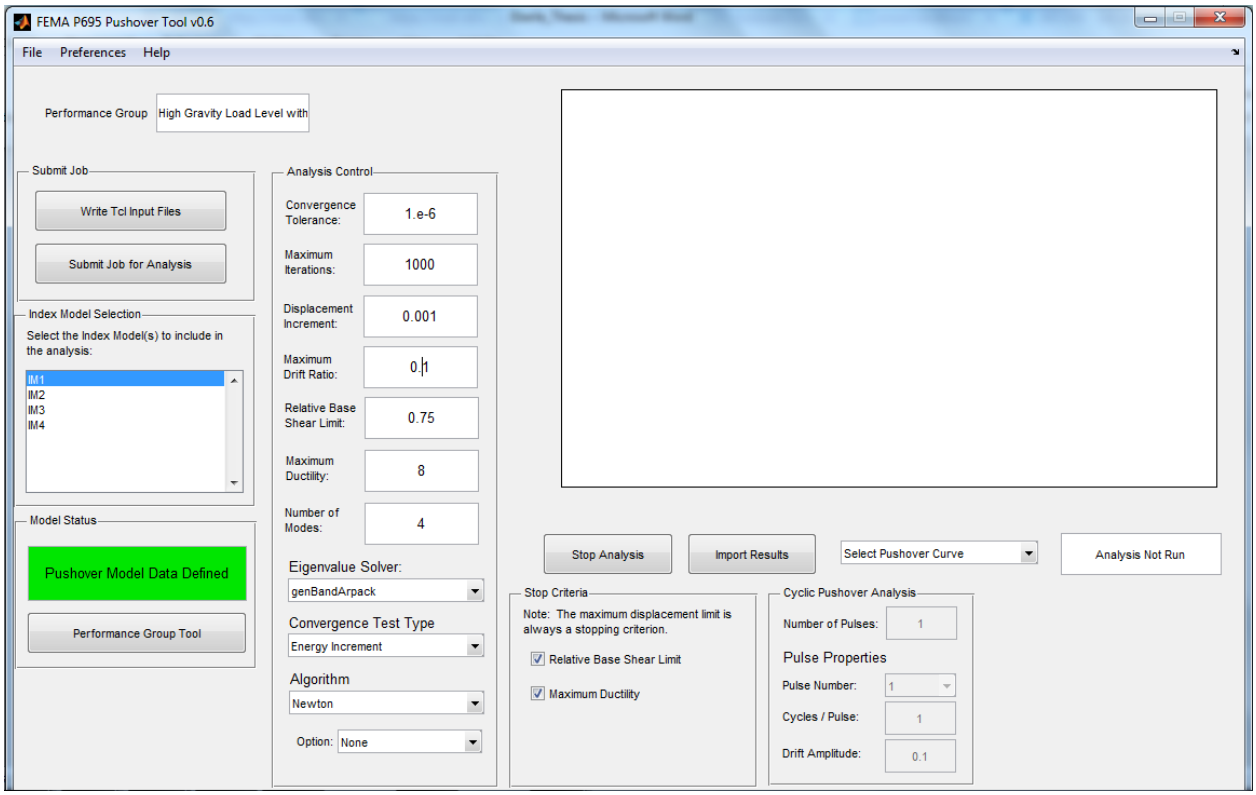

Figure 4.22: Pushover tool within P-695 toolkit

The pushover tool conducts two important analyses for each index archetype. The first analysis is an eigenvalue analysis which calculates the natural periods of vibration for the first n modes, where n is the number of modes requested by the toolkit input. The periods of vibration are used later within the P-695 process to define modal damping for the models. The second analyses conducted by the pushover tool are static pushover analyses. Within a typical P-695 evaluation, a pushover curve would be expected to look like that of the figure on the right of Figure 4.23, however because of the extensively linear nature of the models being analyzed, the resulting pushover curves are linear like the figure on the left.

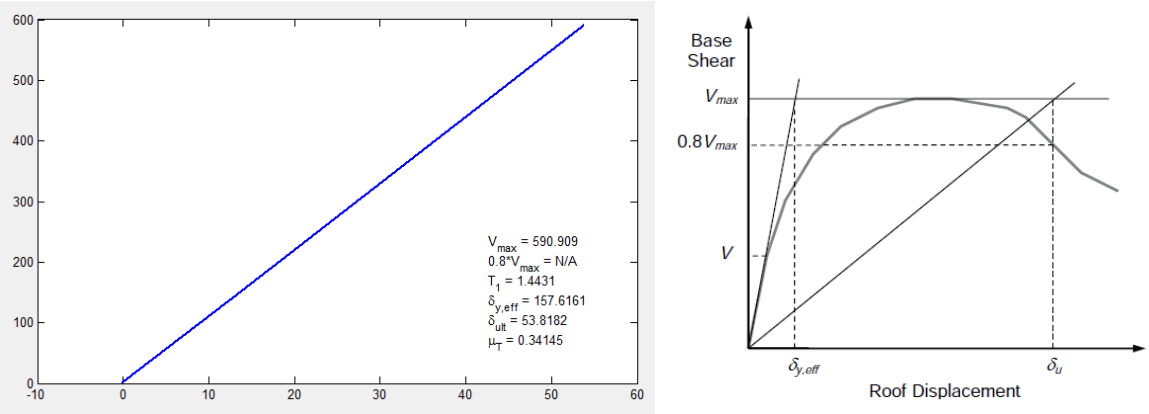

Figure 4.23: Linear pushover curve resulting from analysis (left) and typical pushover curve for extensively nonlinear system (right)

Typically the pushover curve is used to calculate the static overstrength and period based ductility of a given system, but the linear pushover curves resulting from analysis of the provided arch designs do not allow these values to be determined in this manner. Rather, the period based ductility was determined to be the minimum value used in P-695 of 1.0 due to the lack of nonlinear behavior of the structure. This assumption was validated by Charles Kircher, Project Technical Director for FEMA P-695 project

4.4.3 P-695 Ground Motions

The third module within the P-695 toolkit is the ground motion tool. This tool scales the selected ground motions from their recorded accelerations to the MCE level required in P-695. As previously mentioned, the far-field set is used for all evaluations within this project. These ground motion acceleration records are scaled by multiplying by two factors including the anchoring scale factor and the normalization scale factor. These scale factors are functions of the damping ratio, fundamental period of the structure, and SDC. The anchoring scale factor, which is the same for each ground motion within the set, ensures that the median spectral acceleration of the record set matches the spectral acceleration at the fundamental period of the index archetype (FEMA 2009). The second factor applied is the normalization scaling factor which varies for each component pair. This factor is intended to remove variability between records due to several site, event, and distance differences without eliminating record-to-record variability (FEMA 2009). The ground motion tool seen in Figure 4.24 multiplies the ground motion records by the scale factors to create the MCE level ground motions to be used for the dynamic analyses.

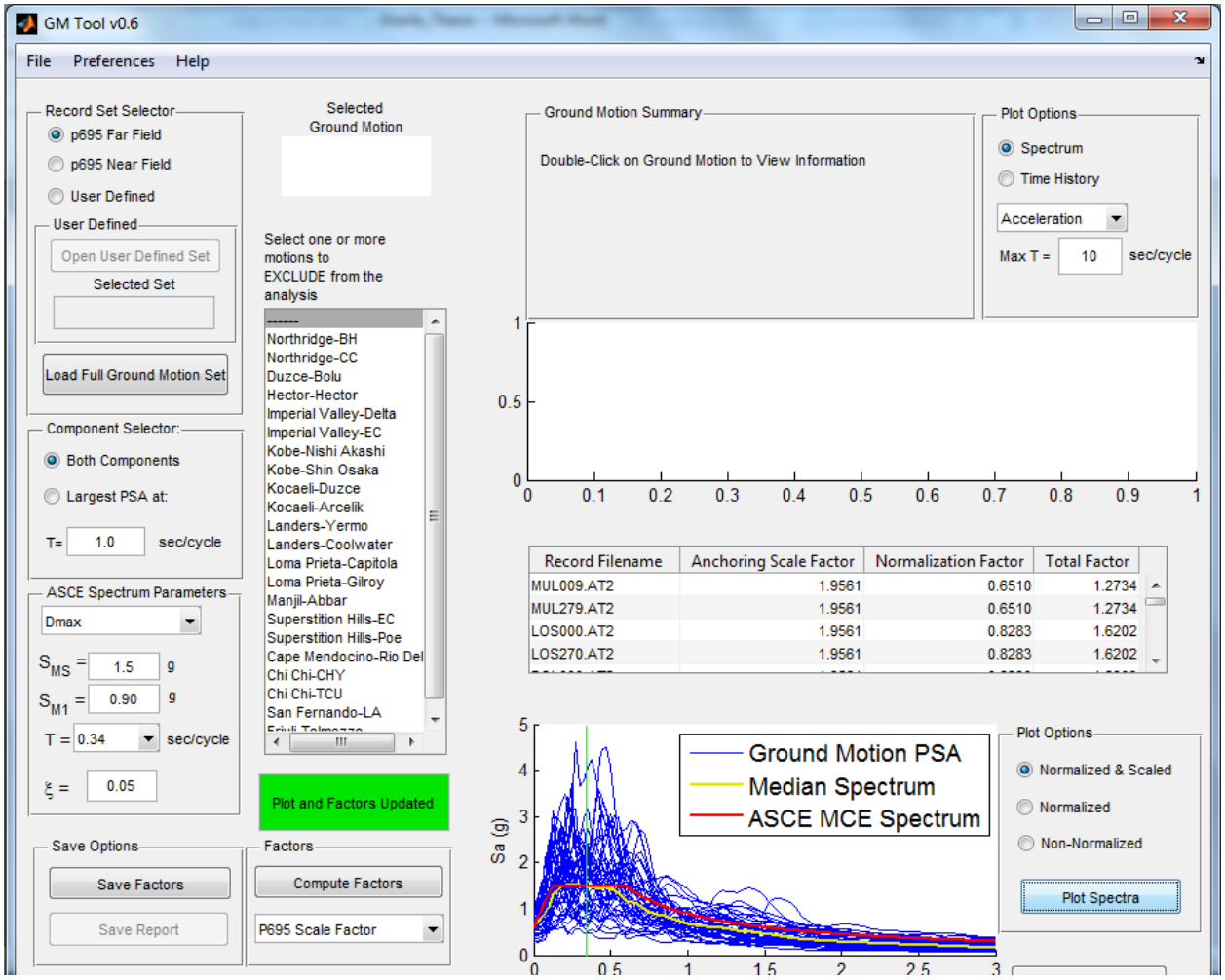

Figure 4.24: Ground motion module within P-695 toolkit

4.4.4 IDA Tool

The Incremental Dynamic Analysis (IDA) tool within the toolkit is used to conduct the IDA analyses required for P-695 evaluations. An IDA is like the dynamic version of a static pushover analysis, however rather than increasing the lateral load applied to the structure, the analysis increments the scale factor applied to the previously calculated MCE level ground motions. The purpose of an IDA is to determine the scale factor at which the structural system collapses, similar to how the purpose of a pushover analysis is to determine the base shear at which the structure collapses. The toolkit IDA module can be seen in Figure 2.25.

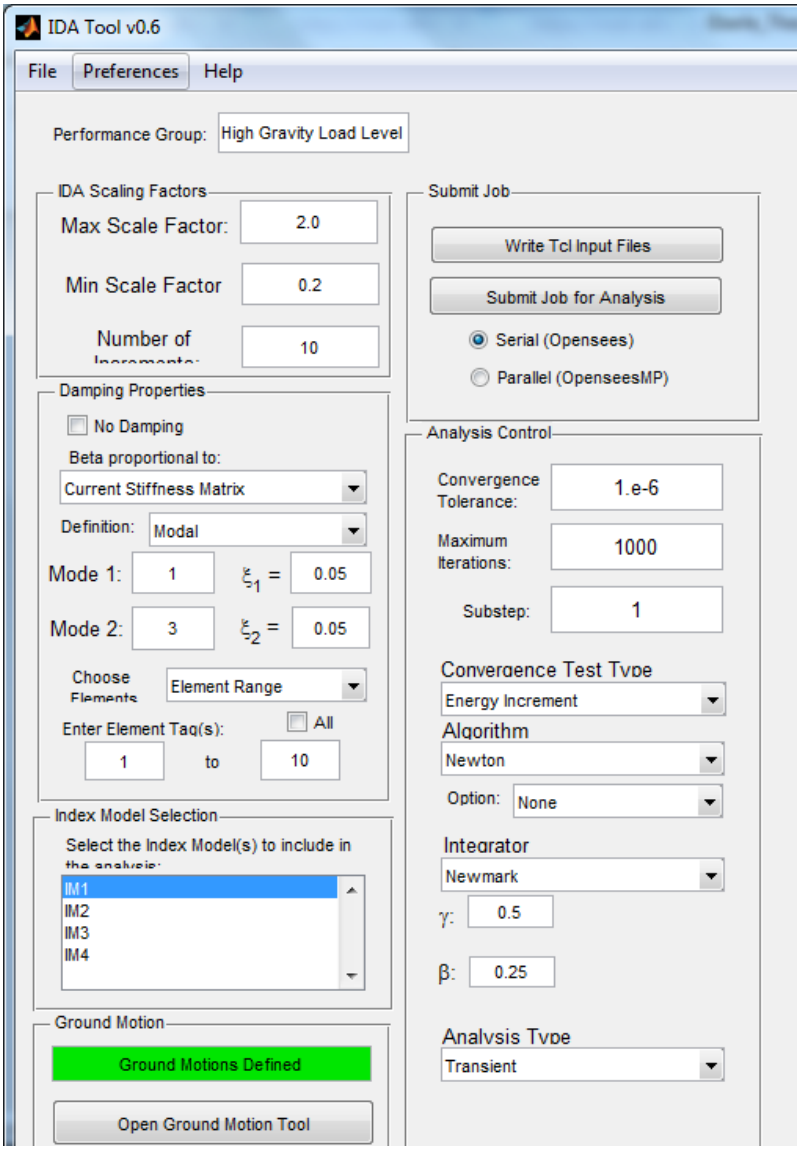

Figure 4.25: IDA toolkit module

The IDA tool allows the user to define the maximum scale factor for analysis, the minimum scale factor for analysis, and the number of scale factors to analyze. In highly nonlinear structures, many scale factors would need to be analyzed to precisely determine the CMR. As previously defined, the CMR is the lowest scale factor at which half of the ground motions cause collapse. The IDA tool also allows the user to apply damping to the elements within the structure. For this project, modal damping was applied with a damping ratio equal to 2.5% of critical for the quad elements within the arch. The last option that the IDA tool allows is for the user to define the analysis controls such as convergence type, integrator, substep etc.

4.5 Non-Simulated Collapse Limits

The Non-Simulated Collapse (NSC) limits represent a failure of the structural system when one or more of them are reached. The NSC limits defined for the three-hinge glulam Tudor arches include:

- bending stress limits for the glulam

- failure of the peak connection due to shear
- failure of the base connection due to outward shear
- failure of the base connection due to inward shear

4.5.1 Glulam Failure Limit

As discussed within the literature review, the glulam material has an expected strength of 7010 psi. To determine the location of maximum stresses within the arch, a small study was conducted where a lateral point load was applied at the peak of the arch and the longitudinal bending stresses along the outside and inside surfaces of the arch were monitored. The results from this study showed that the location of maximum stresses occurred near the arm and leg tangent points but not exactly at them. Because of this, stresses were measured on the outer faces of the member for several elements on each side of the arm and leg tangent points to ensure that the maximum stress was captured.

4.5.2 Connection Capacities

As previously discussed, designs were provided for a total of 56 different arches encompassing variations in gravity load level, overall arch dimensions, and design R-values. Of the four Non-Simulated Collapse (NSC) failure limits which are checked within the dynamic analyses, only three of them vary from one arch design to the next. The longitudinal stress NSC limit is the same for all arch designs because the arch material is assumed to be the same for all designs; however, the connection capacities have been designed to resist the applied loads for each individual design. As previously mentioned, the nominal connection capacities provided within the arch designs require modification to convert the nominal connection capacities to expected capacities for use in the P-695 process. The factors previously discussed within the literature review were used to convert the connection capacities from their nominal capacity to their expected capacity. All arch connection NSC limits (expected connection capacities) are summarized in Table 4.11. Connection designs that have the same dimensions and therefore the same connection strengths as the design with the next lower R-value are highlighted in red italic.

Table 4.11: Summary of connection strengths for both low (a) and high (b) gravity load levels

Arch ID	R	Base Outward Shear [kips]	Base Inward Shear [kips]	Peak Shear [kips]
1L	1.5	46.10	41.48	*27.33*
	2	34.84	35.10	27.33
	2.5	27.33	22.97	27.16
	3	22.64	18.95	27.16
	4	19.59	17.55	17.24
	5	18.44	17.55	17.15
	Min.	15.28	1.48	13.98
2L	1.5	58.25	33.62	21.99
	2	50.42	20.86	21.90
	2.5	45.38	17.55	19.92
	3	42.92	*17.55*	19.75
	4	*42.92*	*17.55*	*19.75*
	5	*42.92*	*17.55*	*19.75*
	Min.	*42.92*	1.36	*19.75*
3L	1.5	90.81	17.55	25.98
	2	*90.81*	*17.55*	*25.98*
	2.5	*90.81*	*17.55*	*25.98*
	3	*90.81*	*17.55*	*25.98*
	4	*90.81*	*17.55*	*25.98*
	5	*90.81*	*17.55*	*25.98*
	Min.	*90.81*	1.36	*25.98*
4L	1.5	126.77	43.58	32.01
	2	*126.77*	17.55	*32.01*
	2.5	*126.77*	*17.55*	*32.01*
	3	*126.77*	*17.55*	*32.01*
	4	*126.77*	*17.55*	*32.01*
	5	*126.77*	*17.55*	*32.01*
	Min.	*126.77*	1.62	*32.01*

(a)

Arch ID	R	Base Outward Shear [kips]	Base Inward Shear [kips]	Peak Shear [kips]
1H	1.5	68.13	53.14	35.73
	2	52.33	41.73	27.68
	2.5	43.11	35.10	28.44
	3	36.46	22.97	27.12
	4	30.69	*17.55*	26.95
	5	26.89	17.55	26.88
	Min.	19.04	1.39	23.40
2H	1.5	80.49	33.62	21.32
	2	70.53	20.86	21.30
	2.5	63.01	17.55	19.32
	3	57.92	*17.55*	18.62
	4	*52.92*	*17.55*	18.55
	5	*52.92*	*17.55*	*18.55*
	Min.	*52.92*	1.31	*18.55*
3H	1.5	113.95	17.55	36.28
	2	110.49	*17.55*	*36.28*
	2.5	*110.49*	*17.55*	*36.28*
	3	*110.49*	*17.55*	*36.28*
	4	*110.49*	*17.55*	*36.28*
	5	*110.49*	*17.55*	*36.28*
	Min.	*110.49*	1.38	*36.28*
4H	1.5	167.56	48.29	42.07
	2	151.81	17.55	41.98
	2.5	*151.81*	*17.55*	*41.98*
	3	*151.81*	*17.55*	*41.98*
	4	*151.81*	*17.55*	*41.98*
	5	*151.81*	*17.55*	*41.98*
	Min.	*151.81*	1.63	*41.98*

(b)

Chapter 5 : Results and Discussion

5.1 Modal Analysis Results

Within the analyses conducted by the toolkit, the first four periods of vibration for each of the models were calculated for use in applying the modal damping to the elements for dynamic analyses. The first natural period of vibration for each model are summarized in Tables 5.1 and 5.2 along with the fundamental periods calculated using ASCE 7-10 provisions.

Table 5.1: Fundamental period and first period of vibration for low gravity load level designs

Arch ID	R-Value	$T = C_u T_A$ (sec)	T_1 (sec)
1L	1.5	0.34	0.55
	2	0.34	0.77
	2.5	0.34	0.91
	3	0.34	1.12
	4	0.34	1.59
	5	0.34	1.93
	Min.	0.34	3.04
2L	1.5	0.34	0.77
	2	0.34	1.00
	2.5	0.34	1.16
	3	0.34	1.27
	4	0.34	1.27
	5	0.34	1.27
	Min.	0.34	1.27
3L	1.5	0.34	0.87
	2	0.34	0.87
	2.5	0.34	0.87
	3	0.34	0.87
	4	0.34	0.87
	5	0.34	0.87
	Min.	0.34	0.87
4L	1.5	0.47	1.12
	2	0.47	1.12
	2.5	0.47	1.12
	3	0.47	1.12
	4	0.47	1.12
	5	0.47	1.12
	Min.	0.47	1.12

Table 5.2: Fundamental period and first period of vibration for low gravity load level designs

Arch ID	R-Value	$T = C_u T_A$ (sec)	T_1 (sec)
1H	1.5	0.34	0.55
	2	0.34	0.78
	2.5	0.34	1.00
	3	0.34	1.05
	4	0.34	1.35
	5	0.34	1.58
	Min.	0.34	2.94
2H	1.5	0.34	0.71
	2	0.34	0.84
	2.5	0.34	0.98
	3	0.34	1.10
	4	0.34	1.18
	5	0.34	1.18
	Min.	0.34	1.18
3H	1.5	0.34	0.79
	2	0.34	0.83
	2.5	0.34	0.83
	3	0.34	0.83
	4	0.34	0.83
	5	0.34	0.83
	Min.	0.34	0.83
4H	1.5	0.47	1.30
	2	0.47	1.40
	2.5	0.47	1.40
	3	0.47	1.40
	4	0.47	1.40
	5	0.47	1.40
	Min.	0.47	1.40

As these tables show, the first natural period calculated using OpenSees are all greater than the fundamental periods determined using ASCE 7-10 provisions. Also, although the fundamental period calculated using ASCE 7-10 is not dependent on the design R-value, the first period of vibration determined computationally is dependent on the design R-value, as would be expected.

5.2 Dynamic Analysis Results

As previously discussed, P-695 defines the Collapse Margin Ratio as the lowest ground motion intensity at which one-half of the records cause collapse (22 of the 44 ground motion records within the Far-Field Set). This was determined by defining collapse of the structure as the lowest scale factor at which one of the NSC limits previously discussed are reached for each ground motion.

Because of the linear response of the NSC criteria as seen in Figure 5.1, the ground motions were run at multiple scale factors and then a linear interpolation was conducted to determine the exact scale factor at failure.

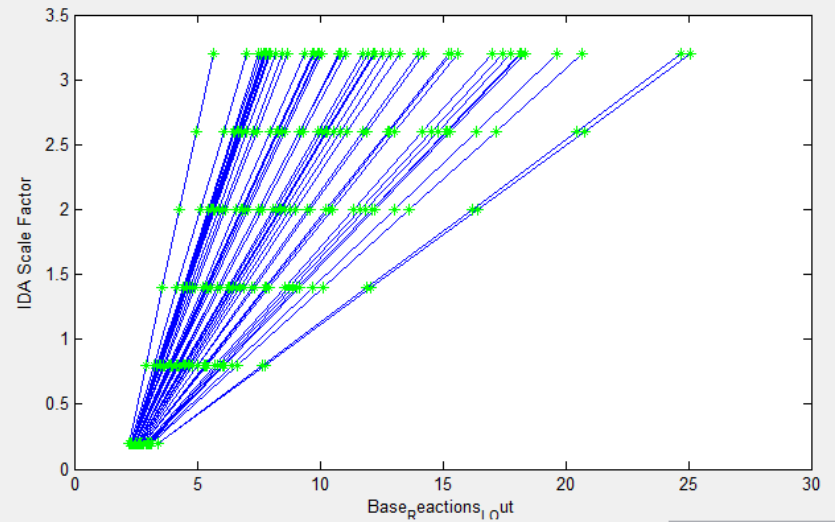

Figure 5.1: IDA curves for Base Reaction Forces

Once the scale factor at failure was determined for each of the 44 ground motions, the scale factors were ordered from lowest to highest and the 22nd scale factor was chosen as the CMR. The CMR's were determined for both the basic designs and the overstrength designs for the arches. Within the arch designs provided, the overstrength combination involves designing and detailing the arch in an attempt to prevent less ductile failure modes from occurring. In particular, the peak shear connections were designed for both basic and overstrength combinations such that the increased capacity of the overstrength combination used for peak shear design might reduce failures within the peak shear connection. The CMR values are presented in Tables 5.3 and 5.4 for both low and high gravity load levels.

Table 5.3: Summary of collapse margin ratios for the low gravity load level

Archetype ID	Performance Group	Arch Index	R-Value	CMR
111	PG-1	1	1.5	0.92
112		2		2.06
113		3		1.67
114		4		2.50
121	PG-2	1	2	1.50
122		2		2.38
123		3		1.67
124		4		1.50
131	PG-3	1	2.5	1.80
132		2		2.05
133		3		1.67
134		4		1.50
141	PG-4	1	3	1.92
142		2		2.30
143		3		1.67
144		4		1.50
151	PG-5	1	4	2.05
152		2		2.30
153		3		1.67
154		4		1.50
161	PG-6	1	5	1.99
162		2		2.30
163		3		1.67
164		4		1.50
171	PG-7	1	Min. Design	1.58
172		2		0.41
173		3		0.35
174		4		0.35

Table 5.4: Summary of collapse margin ratios for the high gravity load level

Archetype ID	Performance Group	Arch Index	R-Value	CMR
211	PG-1	1	1.5	0.69
212		2		0.99
213		3		1.25
214		4		1.97
221	PG-2	1	2	0.88
222		2		1.17
223		3		1.32
224		4		1.38
231	PG-3	1	2.5	1.26
232		2		1.21
233		3		1.32
234		4		1.38
241	PG-4	1	3	1.25
242		2		1.39
243		3		1.32
244		4		1.38
251	PG-5	1	4	1.38
252		2		1.34
253		3		1.32
254		4		1.38
261	PG-6	1	5	1.41
262		2		1.34
263		3		1.32
264		4		1.38
271	PG-7	1	Min. Design	1.08
272		2		0.32
273		3		0.30
274		4		0.35

To better understand the cause of failure within the arches leading to the determined CMR value, the failure limits reached for each arch are summarized in Tables 5.5 and 5.6. These values represent the percentage of ground motions which fail (of the 44 ground motions within the Far-Field set) as a result of the given NSC limit. For example the first failure limit reached for arch ID 1 with a minimum design for 59% of the ground motion records corresponds to base inward shear and for 41% of the ground motion records corresponds to bending stresses within the arch.

Table 5.5: Summary of which NSC limits are causing collapse for low gravity load level given in % of ground motions failing for the given NSC limit

Arch ID	R-Value	Base Outward Shear	Base Inward Shear	Peak Shear	Bending Stresses
1L	1.5	0%	0%	100%	0%
	2	0%	0%	100%	0%
	2.5	0%	0%	100%	0%
	3	0%	0%	0%	100%
	4	0%	0%	21%	79%
	5	0%	0%	0%	100%
	Min.	0%	59%	0%	41%
2L	1.5	0%	0%	100%	0%
	2	0%	97%	3%	0%
	2.5	0%	97%	3%	0%
	3	0%	84%	6%	10%
	4	0%	84%	6%	10%
	5	0%	84%	6%	10%
	Min.	0%	100%	0%	0%
3L	1.5	0%	100%	0%	0%
	2	0%	100%	0%	0%
	2.5	0%	100%	0%	0%
	3	0%	100%	0%	0%
	4	0%	100%	0%	0%
	5	0%	100%	0%	0%
	Min.	0%	100%	0%	0%
4L	1.5	0%	28%	72%	0%
	2	0%	100%	0%	0%
	2.5	0%	100%	0%	0%
	3	0%	100%	0%	0%
	4	0%	100%	0%	0%
	5	0%	100%	0%	0%
	Min.	0%	100%	0%	0%

Table 5.6: Summary of which NSC limits are causing collapse for high gravity load level given in % of ground motions failing for the given NSC limit

Arch ID	R-Value	Base Outward Shear	Base Inward Shear	Peak Shear	Bending Stresses
1H	1.5	0%	0%	100%	0%
	2	0%	0%	100%	0%
	2.5	0%	0%	100%	0%
	3	0%	0%	100%	0%
	4	0%	0%	16%	84%
	5	0%	0%	0%	100%
	Min.	0%	14%	0%	86%
2H	1.5	0%	0%	100%	0%
	2	0%	2%	98%	0%
	2.5	0%	5%	95%	0%
	3	0%	0%	100%	0%
	4	0%	2%	98%	0%
	5	0%	2%	98%	0%
	Min.	0%	100%	0%	0%
3H	1.5	0%	100%	0%	0%
	2	0%	100%	0%	0%
	2.5	0%	100%	0%	0%
	3	0%	100%	0%	0%
	4	0%	100%	0%	0%
	5	0%	100%	0%	0%
	Min.	0%	100%	0%	0%
4H	1.5	0%	29%	71%	0%
	2	0%	100%	0%	0%
	2.5	0%	100%	0%	0%
	3	0%	100%	0%	0%
	4	0%	100%	0%	0%
	5	0%	100%	0%	0%
	Min.	0%	100%	0%	0%

As these results show, the failure limits being reached are dominated by peak shear for the smaller (narrower) arches because of the aspect ratios for those arches. As the results transition from the smaller arches to the larger arches, the NSC limits causing failure change from peak shear to inward forces at the base connection. This transition is the result of the changing aspect ratio which reduces the shear forces in the peak and allows the base shear forces to control.

Along with the previously presented basic load combination results, the IDA results were also compiled for the overstrength load combination. Because the computational models used for the dynamic analyses are not dependent on the NSC limits, the results from the IDA analyses can be used to

determine the overstrength CMR's as well. Do determine the overstrength CMR values, the NSC limit related to peak shear is increased to the overstrength expected capacity. All other NSC limits remain the same because the overstrength combination designs only altered the capacity of the peak shear connection. The results for the overstrength combinations are presented within Appendix B for high and low gravity loads along with the summaries of which NSC limits are causing failure.

5.3 Performance Group Evaluation

The first required step relating to evaluating the performance groups is to determine the Adjusted Collapse Margin Ratios (ACMR). To determine the ACMR, the period based ductility and subsequently the Spectral Shape Factor (SSF) had to first be determined. The period based ductility could not be determined using Eq. 6-6 from P-695 because the limited amount of non-linearity within the models produces a linear pushover curve as seen in Figure 5.2 on the left rather than the expected pushover curve as seen on the right. Because of this linear behavior, it was determined that there is essentially no period based ductility within the structural system and therefore the period based ductility will be taken as the minimum value of 1.0. As previously stated, this assumption was validated by Charles Kircher, Project Technical Director for FEMA P-695 project.

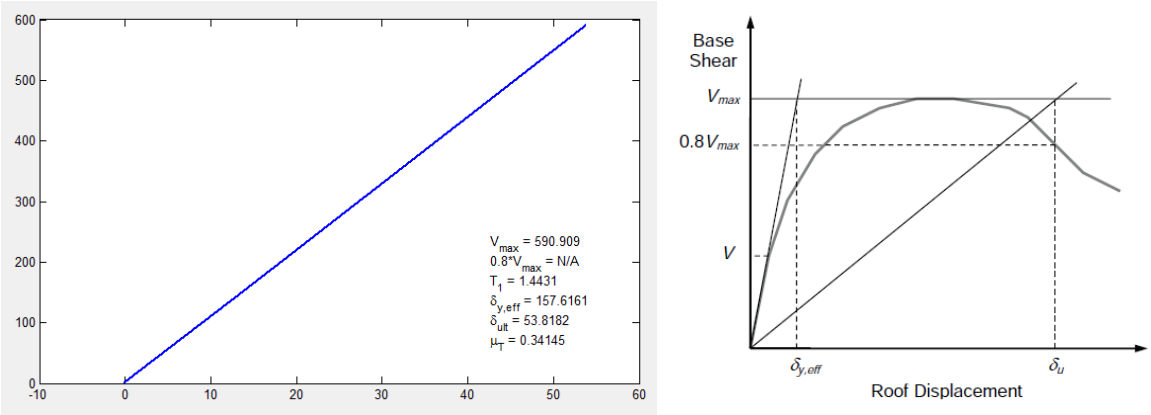

Figure 5.2: Example pushover curve (left) and expected pushover curve (right)

With the period based ductility determined, the SSF was found to be 1.00 for all archetypes from P-695 Tbl. 7-1 (FEMA, 2009b). This is because the SSF is not affected by the fundamental period when the period based ductility, μ_T, is equal to 1.0.

Once the SSF was determined for all archetypes, the Adjusted Collapse Margin Ratio could be found using Eq. 7-1 in P-695 (FEMA, 2009b):

$$ACMR = SSF * CMR \tag{20}$$

Because the Spectral Shape Factor was determined to be 1.0 for all archetypes, the ACMR is simply equal to the CMR for all cases.

To determine whether or not the performance groups under consideration passed the requirements of P-695, the acceptable levels of ACMR needed to be determined. The factors which affect the acceptable ACMR include the record to record and system uncertainties. The record-to-record collapse uncertainty, β_{RTR}, was determined using P-695 Eq. 7-2 to be 0.20 (FEMA, 2009b).

$$\beta_{RTR} = 0.1 + 0.1\mu_T \leq 0.40 \quad (21)$$

$$\beta_{RTR} = 0.1 + 0.1(1.0) = 0.20$$

The system uncertainties include the design requirement uncertainty, test data uncertainty, and modeling uncertainty. The quality of design requirements relates to the confidence in design requirements and design equations used (FEMA, 2009b). Using Table 3-1 of P-695, the quality rating and associated uncertainty of design requirements can be determined. The design requirements used for the arch designs are taken from the NDS for wood construction (AFPA, 2005). The design requirements of the NDS have been used and proven for many years and provide extensive safeguards against failures. Therefore, the uncertainty of design requirements, β_{DR}, was determined to be equal to 0.10.

The quality of test data represents the uncertainty associated with any test data used to characterize any parts of the structural system of interest. For this project, the test data used relates to the adjustment factors used to determine the expected strengths of both the glulam material and the connections. With high confidence in the test results found in research done by others and its relevance to this project, and all individual parts of the system generally understood, the uncertainty of test data, β_{TD}, was determined to be equal to 0.20 from Table 3-2 (FEMA, 2009b).

The last uncertainty parameter used in P-695 is the modeling uncertainty. This uncertainty is related to how well the computational model being used can represent the structural behavior of the system including collapse behavior (FEMA, 2009b). Because finite element models have been used and the models have been checked, there is significant confidence in the ability of the models to represent the behavior of the structural system. This high accuracy in the models coupled with the general ability of the models to encompass effects contributing to collapse, the modeling uncertainty, β_{MDL}, was determined to be equal to 0.20 using Table 5-3 (FEMA, 2009b).

Using the previously defined individual uncertainties, the total system collapse uncertainty, β_{TOT}, was calculated using P-695 Eq. 7-5 (FEMA, 2009b):

$$\beta_{TOT} = \sqrt{\beta_{RTR}^2 + \beta_{DR}^2 + \beta_{TD}^2 + \beta_{MDL}^2} \quad (22)$$

$$\beta_{TOT} = \sqrt{0.20^2 + 0.10^2 + 0.20^2 + 0.20^2} = 0.361$$

Using this equation gives total system collapse uncertainty of 0.361. However, according to P-695, β_{TOT} should be rounded to the nearest 0.025 when calculated using Equation 7-5 (FEMA, 2009b). Therefore, β_{TOT} will be taken as 0.350 for purposes of choosing acceptable ACMR values. Using this value, the acceptable ACMR values were determined using Tbl. 7-3 from P-695 and are given in Table 5.7.

Table 5.7: Summary of Acceptable ACMR values

β_{RTR}	0.2
β_{DR}	0.1
β_{TD}	0.2
β_{MDL}	0.2
β_{TOT}	0.361
Accept. $ACMR_{10\%}$	1.57
Accept. $ACMR_{20\%}$	1.34

From P-695, the average of the ACMR's within a given performance group must be greater than the $ACMR_{10\%}$ and all individual ACMR values within a performance group must be greater than the $ACMR_{20\%}$ for the performance group to pass. If one or both of these criteria are not met, the performance group fails (FEMA, 2009b).

Within Tables 5.8 and 5.9, the performance groups have been evaluated for both the low and high gravity load scenarios.

Table 5.8: Performance group evaluation for low gravity load levels

Archetype ID	Performance Group	Arch Index	R-Value	ACMR	Accept. $ACMR_{20\%}$	PG ACMR	Accept. $ACMR_{10\%}$	Pass/Fail
111	PG-1	1	1.5	0.92	1.34	1.79	1.57	FAIL
112		2		2.06	1.34			
113		3		1.67	1.34			
114		4		2.50	1.34			
121	PG-2	1	2	1.50	1.34	1.76	1.57	PASS
122		2		2.38	1.34			
123		3		1.67	1.34			
124		4		1.50	1.34			
131	PG-3	1	2.5	1.80	1.34	1.76	1.57	PASS
132		2		2.05	1.34			
133		3		1.67	1.34			
134		4		1.50	1.34			
141	PG-4	1	3	1.92	1.34	1.84	1.57	PASS
142		2		2.30	1.34			
143		3		1.67	1.34			
144		4		1.50	1.34			
151	PG-5	1	4	2.05	1.34	1.88	1.57	PASS
152		2		2.30	1.34			
153		3		1.67	1.34			
154		4		1.50	1.34			
161	PG-6	1	5	1.99	1.34	1.86	1.57	PASS
162		2		2.30	1.34			
163		3		1.67	1.34			
164		4		1.50	1.34			
171	PG-7	1	Min. Design	1.58	1.34	0.67	1.57	FAIL
172		2		0.41	1.34			
173		3		0.35	1.34			
174		4		0.35	1.34			

Table 5.9: Performance group evaluation for high gravity load levels

Archetype ID	Performance Group	Arch Index	R-Value	ACMR	Accept. $ACMR_{20\%}$	PG ACMR	Accept. $ACMR_{10\%}$	Pass/Fail
211	PG-1	1	1.5	0.69	1.34	1.22	1.57	FAIL
212		2		0.99	1.34			
213		3		1.25	1.34			
214		4		1.97	1.34			
221	PG-2	1	2	0.88	1.34	1.19	1.57	FAIL
222		2		1.17	1.34			
223		3		1.32	1.34			
224		4		1.38	1.34			
231	PG-3	1	2.5	1.26	1.34	1.29	1.57	FAIL
232		2		1.21	1.34			
233		3		1.32	1.34			
234		4		1.38	1.34			
241	PG-4	1	3	1.25	1.34	1.33	1.57	FAIL
242		2		1.39	1.34			
243		3		1.32	1.34			
244		4		1.38	1.34			
251	PG-5	1	4	1.38	1.34	1.35	1.57	FAIL
252		2		1.34	1.34			
253		3		1.32	1.34			
254		4		1.38	1.34			
261	PG-6	1	5	1.41	1.34	1.36	1.57	FAIL
262		2		1.34	1.34			
263		3		1.32	1.34			
264		4		1.38	1.34			
271	PG-7	1	Min. Design	1.08	1.34	0.51	1.57	FAIL
272		2		0.32	1.34			
273		3		0.30	1.34			
274		4		0.35	1.34			

As seen, some of the performance groups for low gravity load levels are passing the evaluation, however not all and none of the high gravity load level evaluations are passing. The results are, nevertheless, not what might be expected in that the middle R-values are passing rather than the lower R-values. This is thought to possibly be the result of the first natural period of the structure. As the design R-value decreases, the arch members themselves become larger in cross sectional dimension and therefore the system becomes stiffer. This additional stiffness decreases the first natural period of vibration for the arch. Especially for the arch ID 1L, the period of vibration decreases significantly between the design R-values of 2 and 1.5 from 0.765 seconds to 0.550 seconds. This shortening of period could be contributing

to the drastic increase in observed seismic response that is evident in the significant CMR reduction. Another reason that the CMR is decreasing drastically for the low gravity load levels with arch ID 1 is that the connection capacity for basic load combinations does not increase from the design R-value of 2 to the design R-value of 1.5. The peak connection capacity does increase for the high gravity load cases which is why the trend is much more gradual as the R-values decrease. It is because of this problematic arch 1L with design R-value equal to 1.5 that the PG-1 is not passing for the low gravity load levels.

The performance groups were also evaluated for the designs where overstrength combinations have been considered for design of the arch peak connection. The evaluations of these performance groups are provided in Tables 5.10 and 5.11.

Table 5.10: Performance group evaluation for low gravity load levels, considering overstrength combinations

Archetype ID	Performance Group	Arch Index	R-Value	ACMR	Accept. $ACMR_{20\%}$	PG ACMR	Accept. $ACMR_{10\%}$	Pass/Fail
111	PG-1	1	1.5	1.71	1.34	1.98	1.57	PASS
112		2		2.06	1.34			
113		3		1.67	1.34			
114		4		2.50	1.34			
121	PG-2	1	2	2.18	1.34	1.93	1.57	PASS
122		2		2.38	1.34			
123		3		1.67	1.34			
124		4		1.50	1.34			
131	PG-3	1	2.5	1.80	1.34	1.76	1.57	PASS
132		2		2.05	1.34			
133		3		1.67	1.34			
134		4		1.50	1.34			
141	PG-4	1	3	1.92	1.34	1.84	1.57	PASS
142		2		2.30	1.34			
143		3		1.67	1.34			
144		4		1.50	1.34			
151	PG-5	1	4	2.05	1.34	1.88	1.57	PASS
152		2		2.30	1.34			
153		3		1.67	1.34			
154		4		1.50	1.34			
161	PG-6	1	5	1.99	1.34	1.86	1.57	PASS
162		2		2.30	1.34			
163		3		1.67	1.34			
164		4		1.50	1.34			
171	PG-7	1	Min. Design	1.58	1.34	0.67	1.57	FAIL
172		2		0.41	1.34			
173		3		0.35	1.34			
174		4		0.35	1.34			

Table 5.11: Performance group evaluation for high gravity load levels, considering overstrength combinations

Archetype ID	Performance Group	Arch Index	R-Value	ACMR	Accept. $ACMR_{20\%}$	PG ACMR	Accept. $ACMR_{10\%}$	Pass/Fail
211	PG-1	1	1.5	1.26	1.34	1.46	1.57	FAIL
212		2		1.09	1.34			
213		3		1.25	1.34			
214		4		2.22	1.34			
221	PG-2	1	2	1.66	1.34	1.44	1.57	FAIL
222		2		1.42	1.34			
223		3		1.32	1.34			
224		4		1.38	1.34			
231	PG-3	1	2.5	1.85	1.34	1.50	1.57	FAIL
232		2		1.44	1.34			
233		3		1.32	1.34			
234		4		1.38	1.34			
241	PG-4	1	3	1.62	1.34	1.50	1.57	FAIL
242		2		1.68	1.34			
243		3		1.32	1.34			
244		4		1.38	1.34			
251	PG-5	1	4	1.38	1.34	1.41	1.57	FAIL
252		2		1.56	1.34			
253		3		1.32	1.34			
254		4		1.38	1.34			
261	PG-6	1	5	1.41	1.34	1.41	1.57	FAIL
262		2		1.56	1.34			
263		3		1.32	1.34			
264		4		1.38	1.34			
271	PG-7	1	Min. Design	1.08	1.34	0.51	1.57	FAIL
272		2		0.32	1.34			
273		3		0.30	1.34			
274		4		0.35	1.34			

Although many of the individual CMR's have been increased by considering the overstrength combinations for design of the arch peak connectionas seen in Tables 5.10 and 5.11, the effects of using overstrength combinations on the performance groups themselves were not very significant. The one important change when using the overstrength combinations is that the performance group associated with low gravity load levels and a design R-value of 1.5 passes with overstrength combinations where it did not for basic combinations. This is the result of the peak shear capacity being increased and therefore increasing the CMR of arch ID 1.

5.4 Nonlinear IDA Results

As previously mentioned, a small subset of the models was also analyzed including the nonlinearity of the base connection when loaded toward the inside of the arch. Performance group 1 associated with low gravity load levels and a design R-value of 1.5 was chosen for these analyses. The models were created as discussed previously within this report to model the nonlinearity of the base connections. To ensure that the nonlinear models were performing as expected, the base shear at the left side of the arch has been plotted in Figure 5.3 for the ground motion MUL009 from the Far-Field set with a scale factor of 1.133 applied.

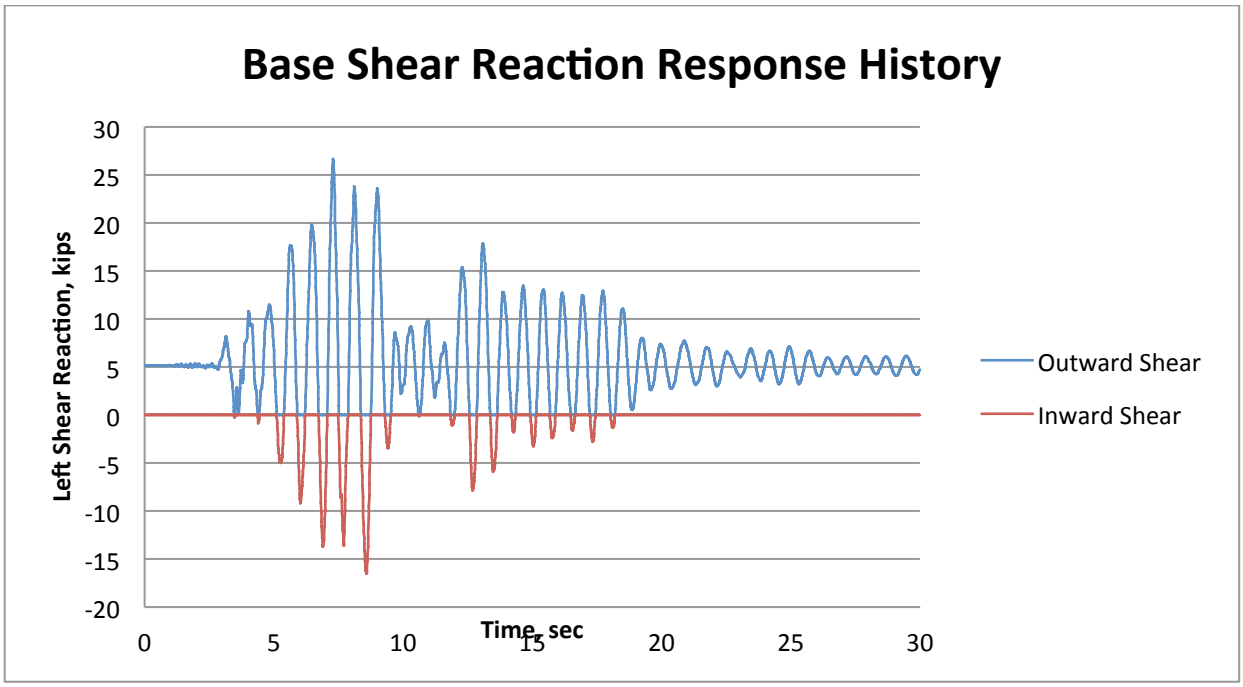

Figure 5.3: Plot of base shear reaction forces at left side of arch for MUL009 ground motion with scale factor of 1.133

Within Figure 5.3, the response of the element being used to represent the stiffness of the connection when the arch is bearing into the shoe is seen in blue, where the response of the nonlinear element which acts when the arch is pulling inward is seen in red. As this plot shows, the model is accurately providing the behavior of the base connection in that the inward shear element resists the shear force when the arch pulls toward the inside, but the outward shear element resists the shear force applied when the arch is providing outward thrust to the connection. With confidence that the elements comprising the base connection were acting at the appropriate times, dynamic analyses moved forward.

Further comparisons were made to provide additional support that the nonlinear elements were indeed providing nonlinear behavior to the system when forces beyond the yield capacity of the bolted connection were applied. To check that this behavior was being observed, two other ground motions was chosen (YER270 and LOS000) from the Far-Field set and the parameters related to the NSC limits were compared for cases where the connection was modeled as linear (fixed) and nonlinear. Figures 5.4 – 5.6 show the resulting forces and stresses for the YER270 ground motion with a scale factor of 1.133.

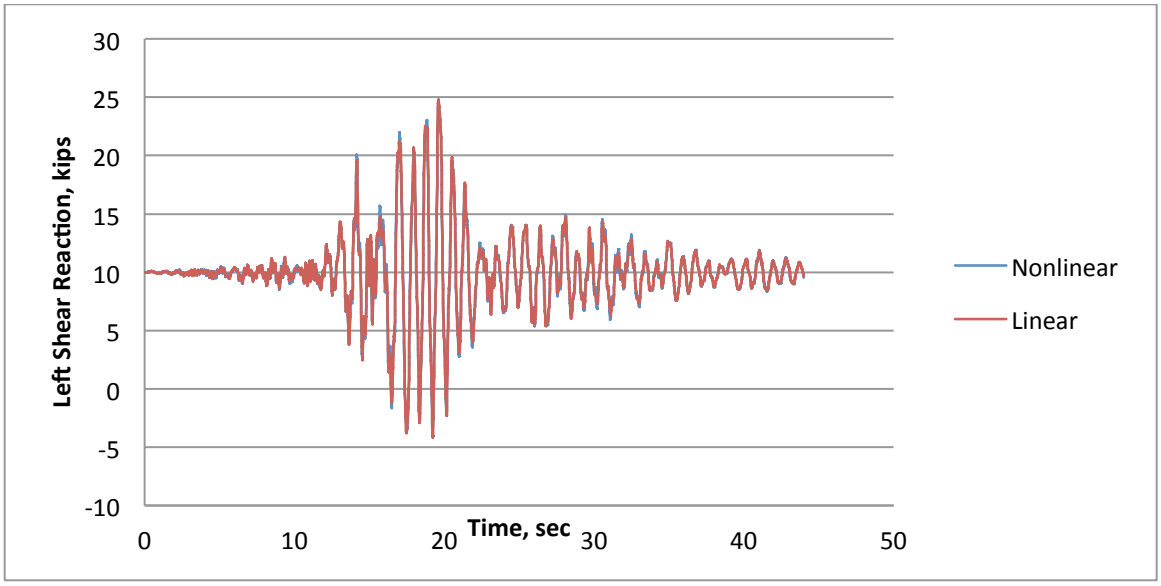

Figure 5.4: Response history plot showing base shear reaction for left side of arch as a function of time

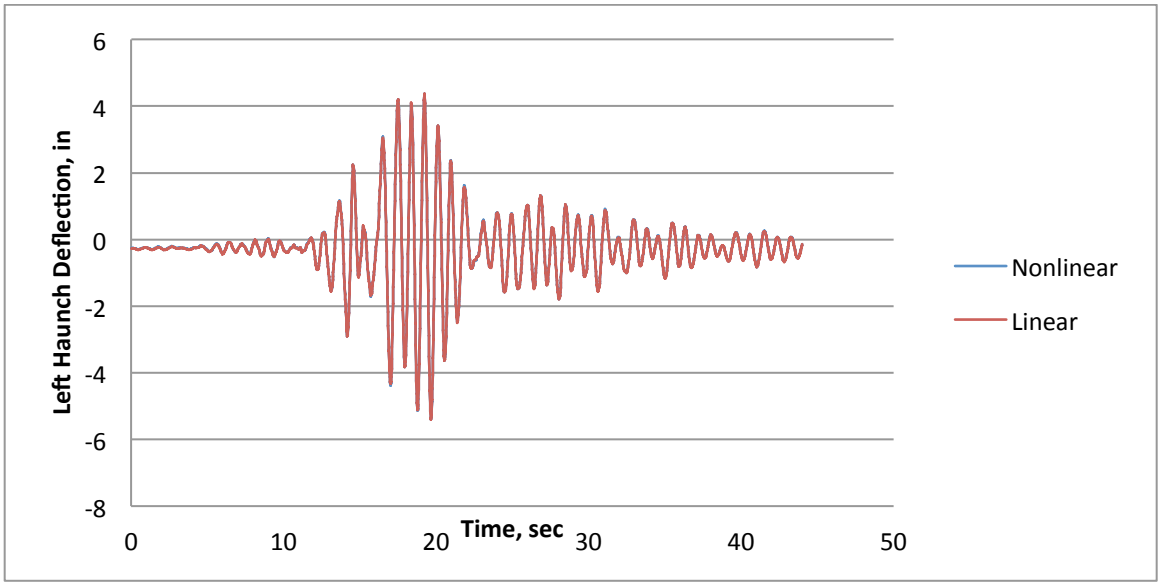

Figure 5.5: Response history plot showing haunch deflection at left haunch as a function of time

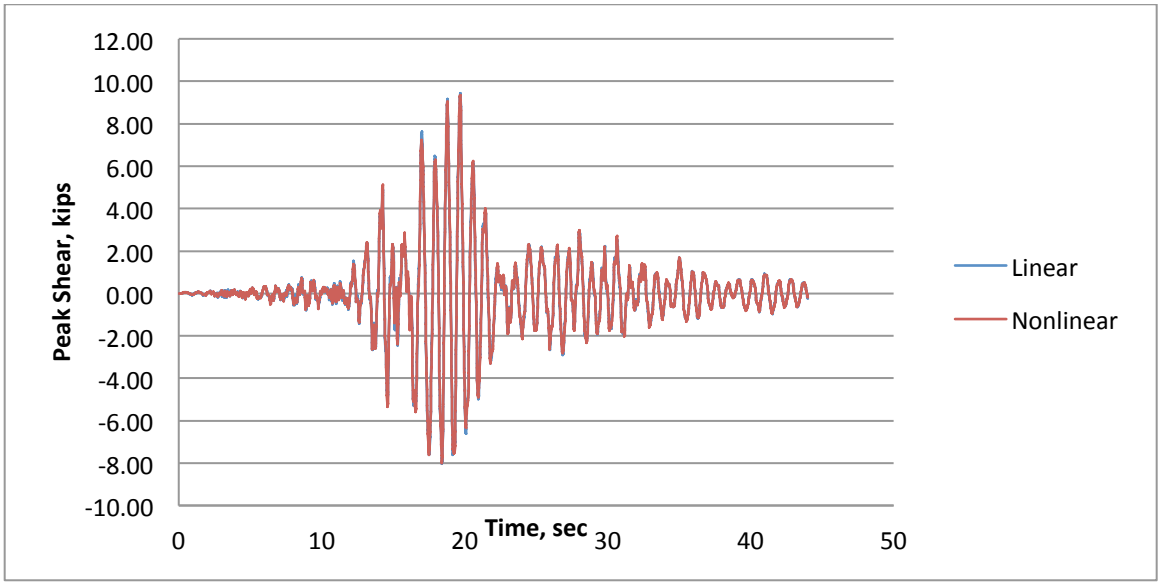

Figure 5.6: Response history plot showing peak shear as a function of time

As Figures 5.4 – 5.6 show, the differences between the linear and nonlinear models are very small at this level of ground motion. Figures 5.7 – 5.9 again show these same resulting forces and stresses for the YER270 ground motion but for a scale factor of 2.067.

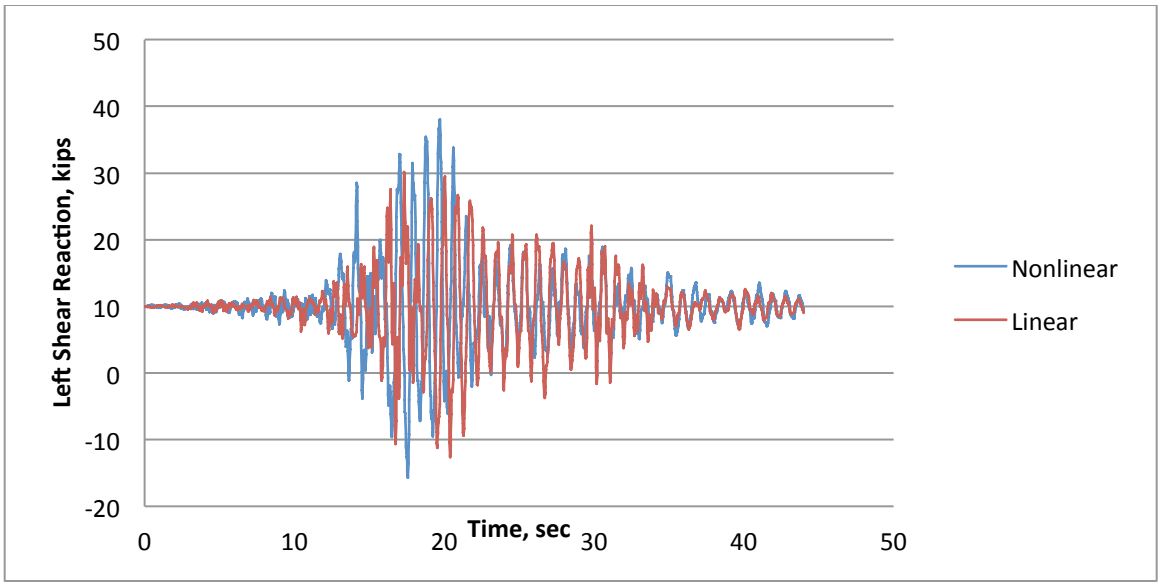

Figure 5.7: Response history plot showing base shear reaction for left side of arch as a function of time

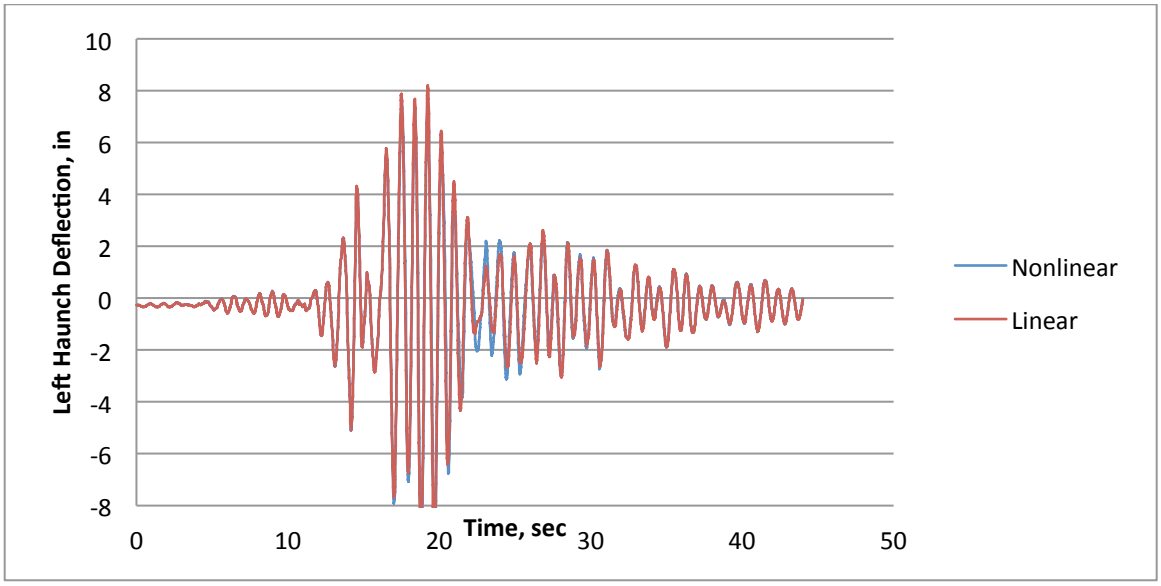

Figure 5.8: Response history plot showing haunch deflection at left haunch as a function of time

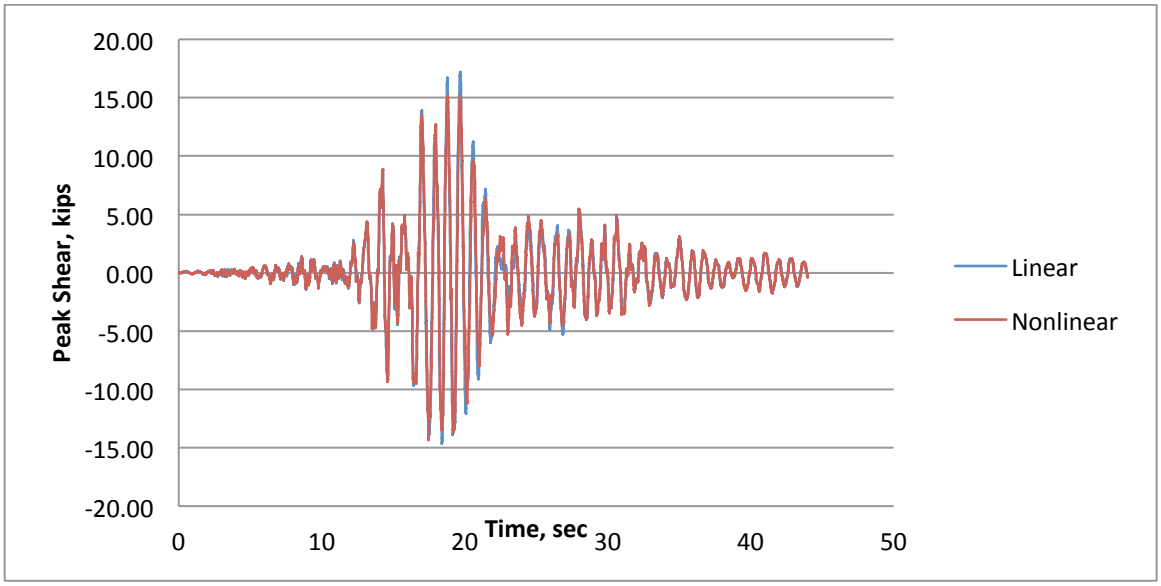

Figure 5.9: Response history plot showing peak shear as a function of time

As Figures 5.7 – 5.9 show, at this larger scale factor significant observable differences can be seen between the linear and nonlinear cases. The largest differences can be seen in the response of the base shear connection but differences are also present for the bending stresses and peak shear forces. The fact that these differences are present for this larger scale factor but not the previous one show that the nonlinear elements within the base connections are acting as they should. The larger ground motion intensities cause the base inward shear forces to become large enough such that they exceed the yield limit of element and behave in a nonlinear fashion as expected. It is also important to note that the resulting base shear forces observed for the nonlinear model actually have greater maximum values than the linear models. This is the result of the unpredictable behavior of nonlinear elements within structures especially when the nonlinearity is limited to the level provided in these models.

Figures 5.7 – 5.12 provide results for ground motion LOS000 with an applied scale factor equal to 1.133.

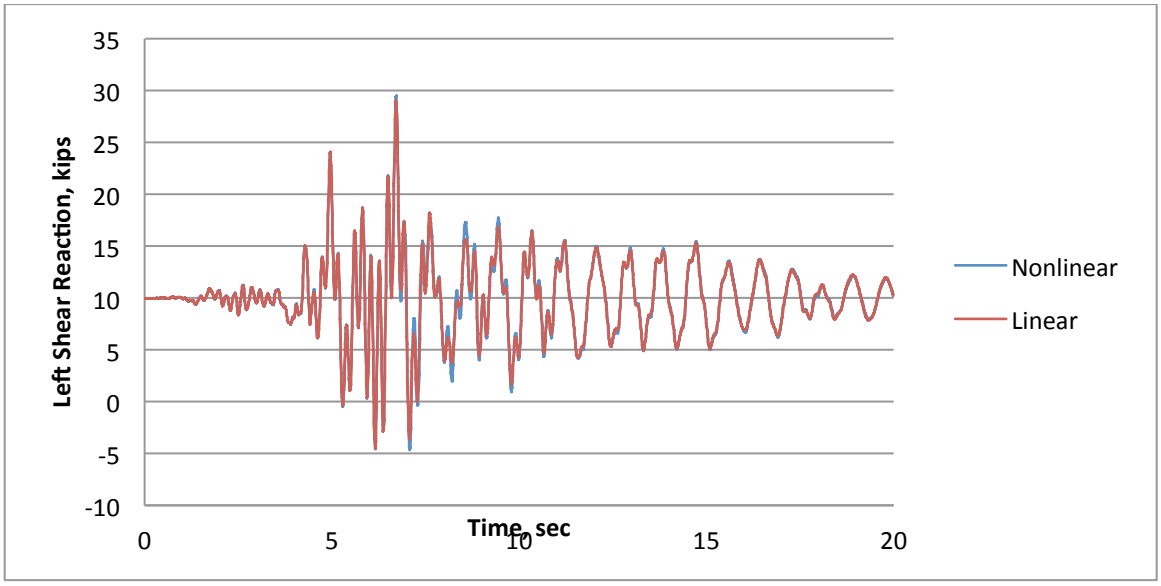

Figure 5.10: Response history plot showing base shear reaction for left side of arch as a function of time

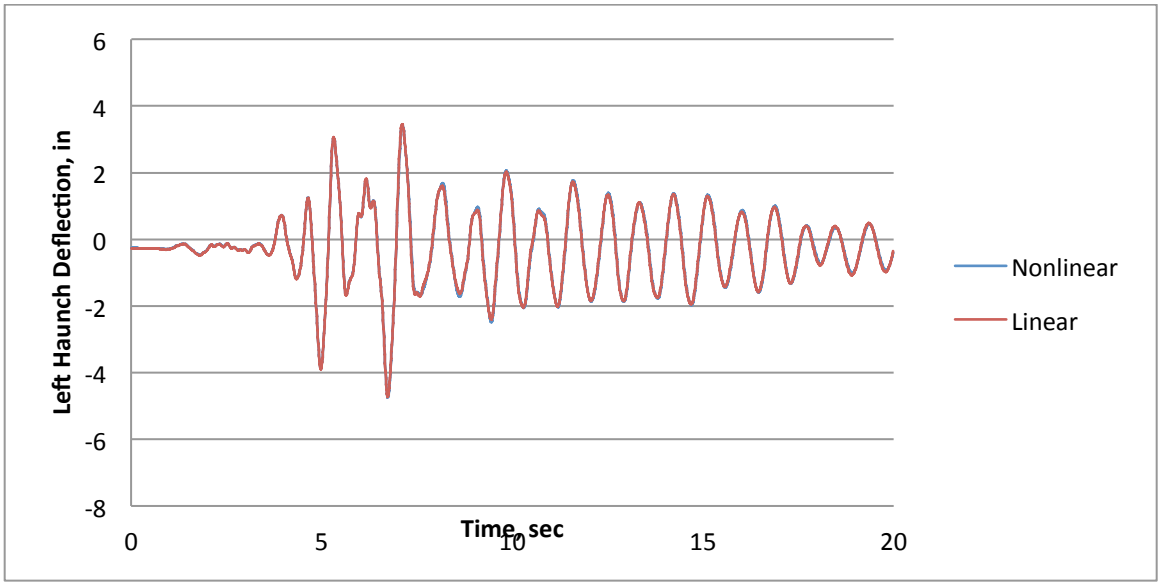

Figure 5.11: Response history plot showing haunch deflection at left haunch as a function of time

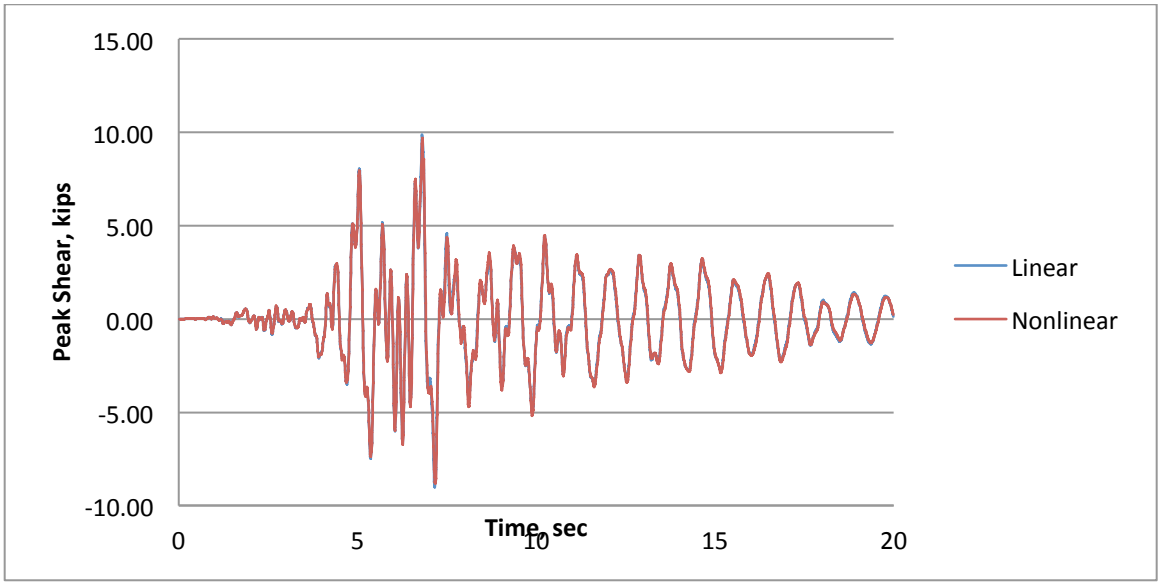

Figure 5.12: Response history plot showing peak shear as a function of time

As Figures 5.10 – 5.12 show, the response of the linear and nonlinear models are again nearly identical because the inward base shear forces are not large enough to activate the nonlinear behavior of the base connection or it has been activated a very limited amount. Figures 5.13 – 5.15 again provide results for ground motion LOS000 but for an applied scale factor of 2.067.

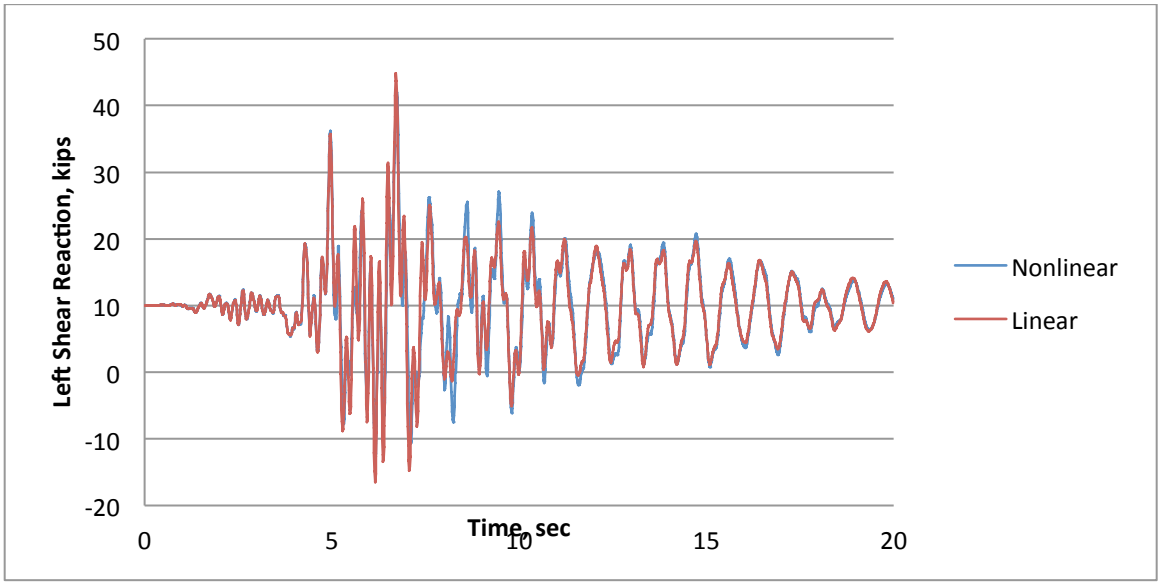

Figure 5.13: Response history plot showing base shear reaction for left side of arch as a function of time

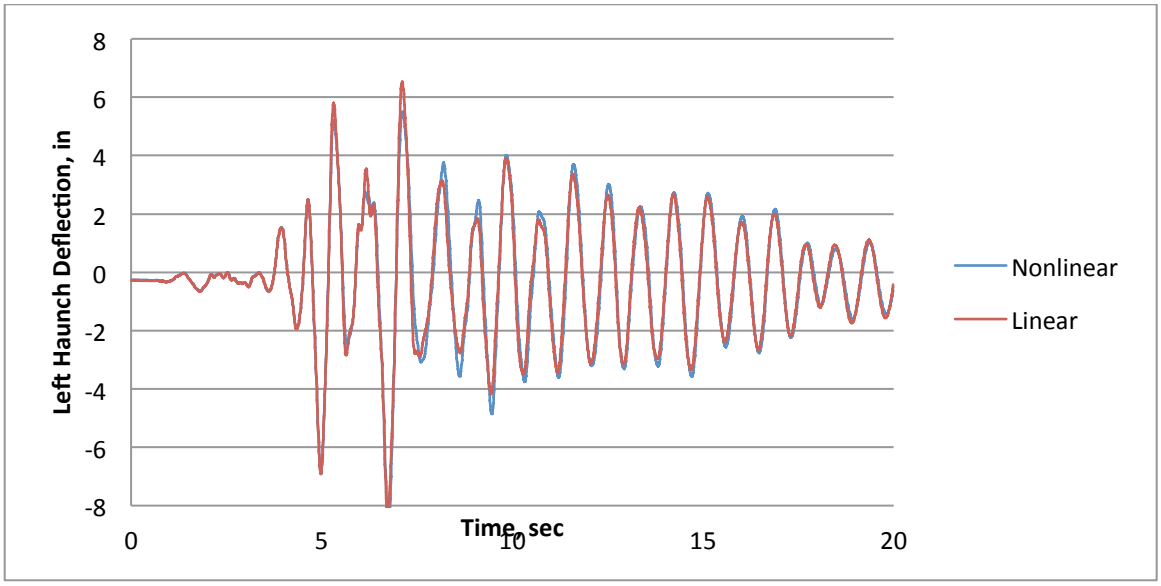

Figure 5.14: Response history plot showing haunch deflection at left haunch as a function of time

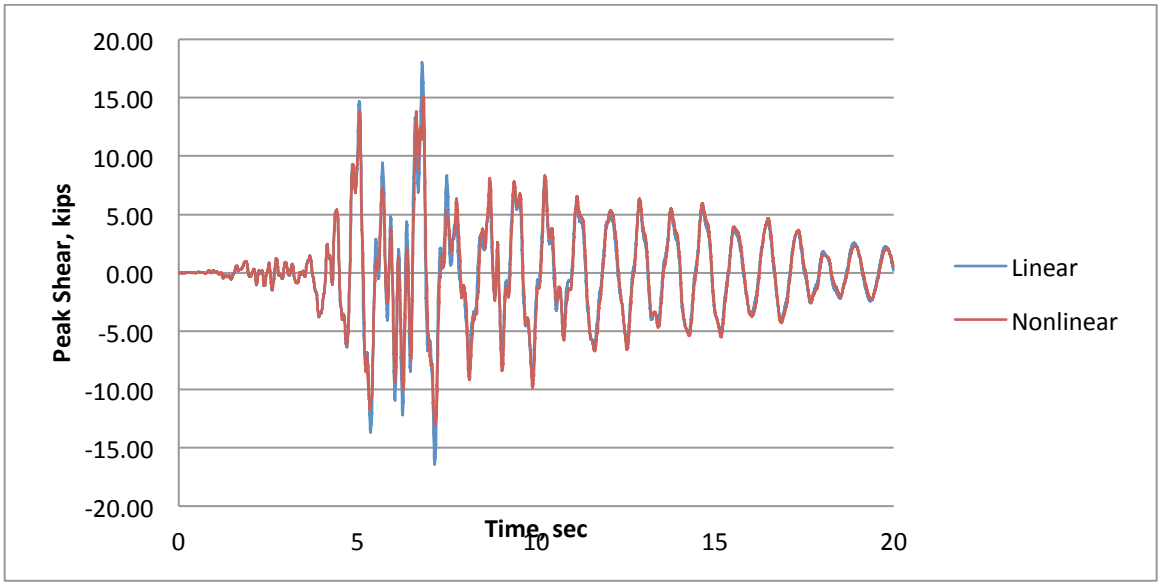

Figure 5.15: Response history plot showing peak shear as a function of time

These results again show that the ground motion intensity has been increased to a level where the nonlinear behavior of the base connection has been activated. This is evident through the fact that the plots of linear and nonlinear response are not the same. The major difference between this set of results and those for ground motion YER270 is that the nonlinear models reduced the observed maximum values of base shear, haunch deflection, and peak shear from the nonlinear results. This further shows that the resulting behavior from adding a limited amount of nonlinear behavior to a model can be unpredictable. From these results, it could be conjectured that the effects of the nonlinear modeling of the base connections on the CMR's could be varied.

With the inclusion of nonlinearity of the base connections, the resulting CMR's for the performance group corresponding to low gravity loads and a design R-value of 1.5 are provided in Table 5.12. Also

provided are the CMR's found for the case when the base connection was modeled as pinned and the amount of difference between the two models.

Table 5.12: CMR results for nonlinear base connection models and comparison the CMR's from linear models

Arch ID	R-Value	Nonlinear CMR	Linear CMR	% Difference	Failure Mode
1L	1.5	1.78	1.71	4.1%	Peak Shear
2L	1.5	1.99	2.06	-3.4%	Peak Shear
3L	1.5	1.93	1.67	15.6%	Base Inward Shear
4L	1.5	2.54	2.50	1.6%	Peak Shear/ Base Inward Shear

As these results demonstrate, the hypothesis that the effects of the nonlinearity on the CMR's would be sporadic is somewhat confirmed. Although one of the arch designs observed a 15% increase in CMR, some of the designs provided a minimal amount of increase, or as can also be seen, one of the designs actually had the CMR decrease when the base connections were modeled as nonlinear. An important thing to note is that the model which provided a significant amount of increase in CMR failed completely due to inward shear at the base connection. Although some of the ground motions for arch ID 4 also failed due to inward shear at the base, failure was controlled for the majority of ground motions by peak shear. Noticing this trend, it is possible that for cases where failure is dominated by inward shear at the base, the CMR could be significantly increased.

Chapter 6 : Conclusions and Recommendations

6.1 Conclusions

The objective of this research project involved determining a seismic response modification factor for three-hinge glulam Tudor arches. In an attempt to meet this objective, P-695 methodology was implemented and incremental dynamic analyses were conducted on each of the provided arch designs for several varied factors. Although some of the performance groups were able to pass for the light gravity load level, none of the performance groups were able to pass for the high gravity load level.

Within P-695, it is required that for a seismic response modification factor to be defined for a given structural system, the performance groups within the low and high gravity load designs must both pass for broad applicability of a given seismic response modification factor. This is a logical requirement in that R-values are not to be dependent on the gravity load applied to a system, but rather are only to be functions of the seismic force resisting system. The issues within this research preventing an R-value from being determined for the given arches are related to the arch designs which were sized for high gravity roof loads. The additional forces and possibly more detrimental the additional masses applied to the arm of the arch are causing the provided designs to fail under the P-695 methodology. Because of this fact, it is suggested that the high gravity load level designs be further investigated.

6.2 Recommendations for Future Research

For an R-value to be determined for the three-hinge glulam Tudor arch systems evaluated within this project, the high gravity load designs will have to be modified in some way to provide CMR values capable of passing the performance group evaluations. This could be achieved in several ways, all of which relate to two fundamental solution methods: increase the capacity of the designs or reduce the demand on the system. The capacity of the system has been designed in accordance with the current design procedures used for glulam arches and therefore those values are set. However if further data supporting increases in connection and/or member capacities could be validated, the failure limits being reached could be increased and therefore the CMR of the models would be increased. For this reason it would be preferable that tests directly relating to the connections being used in design be conducted to determine if further increases in capacities could be attained.

The testing of connections associated with the arch would also provide relevant information related to the behavior of the connections in addition to the capacities. For example if more accurate data could be collected on the base connections, the nonlinear behavior of the bolt bearing due to both shear and overturning moment could be adequately modeled within the computational models and might be able to increase the CMR through added energy dissipation. Another way that the demand on the system could be reduced would be to conduct a full scale test on a three-hinge glulam Tudor arch system. Either dynamic loading or a simple free vibration test would be adequate to provide evidence that a higher damping ratio could be used for the system which would lower the system response as the damping studies have shown.

Additionally, to circumvent the issues which occurred for low gravity load levels using the basic load combinations, it is suggested that the capacity of the peak shear connection be increased. In particular, it is suggested that the peak shear capacity be increased such that the failure of the structural system is

forced into the base connections under inward loading. This requirement would increase the CMR values by increasing the capacity to the capacity of the base connections under inward loading. Additionally, because the nonlinear results show significant benefit when the base connection shear forces control the failure, additional increases in CMR could be observed by taking advantage of the nonlinear behavior of the bolted connections at the base.

References

American Forest & Paper Association. (2005). *National Design Specification (NDS) for Wood Construction.* Washington, DC: American Forest & Paper Association.

American Society of Civil Engineers. (2010). *Minimum design loads for buildings and other structures*. Reston, Va: American Society of Civil Engineers.

American Wood Council. (2013). *Three-Hinge Glulam Tudor Arches.* Washington, DC: American Forest & Paper Association. (Not yet published)

Forest Products Laboratory. (2010). *Wood handbook: Wood as an engineering material*. Madison, WI: United States Department of Agriculture Forest Service.

Federal Emergency Management Agency. (2009a). *NEHRP Recommended Seismic Provisions for New Buildings and Other Structures* (FEMA P-750). Washington, DC: Building Seismic Safety Council.

Federal Emergency Management Agency. (2009b). *Quantification of Building Seismic Performance Factors* (FEMA P-695). Redwood City, CA: Applied Technology Council.

Hernandez, R., Moody, R. C., Falk, R. H. (1995). Fiber Stress Values for Design of Glulam Timber Utility Structures. *Research paper by USDA Forest Products Lab.*

Hernandez, R. Davalos, J. F., Sonti, S. S., Kim, Y., Moody, R. C. (1997). Strength and Stiffness of Reinforced Yellow-Poplar Glued-Laminated Beams. *Research paper by USDA Forest Products Lab.*

Isoda, H. (2000). "Pseudo-Dynamic Test and Evaluation of the Maximum Response of a Glulam Frame Under Big Earthquake Attack". *World Congress on Earthquake Engineering 2000.*

Larson, D., Mirth, R., & Wolfe, R. (2004). Evaluation of Small Diameter Ponderosa Pine Logs in Bending. *Forest Products Journal* 54(12), 52-58.

Linville, J. (2007). Structural Glued Laminated Timber Arches. *STRUCTURE magazine* Feb. 2007.

Longworth, J. (1967). Behavior of Shear Plate Connections in Sloping Grain Surfaces. *Forest Products Journal* 17(7), 49-53.

MATLAB (Version 7.13.0.564(R2011b)) [Computer Software]. Natrick, Massachusetts: MathWorks.

OpenSees (2000). (Version 2.3.2) [Computer Software]. Berkley, CA: University of California.

P-695 Toolkit (2012). (Version 1.0) [Computer Software]. Blacksburg, VA: Virginia Polytechnic Institute and State University.

Portland Bolt & Manufacturing Company (2012a). Shear Plate Installation Procedures. *Shear Plates.* Retrieved April 10, 2013, from http://www.shearplates.com/installation#steps.

Portland Bolt & Manufacturing Company (2012b). Shear Plate Sizes and Dimensions. *Shear Plates.* Retrieved April 10, 2013, from http://www.shearplates.com/sizes.

SAP2000 (2009). (Version 14.0.0) [Computer Software]. Berkley, CA: Computers and Structures, Inc.

Sutoyo, D., and Hall, J. (2006). "Study of Wood-Frame Building Records From the Parkfield and San Simeon Earthquakes". *SMIP06 Seminar Proceedings.*

Wilkinson, T. L. (1968). Strength Evaluation of Round Timber Piles. *Research paper by USDA Forest Products Lab.*

Wilkinson, T. L. (1992). Strength of Bolted Timber Connections with Steel Side Members. *Research paper by USDA Forest Products Lab.*

Wolfe, R. W., & Moody, R. C. (1978). Bending Strength of Water-Soaked Glued Laminated Beams. *Research paper by USDA Forest Products Lab.*

Yeh, C. T., Hartz, B. J., and Brown, C. B. (1971). "Damping Sources in Wood Structures" *Journal of Sound and Vibration*. 19.4 (1971): 411-419. Print.

Appendix A: Arch Model Creation GUI User Guide

A.1 Introduction

The computational models necessary to evaluate the structural behavior of the three-hinge glulam Tudor arches using OpenSees involve large text input files. Because of the finite element modeling deemed necessary to accurately depict the behavior of arches, the text input files vary in length from hundreds to thousands of lines of text. To facilitate the creation of models for analysis, it was determined that a Graphical User Interface (GUI) was needed. This GUI was created in MATLAB because of the availability and ease of GUI creation within MATLAB. Included within the GUI are four MATLAB .m files, one MATLAB .fig file, one folder, and one Microsoft Excel .xlsx file as seen in Figure A.1 in the current folder within the MATLAB command window.

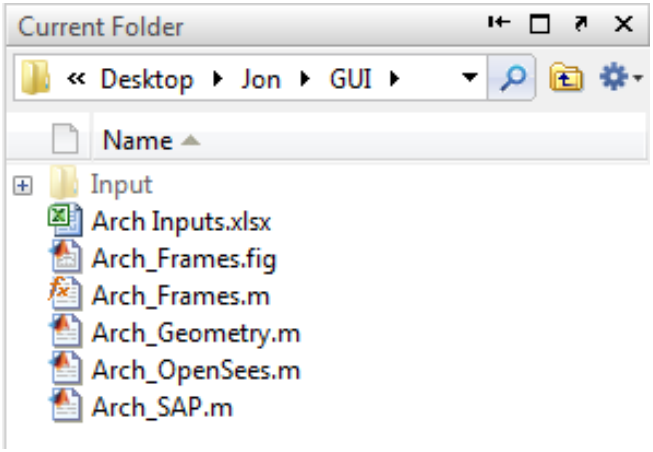

Figure A.1: Current folder of MATLAB command window showing files and folder of GUI

The folder labeled “Input” is the location where all created .tcl files are placed when created by the GUI. The Excel file titled “Arch Inputs” contains the values used for input within the GUI. The Arch_Frames.fig file contains the figure which is viewed when the GUI is run. The Arch_Geometry.m file uses the input parameters from the GUI to create the necessary nodal coordinates and calculate the nodal masses and gravity loads to be applied to the structure. Lastly, the Arch_OpenSees.m and Arch_SAP.m files use the information calculated by the Arch_Geometry.m file to define the model in either OpenSees or SAP2000, respectively.

A.2 GUI Use

To use the GUI, the tool must first be launched by opening MATLAB and making the folder containing the GUI source code files the current folder. This can be done by clicking the “…” button to the right of the current folder as circled in red in Figure A.2.

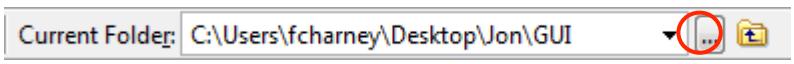

Figure A.2: Locating the GUI source code files and locating them within the current folder

Once the GUI folder has been set to the current folder, the GUI is ready to be launched. To launch the GUI, type Arch_Frames into the Command Window and press return. Once the tool has been launched, the GUI will appear as seen in Figure A.3.

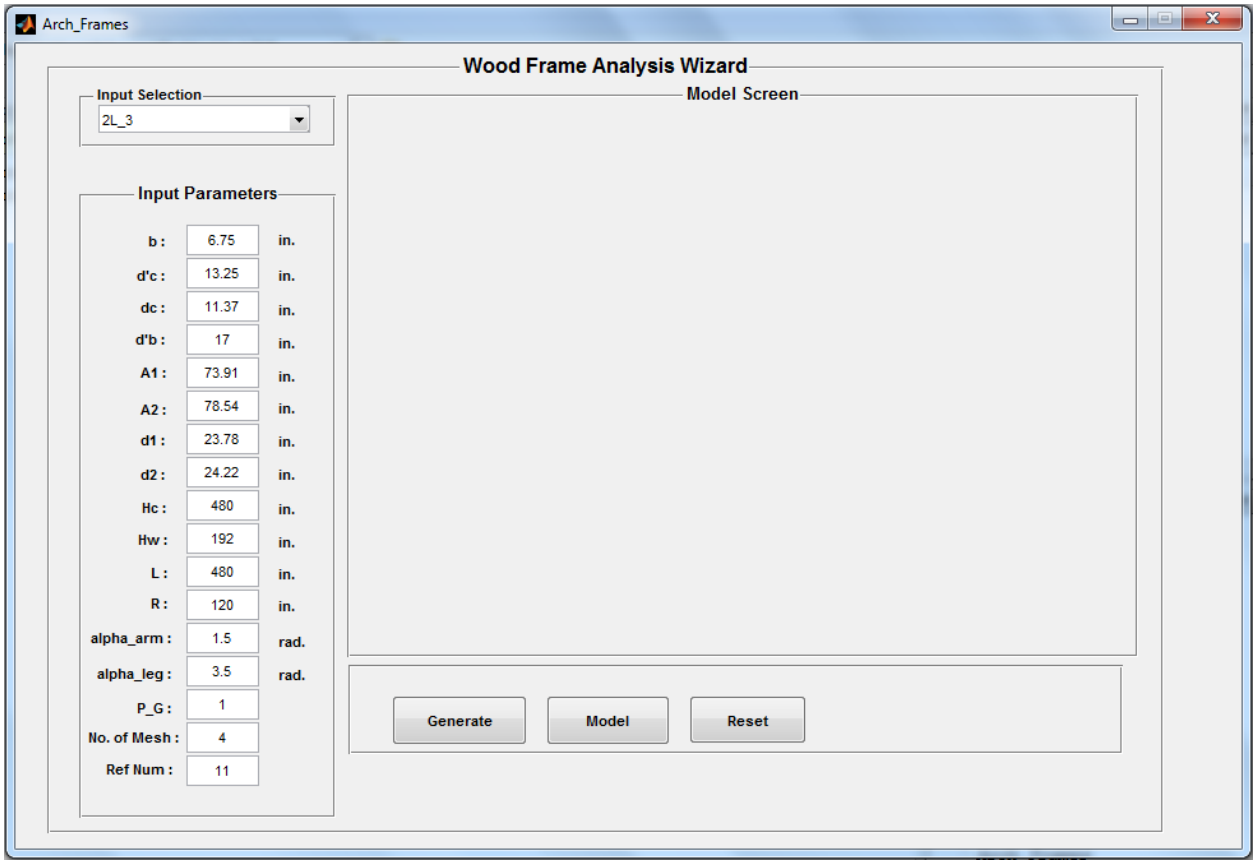

Figure A.3: Model creation GUI

As seen in the above figure, the GUI has four main regions including the input parameters, input selection, control buttons, and model screen. The input parameters region is used to input the values which define the geometry of the arch model. These input parameters are summarized as follows:

b = width of arch in inches

d'c = depth of vertical arch section measured at in units of inches

dc = depth of section at crown measured perpendicular to laminations in units of inches

d'b = depth of section at base measured horizontally in units of inches

A1 = distance from outside of haunch to leg tangent point in units of inches

A2 = distance from outside of haunch to arm tangent point in units of inches

d1 = depth of section at leg tangent point measured horizontally in units of inches

d2 = depth of section at arm tangent point measured perpendicular outside of arm in units of inches

Hc = height of roof at peak in units of inches

Hw = height of wall measured from base to outside of haunch in units of inches

L = half span of Tudor arch in units of inches

R = radius of curvature on inside of haunch section in units of inches

alpha_arm = angle of taper of arm in units of degrees

alpha_leg = angle of taper of leg in units of degrees

P_G = performance group where 1 denotes light gravity loads and 2 denotes heavy gravity loads

No. of Mesh = denotes the number of finite elements across the depth of the arch section

Ref Num = a reference number associated with each arch design to extract relevant information relating to connection capacities for each arch within GUI coding

Although these parameters can be input manually for any given arch dimensions, the parameters for the arch designs used for this project are provided within the AWC white paper. Rather than having to input these parameters manually each time a model is desired to be created, a drop down menu was added to the GUI in the input selection region. This feature allows the user to select any of the 56 arch designs from a drop down list. Doing this automatically inputs the necessary values into the parameter input boxes as seen in Figure A.4 for arch design 2L with a design R-value of 3.

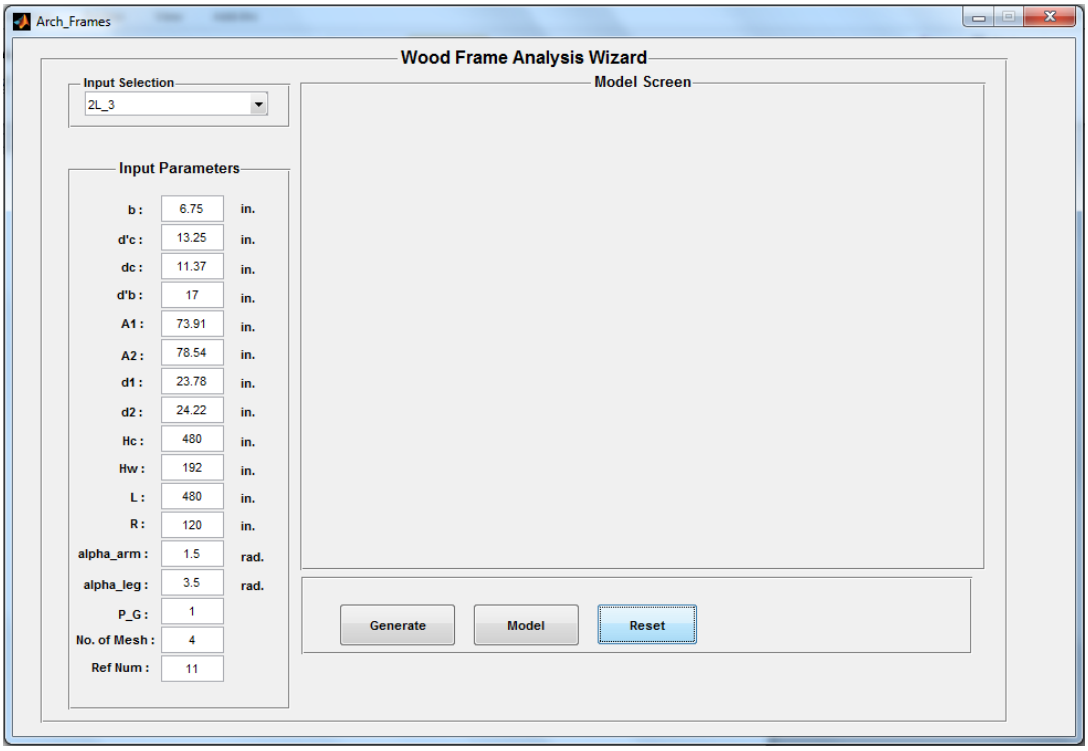

Figure A.4: Model creation GUI where arch 2L with design R-value of 3 has been selected and input values extracted from Excel sheet

Once the necessary input parameters have been defined for the arch design of interest, the model is ready to be created. To create the model, the Generate button must first be clicked. By clicking this button, no visible results are created, rather by clicking this button MATLAB inputs the input parameters into the Arch_Geometry.m file which calculated mesh of the finite element model. The nodal coordinates for each node are calculated based upon the defined geometry. Once these nodal coordinates are defined, the loads and masses associated with each node can also be defined. These forces and masses include components the first of which being the self-weight of the arch which is calculated using an assumed density of the arch material and multiplying it by the volume of each finite element and distributing the forces or masses to the four nodes associated with the element. The second component which contributed to the gravity loads and masses applied to the nodes are related to the gravity loads applied to the roof and walls. These forces or masses are calculated and distributed to the nodes along the outside of the arch where the coverings would be attached based upon tributary area.

After the Generate button has been clicked and the geometry, loads, and masses have been calculated, the Model button can then be clicked to create the computational model. When this button is clicked, the MATLAB code works to create the computational model in either OpenSees or SAP2000. To change which program the model will be created in, the source code contained in the Arch_Frames.m file must be altered. Code lines 513 and 514 relate to which .m file will be accessed to create the model and therefore which program the model will be created for. To create an OpenSees model, the text on line 513 should be active and the text on line 514 should be commented out as seen in Figure A.5.

```
512
513 -    Arch_OpenSees
514      %Arch_SAP;
515
516
517      % --- Executes on button press in pushbutton3.
518      function pushbutton3_Callback(hObject, eventdata, handles)
519      % hObject    handle to pushbutton3 (see GCBO)
520      % eventdata  reserved - to be defined in a future version of MATLAB
521      % handles    structure with handles and user data (see GUIDATA)
522 -    cla(handles.axes1,'reset');
523 -    axis vis3d off
524
525
```

Figure A.5: Arch_Frames.m source code showing code lines which determine what program model is created for

To create a model in SAP2000, the text on line 513 should be commented out and the text on line 514 should be active. Only a limited amount of modeling was done in SAP2000 so the GUI is only currently capable of creating the geometry of the arch. Fixities, masses, loads, and materials must be input manually within the program itself. Where the SAP part of the GUI only creates a preliminary model, the OpenSees model created includes all necessary aspect of the structural model and is ready to analyze once created. Regardless of the program that the model is being created for, when the Model button is clicked, the GUI has also been created such that the geometry of the model is plotted within the model

screen of the GUI. This is helpful to ensure that no errors have occurred during model creation and that no input parameters were drastically wrong. As Figure A.6 shows, the geometry created looks as would be expected for a Tudor arch so the model has been visually confirmed.

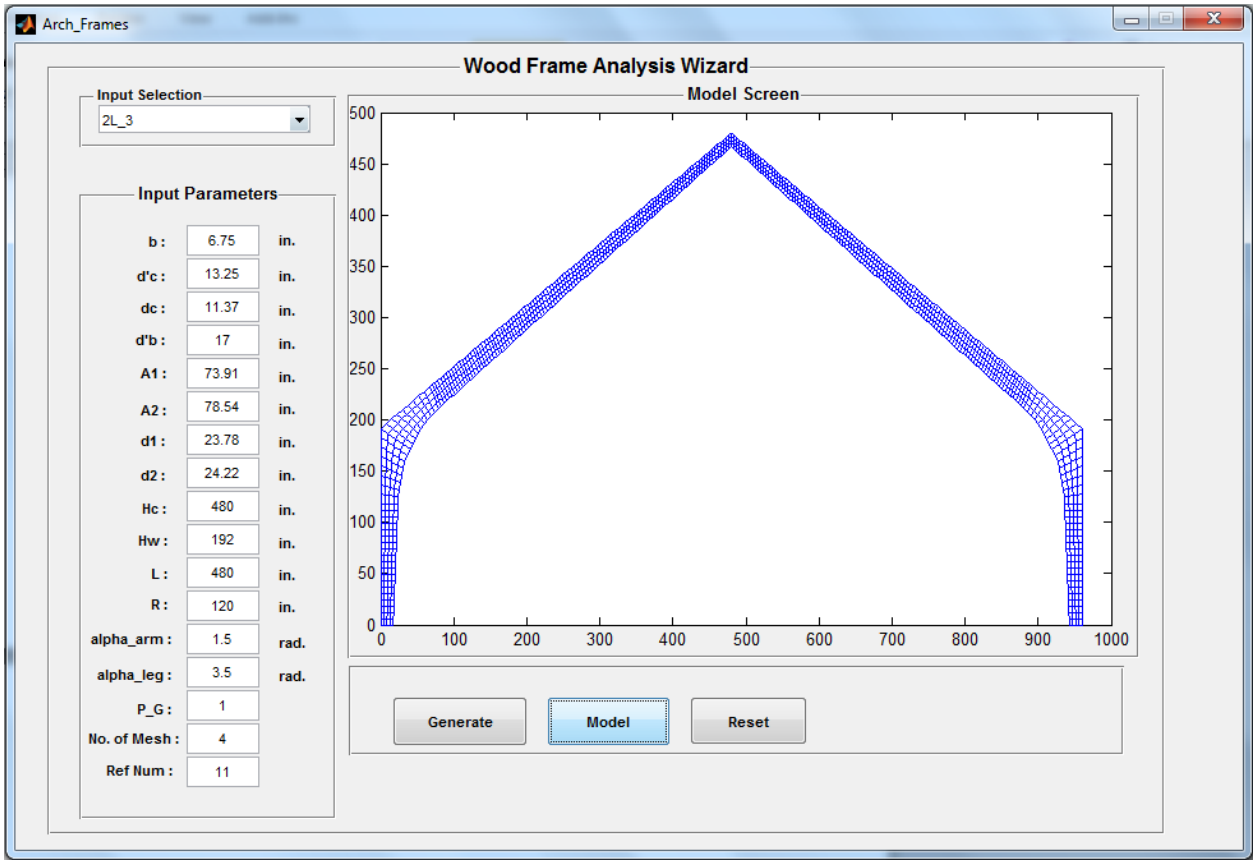

Figure A.6: GUI after Model button has been clicked showing the plotted geometry

For creating OpenSees models, the .tcl input file defining the structural model and the text file which defines the recorder for use within the P-695 toolkit are both created and placed in the input folder previously mentioned.

Appendix B: Additional P-695 Performance Group Evaluations

Presented below are the CMR's for the overstrength combinations for both low and high gravity load. Also summarized in the following tables are the NSC limits causing collapse for the arches.

Table B.1: Summary of collapse margin ratios for the low gravity load level with overstrength combinations

Archetype ID	Performance Group	Arch Index	R-Value	CMR
111	PG-1	1	1.5	1.71
112		2		2.06
113		3		1.67
114		4		2.50
121	PG-2	1	2	2.18
122		2		2.38
123		3		1.67
124		4		1.50
131	PG-3	1	2.5	1.80
132		2		2.05
133		3		1.67
134		4		1.50
141	PG-4	1	3	1.92
142		2		2.30
143		3		1.67
144		4		1.50
151	PG-5	1	4	2.05
152		2		2.30
153		3		1.67
154		4		1.50
161	PG-6	1	5	1.99
162		2		2.30
163		3		1.67
164		4		1.50
171	PG-7	1	Min. Design	1.58
172		2		0.41
173		3		0.35
174		4		0.35

Table B.2: Summary of collapse margin ratios for the high gravity load level with overstrength combinations

Archetype ID	Performance Group	Arch Index	R-Value	CMR
211	PG-1	1	1.5	1.26
212		2		1.48
213		3		1.25
214		4		2.22
221	PG-2	1	2	1.66
222		2		1.42
223		3		1.32
224		4		1.38
231	PG-3	1	2.5	1.85
232		2		1.44
233		3		1.32
234		4		1.38
241	PG-4	1	3	1.62
242		2		1.68
243		3		1.32
244		4		1.38
251	PG-5	1	4	1.38
252		2		1.56
253		3		1.32
254		4		1.38
261	PG-6	1	5	1.41
262		2		1.56
263		3		1.32
264		4		1.38
271	PG-7	1	Min. Design	1.08
272		2		0.32
273		3		0.30
274		4		0.35

Table B.3: Summary of which NSC limits are causing collapse for low gravity load level given in % of ground motions failing for the given NSC limit, overstrength combinations

Arch ID	R-Value	Base Outward Shear	Base Inward Shear	Peak Shear	Bending Stresses
1L	1.5	0%	0%	100%	0%
	2	0%	0%	34%	66%
	2.5	0%	0%	100%	0%
	3	0%	0%	0%	100%
	4	0%	0%	21%	79%
	5	0%	0%	0%	100%
	Min.	0%	59%	0%	41%
2L	1.5	0%	0%	100%	0%
	2	0%	97%	3%	0%
	2.5	0%	97%	3%	0%
	3	0%	84%	6%	10%
	4	0%	84%	6%	10%
	5	0%	84%	6%	10%
	Min.	0%	100%	0%	0%
3L	1.5	0%	100%	0%	0%
	2	0%	100%	0%	0%
	2.5	0%	100%	0%	0%
	3	0%	100%	0%	0%
	4	0%	100%	0%	0%
	5	0%	100%	0%	0%
	Min.	0%	100%	0%	0%
4L	1.5	0%	28%	72%	0%
	2	0%	100%	0%	0%
	2.5	0%	100%	0%	0%
	3	0%	100%	0%	0%
	4	0%	100%	0%	0%
	5	0%	100%	0%	0%
	Min.	0%	100%	0%	0%

Table B.4: Summary of which NSC limits are causing collapse for high gravity load level given in % of ground motions failing for the given NSC limit, overstrength combinations

Arch ID	R-Value	Base Outward Shear	Base Inward Shear	Peak Shear	Bending Stresses
1H	1.5	0%	0%	100%	0%
	2	0%	0%	100%	0%
	2.5	0%	0%	51%	49%
	3	0%	24%	2%	74%
	4	0%	0%	16%	84%
	5	0%	0%	0%	100%
	Min.	0%	14%	0%	86%
2H	1.5	0%	7%	93%	0%
	2	0%	100%	0%	0%
	2.5	0%	100%	0%	0%
	3	0%	98%	2%	0%
	4	0%	100%	0%	0%
	5	0%	100%	0%	0%
	Min.	0%	100%	0%	0%
3H	1.5	0%	100%	0%	0%
	2	0%	100%	0%	0%
	2.5	0%	100%	0%	0%
	3	0%	100%	0%	0%
	4	0%	100%	0%	0%
	5	0%	100%	0%	0%
	Min.	0%	100%	0%	0%
4H	1.5	0%	100%	0%	0%
	2	0%	100%	0%	0%
	2.5	0%	100%	0%	0%
	3	0%	100%	0%	0%
	4	0%	100%	0%	0%
	5	0%	100%	0%	0%
	Min.	0%	100%	0%	0%

Appendix C: Results from Damping Study

The following tables provide the Collapse Margin Ratio (CMR) values for the arch designs with 0.5% damping included in the model. All CMR values were calculated utilizing designs with basic load combination rather than overstrength. Because of the time constraints related to running all 56 arch designs for each damping ratio, only 2 IDA scale factors were run and the CMR values were linearly interpolated. Although this linear interpolation is not exact due to small amounts of nonlinearity within the models, the values should be accurate enough such that comparisons between the damping ratios should be valid, as similar amounts of error should be present within each damping ratio.

Table C.1: Summary of collapse margin ratios for the low gravity load level with ζ = 0.005

Archetype ID	Performance Group	Arch Index	R-Value	CMR
111	PG-1	1	1.5	0.61
112		2		1.53
113		3		1.06
114		4		1.81
121	PG-2	1	2	1.14
122		2		1.71
123		3		1.06
124		4		0.86
131	PG-3	1	2.5	1.42
132		2		1.64
133		3		1.06
134		4		0.86
141	PG-4	1	3	1.45
142		2		1.75
143		3		1.06
144		4		0.86
151	PG-5	1	4	1.70
152		2		1.75
153		3		1.06
154		4		0.86
161	PG-6	1	5	1.55
162		2		1.75
163		3		1.06
164		4		0.86
171	PG-7	1	Min. Design	0.88
172		2		0.32
173		3		0.27
174		4		0.26

Table C.2: Summary of collapse margin ratios for the high gravity load level with ζ = 0.005

Archetype ID	Performance Group	Arch Index	R-Value	CMR
211	PG-1	1	1.5	0.49
212		2		0.76
213		3		0.70
214		4		1.35
221	PG-2	1	2	0.61
222		2		0.96
223		3		0.71
224		4		0.73
231	PG-3	1	2.5	0.97
232		2		0.96
233		3		0.71
234		4		0.73
241	PG-4	1	3	0.97
242		2		1.07
243		3		0.71
244		4		0.73
251	PG-5	1	4	1.09
252		2		1.00
253		3		0.71
254		4		0.73
261	PG-6	1	5	1.11
262		2		1.00
263		3		0.71
264		4		0.73
271	PG-7	1	Min. Design	0.57
272		2		0.26
273		3		0.24
274		4		0.25

The average of the CMR values for the low and high gravity load levels are 1.15 and 0.77, respectively. The values within the next two tables represent the percentage of ground motions which fail (of the 44 ground motions within the Far-Field set) as a result of the given NSC limit. Looking at these will provide the opportunity to determine why the arch models are failing.

Table C.3: Summary of which NSC limits are causing collapse for low gravity load level given in % of ground motions failing for the given NSC limit with $\zeta = 0.005$

Arch ID	R-Value	Base Outward Shear	Base Inward Shear	Peak Shear	Bending Stresses
1L	1.5	0%	0%	100%	0%
	2	0%	0%	100%	0%
	2.5	0%	0%	93%	7%
	3	0%	0%	0%	100%
	4	0%	0%	22%	78%
	5	0%	0%	0%	100%
	Min.	0%	100%	0%	0%
2L	1.5	0%	0%	100%	0%
	2	0%	100%	0%	0%
	2.5	0%	100%	0%	0%
	3	0%	100%	0%	0%
	4	0%	100%	0%	0%
	5	0%	100%	0%	0%
	Min.	0%	100%	0%	0%
3L	1.5	0%	100%	0%	0%
	2	0%	100%	0%	0%
	2.5	0%	100%	0%	0%
	3	0%	100%	0%	0%
	4	0%	100%	0%	0%
	5	0%	100%	0%	0%
	Min.	0%	100%	0%	0%
4L	1.5	0%	56%	44%	0%
	2	0%	100%	0%	0%
	2.5	0%	100%	0%	0%
	3	0%	100%	0%	0%
	4	0%	100%	0%	0%
	5	0%	100%	0%	0%
	Min.	0%	100%	0%	0%

Table C.4: Summary of which NSC limits are causing collapse for low gravity load level given in % of ground motions failing for the given NSC limit with ζ = 0.005

Arch ID	R-Value	Base Outward Shear	Base Inward Shear	Peak Shear	Bending Stresses
1H	1.5	0%	0%	100%	0%
	2	0%	0%	100%	0%
	2.5	0%	0%	100%	0%
	3	0%	0%	100%	0%
	4	0%	0%	18%	82%
	5	0%	0%	0%	100%
	Min.	0%	100%	0%	0%
2H	1.5	0%	0%	100%	0%
	2	0%	23%	77%	0%
	2.5	0%	52%	48%	0%
	3	0%	39%	61%	0%
	4	0%	27%	73%	0%
	5	0%	27%	73%	0%
	Min.	0%	100%	0%	0%
3H	1.5	0%	100%	0%	0%
	2	0%	100%	0%	0%
	2.5	0%	100%	0%	0%
	3	0%	100%	0%	0%
	4	0%	100%	0%	0%
	5	0%	100%	0%	0%
	Min.	0%	100%	0%	0%
4H	1.5	0%	52%	48%	0%
	2	0%	100%	0%	0%
	2.5	0%	100%	0%	0%
	3	0%	100%	0%	0%
	4	0%	100%	0%	0%
	5	0%	100%	0%	0%
	Min.	0%	100%	0%	0%

The next set of presented results is that of the models used for analysis involving a damping ratio equal to 2.5% of critical.

Table C.5: Summary of collapse margin ratios for the low gravity load level with ζ = 0.025

Archetype ID	Performance Group	Arch Index	R-Value	CMR
111	PG-1	1	1.5	0.78
112		2		2.06
113		3		1.44
114		4		2.48
121	PG-2	1	2	1.45
122		2		2.31
123		3		1.44
124		4		1.22
131	PG-3	1	2.5	1.80
132		2		1.95
133		3		1.44
134		4		1.22
141	PG-4	1	3	1.91
142		2		2.21
143		3		1.44
144		4		1.22
151	PG-5	1	4	2.04
152		2		2.21
153		3		1.44
154		4		1.22
161	PG-6	1	5	1.96
162		2		2.21
163		3		1.44
164		4		1.22
171	PG-7	1	Min. Design	1.09
172		2		0.35
173		3		0.30
174		4		0.29

Table C.6: Summary of collapse margin ratios for the high gravity load level with ζ = 0.025

Archetype ID	Performance Group	Arch Index	R-Value	CMR
211	PG-1	1	1.5	0.63
212		2		0.99
213		3		0.90
214		4		1.86
221	PG-2	1	2	0.83
222		2		1.17
223		3		0.95
224		4		0.92
231	PG-3	1	2.5	1.23
232		2		1.18
233		3		0.95
234		4		0.92
241	PG-4	1	3	1.21
242		2		1.34
243		3		0.95
244		4		0.92
251	PG-5	1	4	1.35
252		2		1.27
253		3		0.95
254		4		0.92
261	PG-6	1	5	1.37
262		2		1.27
263		3		0.95
264		4		0.92
271	PG-7	1	Min. Design	0.68
272		2		0.28
273		3		0.26
274		4		0.27

The average of the CMR values for the low and high gravity load levels are 1.51 and 0.98, respectively. The values within the next two tables represent the percentage of ground motions which fail (of the 44 ground motions within the Far-Field set) as a result of the given NSC limit. Looking at these will again provide the opportunity to determine why the arch models are failing and also determine if the failure mechanisms are changing with the added damping.

Table C.7: Summary of which NSC limits are causing collapse for low gravity load level given in % of ground motions failing for the given NSC limit with $\zeta = 0.025$

Arch ID	R-Value	Base Outward Shear	Base Inward Shear	Peak Shear	Bending Stresses
1L	1.5	0%	0%	100%	0%
	2	0%	0%	100%	0%
	2.5	0%	0%	100%	0%
	3	0%	0%	0%	100%
	4	0%	0%	21%	79%
	5	0%	0%	0%	100%
	Min.	0%	100%	0%	0%
2L	1.5	0%	0%	100%	0%
	2	0%	97%	3%	0%
	2.5	0%	97%	3%	0%
	3	0%	97%	3%	0%
	4	0%	97%	3%	0%
	5	0%	97%	3%	0%
	Min.	0%	100%	0%	0%
3L	1.5	0%	100%	0%	0%
	2	0%	100%	0%	0%
	2.5	0%	100%	0%	0%
	3	0%	100%	0%	0%
	4	0%	100%	0%	0%
	5	0%	100%	0%	0%
	Min.	0%	100%	0%	0%
4L	1.5	0%	41%	59%	0%
	2	0%	100%	0%	0%
	2.5	0%	100%	0%	0%
	3	0%	100%	0%	0%
	4	0%	100%	0%	0%
	5	0%	100%	0%	0%
	Min.	0%	100%	0%	0%

Table C.8: Summary of which NSC limits are causing collapse for high gravity load level given in % of ground motions failing for the given NSC limit with $\zeta = 0.025$

Arch ID	R-Value	Base Outward Shear	Base Inward Shear	Peak Shear	Bending Stresses
1H	1.5	0%	0%	100%	0%
	2	0%	0%	100%	0%
	2.5	0%	0%	100%	0%
	3	0%	0%	100%	0%
	4	0%	0%	14%	86%
	5	0%	0%	0%	100%
	Min.	0%	100%	0%	0%
2H	1.5	0%	0%	100%	0%
	2	0%	16%	84%	0%
	2.5	0%	48%	52%	0%
	3	0%	27%	73%	0%
	4	0%	21%	79%	0%
	5	0%	21%	79%	0%
	Min.	0%	100%	0%	0%
3H	1.5	0%	100%	0%	0%
	2	0%	100%	0%	0%
	2.5	0%	100%	0%	0%
	3	0%	100%	0%	0%
	4	0%	100%	0%	0%
	5	0%	100%	0%	0%
	Min.	0%	100%	0%	0%
4H	1.5	0%	50%	50%	0%
	2	0%	100%	0%	0%
	2.5	0%	100%	0%	0%
	3	0%	100%	0%	0%
	4	0%	100%	0%	0%
	5	0%	100%	0%	0%
	Min.	0%	100%	0%	0%

The next set of results corresponds to a damping ratio of 5% critical and is provided below.

Table C.9: Summary of collapse margin ratios for the low gravity load level with ζ = 0.05

Archetype ID	Performance Group	Arch Index	R-Value	CMR
111	PG-1	1	1.5	0.95
112		2		2.24
113		3		1.86
114		4		2.78
121	PG-2	1	2	1.60
122		2		2.73
123		3		1.86
124		4		1.38
131	PG-3	1	2.5	2.05
132		2		2.47
133		3		1.86
134		4		1.38
141	PG-4	1	3	2.14
142		2		2.66
143		3		1.86
144		4		1.38
151	PG-5	1	4	2.27
152		2		2.66
153		3		1.86
154		4		1.38
161	PG-6	1	5	2.14
162		2		2.66
163		3		1.86
164		4		1.38
171	PG-7	1	Min. Design	1.20
172		2		0.39
173		3		0.33
174		4		0.31

Table C.10: Summary of collapse margin ratios for the high gravity load level with ζ = 0.05

Archetype ID	Performance Group	Arch Index	R-Value	CMR
211	PG-1	1	1.5	0.75
212		2		1.17
213		3		1.05
214		4		2.22
221	PG-2	1	2	0.91
222		2		1.30
223		3		1.07
224		4		1.12
231	PG-3	1	2.5	1.35
232		2		1.38
233		3		1.07
234		4		1.12
241	PG-4	1	3	1.35
242		2		1.51
243		3		1.07
244		4		1.12
251	PG-5	1	4	1.47
252		2		1.48
253		3		1.07
254		4		1.12
261	PG-6	1	5	1.59
262		2		1.48
263		3		1.07
264		4		1.12
271	PG-7	1	Min. Design	0.80
272		2		0.30
273		3		0.27
274		4		0.29

The average of the CMR values for the low and high gravity load levels are 1.77 and 1.13, respectively. The values within the next two tables represent the percentage of ground motions which fail (of the 44 ground motions within the Far-Field set) as a result of the given NSC limit.

Table C.11: Summary of which NSC limits are causing collapse for low gravity load level given in % of ground motions failing for the given NSC limit with ζ = 0.05

Arch ID	R-Value	Base Outward Shear	Base Inward Shear	Peak Shear	Bending Stresses
1L	1.5	0%	0%	100%	0%
	2	0%	0%	100%	0%
	2.5	0%	0%	100%	0%
	3	0%	0%	0%	100%
	4	0%	0%	21%	79%
	5	0%	0%	0%	100%
	Min.	0%	98%	0%	2%
2L	1.5	0%	0%	100%	0%
	2	0%	100%	0%	0%
	2.5	0%	100%	0%	0%
	3	0%	96%	4%	0%
	4	0%	96%	4%	0%
	5	0%	96%	4%	0%
	Min.	0%	100%	0%	0%
3L	1.5	0%	100%	0%	0%
	2	0%	100%	0%	0%
	2.5	0%	100%	0%	0%
	3	0%	100%	0%	0%
	4	0%	100%	0%	0%
	5	0%	100%	0%	0%
	Min.	0%	100%	0%	0%
4L	1.5	0%	23%	77%	0%
	2	0%	100%	0%	0%
	2.5	0%	100%	0%	0%
	3	0%	100%	0%	0%
	4	0%	100%	0%	0%
	5	0%	100%	0%	0%
	Min.	0%	100%	0%	0%

Table C.12: Summary of which NSC limits are causing collapse for high gravity load level given in % of ground motions failing for the given NSC limit with ζ = 0.05

Arch ID	R-Value	Base Outward Shear	Base Inward Shear	Peak Shear	Bending Stresses
1H	1.5	0%	0%	100%	0%
	2	0%	0%	100%	0%
	2.5	0%	0%	100%	0%
	3	0%	0%	100%	0%
	4	0%	0%	12%	88%
	5	0%	0%	0%	100%
	Min.	0%	91%	0%	9%
2H	1.5	0%	0%	100%	0%
	2	0%	16%	84%	0%
	2.5	0%	40%	60%	0%
	3	0%	20%	80%	0%
	4	0%	13%	88%	0%
	5	0%	13%	88%	0%
	Min.	0%	100%	0%	0%
3H	1.5	0%	100%	0%	0%
	2	0%	100%	0%	0%
	2.5	0%	100%	0%	0%
	3	0%	100%	0%	0%
	4	0%	100%	0%	0%
	5	0%	100%	0%	0%
	Min.	0%	100%	0%	0%
4H	1.5	0%	34%	66%	0%
	2	0%	100%	0%	0%
	2.5	0%	100%	0%	0%
	3	0%	100%	0%	0%
	4	0%	100%	0%	0%
	5	0%	100%	0%	0%
	Min.	0%	100%	0%	0%

The next set of results corresponds to a damping ratio of 5% critical and is provided below.

Table C.13: Summary of collapse margin ratios for the low gravity load level with ζ = 0.10

Archetype ID	Performance Group	Arch Index	R-Value	CMR
111	PG-1	1	1.5	1.11
112		2		2.68
113		3		2.23
114		4		3.17
121	PG-2	1	2	1.89
122		2		3.09
123		3		2.23
124		4		1.58
131	PG-3	1	2.5	2.43
132		2		2.89
133		3		2.23
134		4		1.58
141	PG-4	1	3	2.61
142		2		3.23
143		3		2.23
144		4		1.58
151	PG-5	1	4	2.64
152		2		3.23
153		3		2.23
154		4		1.58
161	PG-6	1	5	2.51
162		2		3.23
163		3		2.23
164		4		1.58
171	PG-7	1	Min. Design	1.21
172		2		0.43
173		3		0.36
174		4		0.33

Table C.14: Summary of collapse margin ratios for the high gravity load level with ζ = 0.10

Archetype ID	Performance Group	Arch Index	R-Value	CMR
211	PG-1	1	1.5	0.89
212		2		1.40
213		3		1.26
214		4		2.70
221	PG-2	1	2	1.07
222		2		1.65
223		3		1.34
224		4		1.21
231	PG-3	1	2.5	1.59
232		2		1.68
233		3		1.34
234		4		1.21
241	PG-4	1	3	1.57
242		2		1.69
243		3		1.34
244		4		1.21
251	PG-5	1	4	1.81
252		2		1.79
253		3		1.34
254		4		1.21
261	PG-6	1	5	1.82
262		2		1.79
263		3		1.34
264		4		1.21
271	PG-7	1	Min. Design	0.78
272		2		0.33
273		3		0.29
274		4		0.29

The average of the CMR values for the low and high gravity load levels are 2.08 and 1.33, respectively. The values within the next two tables represent the percentage of ground motions which fail (of the 44 ground motions within the Far-Field set) as a result of the given NSC limit.

Table C.15: Summary of which NSC limits are causing collapse for low gravity load level given in % of ground motions failing for the given NSC limit with ζ = 0.10

Arch ID	R-Value	Base Outward Shear	Base Inward Shear	Peak Shear	Bending Stresses
1L	1.5	0%	0%	100%	0%
	2	0%	0%	100%	0%
	2.5	0%	0%	93%	7%
	3	0%	0%	0%	100%
	4	0%	0%	32%	68%
	5	0%	0%	0%	100%
	Min.	0%	100%	0%	0%
2L	1.5	0%	0%	100%	0%
	2	0%	86%	14%	0%
	2.5	0%	97%	3%	0%
	3	0%	93%	3%	3%
	4	0%	93%	3%	3%
	5	0%	93%	3%	3%
	Min.	0%	100%	0%	0%
3L	1.5	0%	100%	0%	0%
	2	0%	100%	0%	0%
	2.5	0%	100%	0%	0%
	3	0%	100%	0%	0%
	4	0%	100%	0%	0%
	5	0%	100%	0%	0%
	Min.	0%	100%	0%	0%
4L	1.5	0%	34%	66%	0%
	2	0%	100%	0%	0%
	2.5	0%	100%	0%	0%
	3	0%	100%	0%	0%
	4	0%	100%	0%	0%
	5	0%	100%	0%	0%
	Min.	0%	100%	0%	0%

Table C.16: Summary of which NSC limits are causing collapse for high gravity load level given in % of ground motions failing for the given NSC limit with ζ = 0.10

Arch ID	R-Value	Base Outward Shear	Base Inward Shear	Peak Shear	Bending Stresses
1H	1.5	0%	0%	100%	0%
	2	0%	0%	100%	0%
	2.5	0%	0%	100%	0%
	3	0%	0%	100%	0%
	4	0%	0%	10%	90%
	5	0%	0%	0%	100%
	Min.	0%	100%	0%	0%
2H	1.5	0%	0%	100%	0%
	2	0%	20%	80%	0%
	2.5	0%	53%	47%	0%
	3	0%	27%	73%	0%
	4	0%	19%	81%	0%
	5	0%	19%	81%	0%
	Min.	0%	100%	0%	0%
3H	1.5	0%	100%	0%	0%
	2	0%	100%	0%	0%
	2.5	0%	100%	0%	0%
	3	0%	100%	0%	0%
	4	0%	100%	0%	0%
	5	0%	100%	0%	0%
	Min.	0%	100%	0%	0%
4H	1.5	0%	49%	51%	0%
	2	0%	100%	0%	0%
	2.5	0%	100%	0%	0%
	3	0%	100%	0%	0%
	4	0%	100%	0%	0%
	5	0%	100%	0%	0%
	Min.	0%	100%	0%	0%

Summary and Conclusion

The results from all of the analyses are summarized below by using the average of each gravity load level group as previously mentioned. The percentage of increase or decrease in CMR from the original case with the damping ratio set to 0.025 to the case of interest is also provided within this table.

Table C.17: Summary of average CMR values and their deviation from the CMR with damping set to 0.025

Damping Ratio, ζ	CMR		Δ_{CMR} from ζ = 0.025	
	Gravity Load Level		Gravity Load Level	
	Low	High	Low	High
0.005	1.15	0.77	-24%	-21%
0.025	1.51	0.98	0%	0%
0.05	1.77	1.13	17%	15%
0.1	2.08	1.33	38%	36%

These results show that damping applied to a structure has a significant impact on the CMR of the system. From the table, it can be seen that if the damping ratio typically assumed for timber material only was used, the CMR values would be expected to be decreased by over 20% on average which is a significant impact. Also, it can be seen from these results that an increase in damping ratio could potentially provide a significant increase to the CMR values observed. By increasing the damping to 5% of critical, increases of at least 15 % on average would be expected. A damping ratio of 5% is probably not unreasonable for a system such as this, in fact from the previously discussed research, it is certainly possible that the damping ratio of one of these systems is likely somewhere between 5 and 10% but without information on this particular structural system, it would be difficult to defend a reason to significantly increase the damping ratio.